Master thesis - Electrical Engineering

Analysis of three dimensional array antenna elements to achieve asymmetric active element patterns

Ralph van Schelven 4162188

Delft University of Technology

September 20, 2017

TU Delft Delft University of Technology

TNO

Master-track Telecommunications,
Faculty of Electrical Engineering,
Mathematics and Computer Science

Challenge the future

Analysis of three dimensional array antenna elements to achieve asymmetric active element patterns
(September 20, 2017)

Preface

Typical antenna arrays are designed such that the active element pattern is symmetric around the broadside direction. However, applications exist, for example in satellite communication, where a symmetric pattern is not needed or even unwanted. This angular selectivity can be achieved using asymmetric elements. However, it is known that for well sampled infinite arrays the asymmetry of the active element pattern disappears. Although designs of under-sampled antenna arrays achieving an asymmetric active element pattern have been presented in literature, the fundamental properties of this type of arrays in terms of radiation characteristics have not been investigated in detail. This thesis studies the asymmetry in the active element pattern of a finite linear array of asymmetric elements. To this end an in-house method of moments code is developed in Matlab to simulate tilted dipoles in free space and in the proximity of a ground plane. The dependency of the asymmetry of the active element pattern on the inter-element distance, the skew angle of the elements and the number of elements in the array is analyzed and design rules are derived. Using entire domain basis functions, closed form expressions for spectral integrals and the periodicity of the array the implemented code enables the simulation of large arrays in a much shorter time compared to commercially available software, such as CST.

Regarding the choice of antenna element, a dipole bent into a Z-shape is proposed as an alternative for a tilted dipole. This type of dipole can be defined to have an equivalent radiation pattern to that of a tilted dipole. This shape of dipole can be implemented using standard PCB technology using horizontal metal strips and vertical vias. The Z-shaped dipoles are analyzed using a method of moments code based on horizontal and vertical dipoles. The spectral Green's function of stratified media can be included in the spectral domain expressions to account for the presence of dielectric slabs in realistic designs.

This thesis is submitted in partial fulfillment of the requirements for the degree of Master of Science in Electrical Engineering at Delft University of Technology.

Ralph van Schelven
Delft, September 20, 2017

Acknowledgments

First of all I would like to thank the teachers of the electromagnetism courses here at TU Delft. You have shown me the beauty of this field and have inspired me to take this direction in my studies.

I would like to thank my supervisors: Daniele, Stefania, Erio and Cristina.

Daniele, you spent a lot of time teaching me about the method of moments and how to do the mathematics involved. You helped me by being critical of my work and making me think about the results. Even though you are very busy, you were always able to help me with any questions.

Although being always very busy, Stefania was able to make some time to look at my work and give me tips and feedback. You were always very enthusiastic, which motivated me to keep going.

After my internship Erio kept supervising me for my thesis work as well. Although you were very busy working on your own projects, I could come to you both for questions and to get a coffee. Besides advising me on my work you helped me think about my future after graduating and together with Stefania tried to get me a PhD position at TNO. I cannot even begin to tell both of you how much I appreciated that.

The person I am sure I bothered the most with questions was Cristina. Being very involved in the project, and only one room away, you were my go to person for questions and panic. You never told me to come back later and immediately dropped your own work to think with me about a problem I had. Besides a supervisor you became a friend and I am looking forward to all the coffees and big hot chocolates we'll get in the years to come.

I am feeling truly lucky to have had the four of you as my supervisors the past year.

Of course I thank my roommates for all the fun we had during and after work. Alicia, Arturo, Cantika, Diego, Harshitha, Sjoerd and Zhengzheng, you made the office my second home. I want to thank Harshitha for answering any quick questions I had regarding the method of moments and basis functions and everything else. Being only two meters away you were even closer than Cristina and I enjoyed talking together about both our projects. Besides my roommates I want to mention also the rest of the Terahertz sensing group for creating a nice, comfortable environment to work.

I want to thank my friends from my board, the rest of the ETV and from JC Schot for the fun nights and for the random messages in group chats, providing some welcome distractions from work every now and then.

And finally I would like to thank my parents, who have always been there for me. You have supported me all my life and patiently listened to all my stories and problems. Knowing I can always count on you makes everything more easy. Thank you.

Analysis of three dimensional array antenna elements to achieve asymmetric active element patterns

This thesis is submitted in partial fulfillment of the requirements for the degree of

Master of Science

in

Electrical Engineering

by

Ralph van Schelven
born in Dordrecht, The Netherlands

The work presented in this thesis was performed at:

Tera-Hertz Sensing Group
Department of Microelectronics
Faculty of Electrical Engineering, Mathematics and Computer Science
Delft University of Technology

Department of Radar Technology
Oude Waalsdorperweg, The Hague
TNO

Delft University of Technology
Department of Electrical Engineering

The undersigned hereby certify that they have read and recommend to the Faculty of Electrical Engineering, Mathematics and Computer Science for acceptance a thesis entitled **"Analysis of three dimensional array antenna elements to achieve asymmetric active element patterns "** by **Ralph van Schelven** in partial fulfillment of the requirements for the degree of **Master of Science***.

Dated: September 29, 2017

Chairman:

prof. dr. Andrea Neto

Advisor:

dr. Daniele Cavallo

Committee Members:

dr. Bert Kooij

dr. Stefania Monni

*The daily supervisors for the duration of the thesis work were Cristina Yepes from the TU Delft and Erio Gandini from TNO.

Contents

List of Figures

Chapter 1

Introduction

1.1 Background

In the world of today it is more and more desired to be connected every time, everywhere. We want to be able to connect to the internet with our mobile phones and laptops on the train and while flying. Our cars download traffic information in order to plan the fastest route from the internet while driving. In order to facilitate the satellite communication for these vehicles, a demand arises for lightweight, low-profile steerable-beam antennas [1], [2], [3]. It is desirable that these antennas can be integrated on cars and planes, without significantly affect the aerodynamics and the aesthetics of the vehicle.

A relevant recent application, considered in [4], is in-flight entertainment. For such application, antenna arrays located on airplanes for satellite communication applications, are typically required to be able to scan to very large scan angles (close to hemispherical). However, planar antenna arrays typically experience scan loss, i.e. a reduction of gain when the main beam is pointed away from broadside. To increase the scan range, multi-panel configurations have been proposed in [4] or conformal arrays in [5], but the height of the structure affects the aerodynamics of the airplanes to a too large extent. To obtain wide-scan capability while still maintaining a low antenna profile, hybrid scanning mechanism have been proposed in [1], [3], [6] and [7]. The beam is scanned electronically from broadside to a positive, as high as possible, angle and by rotation of the array along the azimuth full coverage is achieved.

New technologies, such as 3D-printing and additive manufacturing, enable new possibilities in the design of antenna arrays. Figure 1.1a shows a preliminary design of the antenna proposed in [1]. The array elements are placed at a skew angle to maximize the radiation to high elevation angles in one direction, as shown in figure 1.1b. The array is designed to shape the active element pattern to be asymmetric. Also at TNO, an array consisting of skewed patches is currently being developed. Although some designs employing skewed antenna elements have been presented in the literature, the fundamental properties of this type of arrays in terms of radiation characteristics have not been investigated in detail.

Achieving asymmetric patterns with large antenna arrays is not an easy task. That is because, as shown in [8], the active element pattern for infinite arrays is always symmetric (equal for scanning to $+\theta_{scan}$ or $-\theta_{scan}$) when the array is dimensioned such that no grating lobes occur. This property is valid for any generic current distribution on the antenna element, thus also in the case of asymmetric or tilted elements. However, outside of the grating lobe free region asymmetry can be achieved. Therefore, for a large array, the inter-element distance must be increased in order to achieve higher asymmetry in the active element pattern. Also, the theory described in [8] considers only infinite arrays. Thus a certain degree of asymmetry can be still

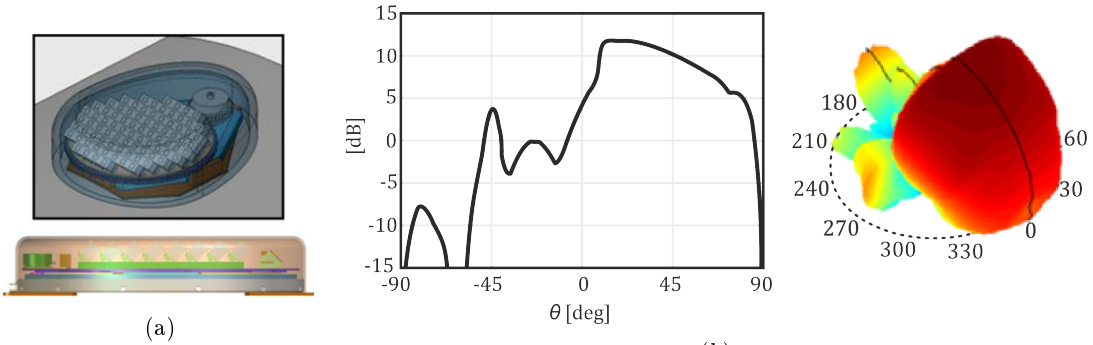

(a) (b)

Figure 1.1: A preliminary design of a low-profile steerable beam antenna as proposed in [1]. The elements are placed under a skew angle to provide the asymmetry. a) Model of the antenna. b) Simulated radiation pattern of the antenna.

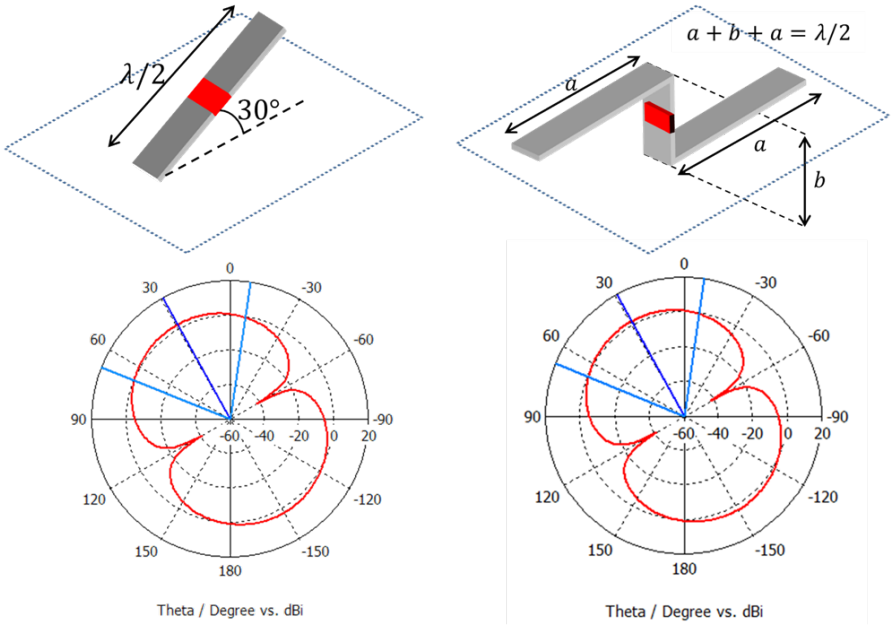

Figure 1.2: An alternative to implement skewed dipoles using bent dipoles shaped like a Z. It can be seen that the radiation patterns of the two dipoles show a good agreement.

achieved for finite arrays. The dependence of the asymmetry properties on the size of the array can be studied.

Regarding the choice of the antenna element, skewed dipoles can be considered. An alternative to tilted dipoles can be a dipole that is bent into a Z-shape, partly horizontally and partly vertically oriented. It is shown in figure 1.2 that a Z-shaped dipole can be defined to have an equivalent radiation pattern as that of a skewed dipole. Such a Z-shaped dipole can be implemented using standard PCB technology, using horizontal metal patches and vertical vias.

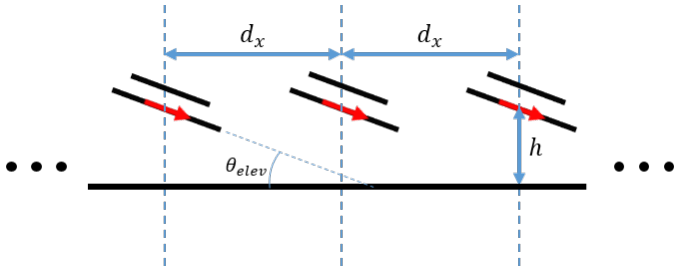

Figure 1.3: Linear array of skewed stacked dipoles above an infinite ground plane and their images. The displacement in x-direction between the dipoles is d_x and the distance between the centers of the excited dipoles and the ground plane is h. The skew angle between the dipoles and the ground plane is θ_{elev}.

1.2 Objectives of this thesis

This work aims to find design rules for a linear array with an asymmetric active element pattern. Specifically the dependency of the asymmetry on the number of elements, the periodicity of the array and the skew angle of the elements is investigated. To this end, a theoretical analysis of simple asymmetric structures can constitute a relevant tool to derive trade-offs that will represent the basis for practical designs and implementations of asymmetric arrays. A method of moments (MoM) code is developed to find the radiation pattern and the active element pattern of a linear array of skewed dipoles. An example of such a linear array, located above an infinite ground plane, is shown in figure 1.3. The method of moments code is implemented in Matlab and validated using CST studio suite. The thesis gives the expressions of the impedance and the forcing terms of the method of moments both in the spatial and the spectral domain. However, all results shown in the thesis are made using the spectral domain calculations. Using the method of moments code the dependence of the asymmetry of the active element pattern on the number of array elements, periodicity and skew angle is evaluated and discussed.The implemented method of moments code enables the simulation of large arrays in a much shorter time compared to commercially available software, such as CST.

As an alternative for skewed dipoles, dipoles bent into a Z-shape are proposed. The method of moments code to analyze these elements is then based on expressions to simulate dipoles oriented along x and z. Because the Z-shaped dipoles consist of horizontal and vertical parts, the spectral Green's function of stratified media can be included in the spectral domain expressions, which is necessary to account for the presence of dielectric slabs in realistic designs.

A spectral method of moments to simulate dipoles and slots bent in the xy-plane was previously presented in [9]. However, z-oriented currents where not considered in that work, while this thesis addresses the problem of generalizing the spectral coupling integral to include structures along z.

1.3 Thesis outline

This thesis is organized as follows:

The method of moments for horizontal dipoles is explained in chapter 2. The expressions for the impedances and the forcing terms are derived in the spatial domain, before being rewritten in the spectral domain. Two types of basis functions are considered: an entire domain basis function and piecewise linear basis functions.

Chapter 3 deals with the analysis of non-parallel dipoles. The expressions for the method

of moments for dipoles oriented along x and z are derived. Subsequently, dipoles skewed under arbitrary angle with respect to each other are considered.

Using the method described in the previous chapters to simulate the active element pattern of skewed dipoles above a ground plane, chapter 4 describes the analysis on the asymmetry of the active element pattern while varying the number of elements in the array, the inter-element spacing and the skew angle of the elements. The asymmetry for linear arrays of both dipoles and directive elements is analyzed. Design rules are derived for the asymmetry of the active element pattern.

An alternative for skewed dipoles using Z-shaped dipoles is considered in chapter 5. A method of moments code is developed to calculate the radiation patterns of this Z-shaped dipole. Such structure is somewhat more complicated to analyze because of non-convergent spectral integrals arising from the electrical connection between z- and x-oriented strips. A possible solution to solve this issue is suggested.

A conclusion on the performed work can be found in chapter 6, as well as potential future developments.

Chapter 2

MoM for finite arrays of horizontal dipoles

This chapter focuses on the backbone of the work performed for this thesis: the method of moments. First the method of moments for a finite number of horizontal dipoles made of a perfect electric conductor (PEC) is presented in section 2.1. The expressions of the mutual and self impedance and the forcing terms are derived in the spatial domain and rewritten to the spectral domain. The electric far field radiated by the dipoles is calculated and the radiation pattern is found. Two different types of basis functions are then considered in the following sections to solve the problem. In particular, entire domain basis functions are used in section 2.2 and piecewise linear basis functions in section 2.3.

2.1 MoM for dipoles made of a PEC

The starting point of the method of moments is to impose the boundary conditions for the problem at hand.

Let us consider a single planar dipole made of perfect electric conductor and located in the xy-plane, fed by an infinite transmission line as shown in figure 2.1a. The dipole is centered in the origin of the Cartesian reference system. The transmission line feeding the dipole can be represented as a Thévenin network consisting of a voltage source and a generator impedance as shown in figure 2.1b. The source voltage is equal to the open-circuit voltage at the terminals of the dipole and is therefore equal to $v_0 = v^+(1+\Gamma) = 2v^+$. Considering a semi-infinite feeding transmission line, the Thévenin impedance is equal to the characteristic impedance of line z_0.

For a dipole made of perfect electric conductor, the condition to be satisfied on the dipole is:

$$\hat{\boldsymbol{n}} \times \boldsymbol{e}_{tot} = z_{surf}\boldsymbol{j} \tag{2.1}$$

where $\hat{\boldsymbol{n}}$ is the unit vector normal to the dipole and $\boldsymbol{e}_{tot}$ is the total electric field at the surface of the dipole. z_{surf} is the surface impedance on the dipole and $\boldsymbol{j}$ is the current along the dipole. Since the dipole is made of perfect electric conductor $z_{surf} = 0$ on the dipole arms and $z_{surf} = z_0$ on the gap.

$$z_{surf}(x,y) = \frac{z_0}{\delta}\,\mathrm{rect}_{w,\delta}(x,y)\,. \tag{2.2}$$

The total electric field can be decomposed in the incident field, $\boldsymbol{e}_{inc}$, and the scattered field, $\boldsymbol{e}_{scat}$, such that:

$$\begin{aligned} \hat{\boldsymbol{n}} \times (\boldsymbol{e}_{inc} + \boldsymbol{e}_{scat}) &= z_{surf}\boldsymbol{j} \\ -\hat{\boldsymbol{n}} \times \boldsymbol{e}_{scat} + z_{surf}\boldsymbol{j} &= \hat{\boldsymbol{n}} \times \boldsymbol{e}_{inc}\,. \end{aligned} \tag{2.3}$$

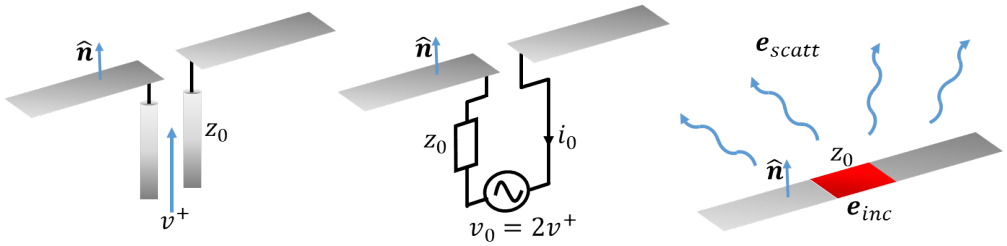

Figure 2.1: The dipole under consideration. a) A dipole fed by a transmission line. b) The transmission line can be represented by a Thévenin equivalent circuit. c) The incident field and the scattered field.

The incident electric field is the field induced due to the voltage in the gap and is assumed constant:

$$\hat{\boldsymbol{n}} \times \boldsymbol{e}_{inc}(x,y) = \frac{v_0}{\delta}\,\mathrm{rect}_{w,\delta}(x,y)\hat{\boldsymbol{x}} \tag{2.4}$$

where δ is the length of the port, w is the width of the dipole. The scattered field is the field radiated from the dipole, as shown in figure 2.1c.

By using the equivalence theorem, the original problem of a dipole made of perfect electric conductor can be expressed as equivalent currents in free space. A surface S enclosing a volume V is defined just around the dipole, as shown in figure 2.2a. The fields inside S, $\boldsymbol{e}_1$ and $\boldsymbol{h}_1$, are chosen to be 0. The equivalent currents need to satisfy the boundary conditions:

$$\boldsymbol{j}'_{eq} = \hat{\boldsymbol{n}} \times (\boldsymbol{h}_2 - \boldsymbol{h}_1) \tag{2.5}$$

$$\boldsymbol{m}'_{eq} = -\hat{\boldsymbol{n}} \times (\boldsymbol{e}_2 - \boldsymbol{e}_1) \tag{2.6}$$

where $\boldsymbol{h}_1$, $\boldsymbol{e}_1$ and $\boldsymbol{h}_2$, $\boldsymbol{e}_2$ are the magnetic and electric fields just inside and outside S, respectively. Since the fields outside the surface S must be equal to the original problem, we know from equation (2.1) that $\hat{\boldsymbol{n}} \times \boldsymbol{e}_2 = 0$ on the dipole arms. Therefore, the equivalent magnetic current $\boldsymbol{m}'_{eq}$ vanishes on the metal leaving only an equivalent electric current $\boldsymbol{j}'_{eq}$ as can be seen in figure 2.2b. Due to the continuity of the field, i.e. the electric field below the gap $\boldsymbol{e}_2^-$ and the electric field above the gap $\boldsymbol{e}_2^+$ are equal, the magnetic current vanishes also in the gap. The dipole is oriented along x, such that $\hat{\boldsymbol{n}} = \hat{\boldsymbol{z}}$ on top of the dipole and $\hat{\boldsymbol{n}} = -\hat{\boldsymbol{z}}$ on the bottom. Assuming the dipoles to be very thin and since the magnetic field just above the dipole, $\boldsymbol{h}_2^+$, is equal but opposite to the magnetic field just below the dipole, $\boldsymbol{h}_2^-$, the total equivalent current can be expressed as:

$$\boldsymbol{j}_{eq} = \hat{\boldsymbol{z}} \times \boldsymbol{h}_2^+ - \hat{\boldsymbol{z}} \times \boldsymbol{h}_2^- = 2\boldsymbol{j}'_{eq} \tag{2.7}$$

in free space which is shown in figure 2.2c.

The scattered field can be rewritten as a convolution between the dyadic Green's function describing the electric field due to electric currents, $\boldsymbol{g}^{ej}$, and the equivalent electric current:

$$\boldsymbol{e}_{scat} = \int_{-\infty}^{\infty}\int_{-\infty}^{\infty}\int_{-\infty}^{\infty} \boldsymbol{j}_{eq}(\boldsymbol{r}')\boldsymbol{g}^{ej}(\boldsymbol{r},\boldsymbol{r}')d\boldsymbol{r}' \tag{2.8}$$

where $\boldsymbol{r}' \equiv (x',y',z')$ and $\boldsymbol{r} \equiv (x,y,z)$ are the source and observation points respectively.

The equivalent current is written as an unknown coefficient $i_{n'}$ multiplied by a known basis function $\boldsymbol{b}_{n'}$. Once the weighting term $i_{n'}$ is calculated the current distribution over the dipoles is

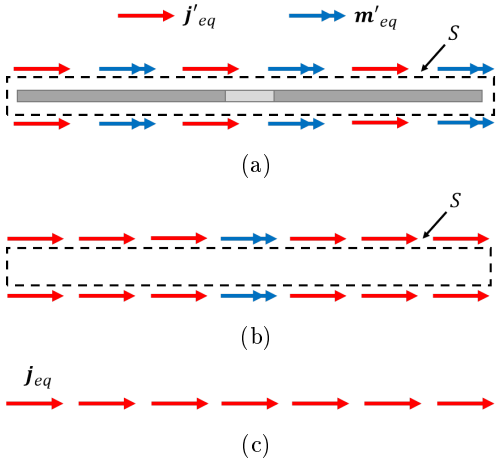

Figure 2.2: Visual representation of the equivalence theorem considering a thin dipole made of perfect electric conductor. a) Defining a surface S around the dipole and the equivalent currents $\boldsymbol{j'}_{eq}$ and $\boldsymbol{m'}_{eq}$. b) Satisfying the boundary conditions the magnetic currents vanish everywhere except on the gap. c) Due to the continuity of the fields, the magnetic current in the gap vanishes and, assuming a thin dipole, an equivalent electric current $\boldsymbol{j}_{eq} = 2\boldsymbol{j'}_{eq}$ remains.

known. Both sides of the integral equation are projected on the same known current distribution. This current distribution is called the test function $\boldsymbol{t}_n$. Projecting both sides of the electric field integral equation on the test function gives:

$$\begin{gathered}\langle -\hat{\boldsymbol{n}} \times \boldsymbol{e}_{scat}(\boldsymbol{r}) + z_{surf}\boldsymbol{j}(\boldsymbol{r}), \boldsymbol{t}_n(\boldsymbol{r})\rangle = \langle \hat{\boldsymbol{n}} \times \boldsymbol{e}_{inc}(\boldsymbol{r}), \boldsymbol{t}_n(\boldsymbol{r})\rangle \\ -\sum_{n'=1}^{N} i_{n'}\langle \hat{\boldsymbol{n}} \times (\boldsymbol{g}^{ej}(\boldsymbol{r}) * \boldsymbol{b}_{n'}(\boldsymbol{r})), \boldsymbol{t}_n(\boldsymbol{r})\rangle + \langle z_{surf}\boldsymbol{j}(\boldsymbol{r}), \boldsymbol{t}_n(\boldsymbol{r})\rangle = \langle \hat{\boldsymbol{n}} \times \boldsymbol{e}_{inc}(\boldsymbol{r}), \boldsymbol{t}_n(\boldsymbol{r})\rangle\end{gathered} \tag{2.9}$$

where $\langle \boldsymbol{f}_1, \boldsymbol{f}_2\rangle = \int_{-\infty}^{\infty}\int_{-\infty}^{\infty}\int_{-\infty}^{\infty} \boldsymbol{f}_1(\boldsymbol{r}) \cdot \boldsymbol{f}_2^*(\boldsymbol{r}) d\boldsymbol{r}$ and N is the number of basis functions. Defining the impedance terms as

$$Z_{nn'} = \langle \hat{\boldsymbol{n}} \times (\boldsymbol{g}^{ej}(\boldsymbol{r}) * \boldsymbol{b}_{n'}(\boldsymbol{r})), \boldsymbol{t}_n(\boldsymbol{r})\rangle \tag{2.10}$$

and assuming that the current is constant in the gap:

$$\langle z_{surf}\boldsymbol{j}(\boldsymbol{r}), \boldsymbol{t}_n(\boldsymbol{r})\rangle = z_0 i_0 \langle \frac{1}{\delta}\,\mathrm{rect}_{w,\delta}(x,y)\hat{\boldsymbol{x}}, \boldsymbol{t}_n(\boldsymbol{r})\rangle = z_0 i_0 p_n\,. \tag{2.11}$$

The forcing terms are defined as

$$v_n = \langle \hat{\boldsymbol{n}} \times \boldsymbol{e}_{inc}(\boldsymbol{r}), \boldsymbol{t}_n(\boldsymbol{r})\rangle = \frac{v_0}{\delta}\langle \mathrm{rect}_{w,\delta}(x,y)\hat{\boldsymbol{x}}, \boldsymbol{t}_n(\boldsymbol{r})\rangle = v_0 p_n\,. \tag{2.12}$$

Thus equation (2.9) can be written in a more compact form as

$$\sum_{n'=1}^{N} Z_{nn'} i_{n'} + z_0 i_0 p_n = v_0 p_n \qquad \forall\, n \tag{2.13}$$

or in matrix notation:

$$\begin{gathered}(\boldsymbol{Z} + z_0\boldsymbol{P}) \cdot \boldsymbol{i} = \boldsymbol{P} \cdot \boldsymbol{v} \\ \boldsymbol{i} = (\boldsymbol{Z} + z_0\boldsymbol{P})^{-1} \cdot (\boldsymbol{P} \cdot \boldsymbol{v})\end{gathered} \tag{2.14}$$

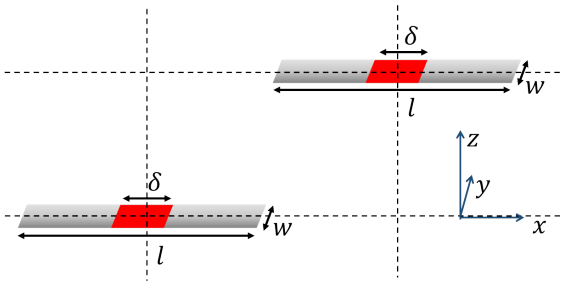

Figure 2.3: Two identical dipoles with lenght l and width w oriented along x, centered at $y = 0$ displaced in x and z. The excitation port has a lenght δ.

where $\boldsymbol{P}$ is a diagonal matrix $\boldsymbol{P} = \text{diag}(p_n)$, whose terms are zero if the n^{th} basis function is defined on the metal, and different from zero if the basis function overlaps with the feeding gap region.

2.1.1 MoM in the spatial domain

Let us consider a finite number M of infinitely thin dipoles oriented along x. The elements can be displaced in x and z. Figure 2.3 shows an example of such an array consisting of two elements.

We define x_n, z_n to be the x- and z-coordinates of the center of the n^{th} basis function. Assuming that the dipole width is small compared to the wavelength, the equivalent current can be considered as oriented along the dipole. The transverse current distribution is assumed to be edge-singular. The basis function can thus be written as:

$$\boldsymbol{b}_n(\boldsymbol{r}') = b_{n,x}(x' - x_n) j_t(y') \delta(z' - z_n) \hat{\boldsymbol{x}} \tag{2.15}$$

where

$$j_t(y') = \frac{2}{w\pi} \frac{\text{rect}_w(y')}{\sqrt{1 - \left(\frac{2y'}{w}\right)^2}} \tag{2.16}$$

and w is the width of the dipole. The test function along x is chosen to be the same as the basis function. The observation domain is chosen to be along the dipole axis $y = 0$. Therefore the test function can be written as:

$$\boldsymbol{t}_n(\boldsymbol{r}) = b_{n,x}(x - x_n)\delta(y)\delta(z - z_n)\hat{\boldsymbol{x}}\,. \tag{2.17}$$

The projection terms p_n can be written explicitly as spatial domain integrals as follows:

$$p_n = \frac{1}{\delta}\langle \text{rect}_{w,\delta}(x,y)\hat{\boldsymbol{x}}, \boldsymbol{t}_n(\boldsymbol{r})\rangle = \frac{1}{\delta}\int_{-\infty}^{\infty} \text{rect}_\delta(x - x_m) b^*_{n,x}(x - x_n)dx\,. \tag{2.18}$$

where the property of the δ-function, $\int_{-\infty}^{\infty} f(\xi)\delta(\xi - \xi_0)d\xi = f(\xi_0)$ is used and x_m is the x-coordinate of the center of the m^{th} dipole. The elements of the impedance matrix defined in equation (2.10) can be written as

$$Z_{xnxn'} = -\int_{x_{n'}-\frac{l_b}{2}}^{x_{n'}+\frac{l_b}{2}} \int_{-\frac{w}{2}}^{\frac{w}{2}} \int_{x_n-\frac{l_b}{2}}^{x_n+\frac{l_b}{2}} b_{n',x}(x' - x_{n'}) j_t(y') g^{ej}_{xx}(x - x', y', z_n - z_{n'}) b^*_{n,x}(x - x_n)dxdy'dx' \tag{2.19}$$

where l_b is the length of the basis function in the x-direction and g^{ej}_{xx} is the xx-component of the Green's function. The forcing terms, as defined in equation (2.12) can be written as:

$$v_{xn} = \frac{v_m}{\delta} \int_{-\infty}^{\infty} \text{rect}_\delta(x - x_m) b^*_{n,x}(x - x_n) dx \,. \tag{2.20}$$

where v_m are the complex excitation voltages .

2.1.2 MoM in the spectral domain

Another way to calculate the unknown coefficients $\boldsymbol{i}$ is to rewrite the equations in the spectral domain. It will be shown that the amount of integrals needed to be calculated is reduced from three to two or even one for most cases.

Using the spectral representation of the xx-component of the free-space Green's function it is known that:

$$g^{ej}_{xx}(\boldsymbol{r} - \boldsymbol{r}') = j\frac{\zeta}{k_0}\frac{1}{(2\pi)^3} \int_{-\infty}^{\infty}\int_{-\infty}^{\infty}\int_{-\infty}^{\infty} \left(k_0^2 - k_x^2\right) \frac{e^{-jk_x(x-x')} e^{-jk_y(y-y')} e^{-jk_z(z-z')}}{k_0^2 - k_x^2 - k_y^2 - k_z^2} dk_x dk_y dk_z \,. \tag{2.21}$$

In appendix C it is shown that, applying the Residue theorem:

$$\int_{-\infty}^{\infty} \frac{e^{-jk_z(z-z')}}{k_0^2 - k_x^2 - k_y^2 - k_z^2} dk_z = \pi j \frac{e^{-j\sqrt{k_0^2 - k_x^2 - k_y^2}|z-z'|}}{\sqrt{k_0^2 - k_x^2 - k_y^2}} \,. \tag{2.22}$$

Substituting equations (2.21) and (2.22) into equation (2.19) gives the following expression for the mutual impedance:

$$\begin{aligned} Z_{xnxn'} = \int_{x_{n'}-\frac{l_b}{2}}^{x_{n'}+\frac{l_b}{2}} \int_{-\frac{w}{2}}^{\frac{w}{2}} \int_{x_n-\frac{l_b}{2}}^{x_n+\frac{l_b}{2}} b_{n',x}(x' - x_{n'}) b^*_{n,x}(x - x_n) j_t(y') \frac{\zeta}{k_0}\frac{1}{8\pi^2} \int_{-\infty}^{\infty}\int_{-\infty}^{\infty} \left(k_0^2 - k_x^2\right) \\ \frac{e^{-jk_x(x-x')} e^{jk_y(y')} e^{-j\sqrt{k_0^2 - k_x^2 - k_y^2}|z_n - z_{n'}|}}{\sqrt{k_0^2 - k_x^2 - k_y^2}} dk_x dk_y dx dy' dx' \,. \end{aligned} \tag{2.23}$$

From equation (2.23) the integral in x' can be extracted and evaluated:

$$\begin{aligned} &\int_{x_{n'}-\frac{l_b}{2}}^{x_{n'}+\frac{l_b}{2}} b_{n',x}(x' - x_{n'}) e^{jk_x x'} dx' \\ &= \int_{-\frac{l_b}{2}}^{\frac{l_b}{2}} b_{n',x}(u) e^{jk_x u} du \, e^{jk_x x_{n'}} \\ &= B_{n',x}(k_x) e^{jk_x x_{n'}} \end{aligned} \tag{2.24}$$

where the change of variables $u = x' - x_{n'}$ is used to center the basis function around the origin. $B_{n'}(k_x)$ can be recognized to be the Fourier transform of the basis function. The exponential,

$e^{jk_x x_{n'}}$, represents the phase shift due to the displacement of the basis function from the origin. Similar steps can be performed for the integrals in y' and in x to obtain:

$$J_t(k_y) = \int_{-\frac{w}{2}}^{\frac{w}{2}} j_t(y') e^{jk_y y'} dy' = J_0\left(\frac{k_y w}{2}\right) \tag{2.25}$$

and

$$B^*_{n,x}(-k_x) e^{-jk_x x_n} = \int_{x_n - \frac{l_b}{2}}^{x_n + \frac{l_b}{2}} b^*_{n,x}(x - x_n) e^{-jk_x x} dx \tag{2.26}$$

where $J_t(k_y)$ is the Fourier transforms of $j_t(y')$ and J_0 is the zeroth order Bessel function. Substituting the Fourier transforms of the basis functions found in equations (2.24), (2.25) and (2.26) into equation (2.23) the expression for the active impedance in the spectral domain is found.

$$Z_{xnxn'} = -\frac{1}{2\pi} \int_{-\infty}^{\infty} B_{n',x}(k_x) B^*_{n,x}(-k_x) D_{nn'}(k_x) e^{-jk_x(x_n - x_{n'})} dk_x \tag{2.27}$$

where $D_{nn'}(k_x) = \frac{1}{2\pi} \int_{-\infty}^{\infty} J_t(k_y) G^{ej}_{xx}(k_x, k_y) e^{-j\sqrt{k_0^2 - k_x^2 - k_y^2}|z_n - z_{n'}|} dk_y$ and

$G^{ej}_{xx}(k_x, k_y) = -\frac{\zeta}{2k_0} \frac{\left(k_0^2 - k_x^2\right)}{\sqrt{k_0^2 - k_x^2 - k_y^2}}$. It is shown in appendix C that the integral in k_y can be solved analytically when $|z_n - z_{n'}| = 0$ or when $|z_n - z_{n'}| \gg w$, resulting in only one integral to be calculated:
If $|z_n - z_{n'}| = 0$

$$D_{nn'}(k_x) = -\frac{\zeta}{4k_0} \left(k_0^2 - k_x^2\right) J_0\left(\sqrt{k_0^2 - k_x^2}\frac{w}{4}\right) H_0^{(2)}\left(\sqrt{k_0^2 - k_x^2}\frac{w}{4}\right) \tag{2.28}$$

If $|z_n - z_{n'}| \gg w$

$$D_{nn'}(k_x) \approx -\frac{\zeta}{4k_0} \left(k_0^2 - k_x^2\right) H_0^{(2)}\left(\sqrt{k_0^2 - k_x^2}|z_n - z_{n'}|\right) . \tag{2.29}$$

Besides the active impedance, also the forcing terms, as found in equation (2.20), can be expressed in the spectral domain:

$$\begin{aligned} v_{xn} &= \int_{x_n - \frac{l_b}{2}}^{x_n + \frac{l_b}{2}} \frac{v_m}{\delta} \operatorname{rect}_\delta(x - x_m) b^*_n(x - x_n) dx \\ &= \int_{x_n - \frac{l_b}{2}}^{x_n + \frac{l_b}{2}} \frac{v_m}{\delta} \left(\frac{1}{2\pi} \int_{-\infty}^{\infty} \delta \operatorname{sinc}\left(\frac{k_x \delta}{2}\right) e^{-jk_x(x - x_m)} dk_x \right) b^*_n(x - x_n) dx . \end{aligned} \tag{2.30}$$

An expression similar to equation (2.26) can be recognized. Therefore the voltage can be written in the spectral domain as:

$$v_{xn} = \frac{v_m}{2\pi} \int_{-\infty}^{\infty} \operatorname{sinc}\left(\frac{k_x \delta}{2}\right) B^*_{n,x}(-k_x) e^{-jk_x(x_n - x_m)} dk_x \tag{2.31}$$

The results presented throughout this thesis are calculated using the spectral representation of the method of moments, because of the closed-form solutions in (2.28) and (2.29), and because this representation, for planar dipoles, can be easily generalized to stratified media.

2.1.3 Radiation pattern

This section will describe how the far field pattern can be found once the current vector $\boldsymbol{i}$ has been calculated. One can imagine a sphere with radius r centered in the origin. Every point on the surface of this sphere can be expressed in terms of two angles: the elevation angle θ and the azimuthal angle ϕ, where $\theta = 0$ is along the positive z-axis and $\phi = 0$ is along the positive x-axis. Every point on the surface of this sphere can be expressed in Cartesian coordinates as:

$$\begin{aligned} x &= r\sin\theta\cos\phi \\ y &= r\sin\theta\sin\phi \\ z &= r\cos\theta\,. \end{aligned} \tag{2.32}$$

The electric field due to an electric current source can be found in any point $\boldsymbol{r}$ by calculating the convolution between the equivalent current, $\boldsymbol{j}_{eq}$, and the dyadic Green's function, $\boldsymbol{g}^{ej}$, evaluated in the point (x, y, z). Since convolution in the spatial domain is equivalent to multiplication in the spectral domain the electric field can be found as:

$$\boldsymbol{E}(x,y,z) = \frac{1}{(2\pi r)^2}\int_{-\infty}^{\infty}\int_{-\infty}^{\infty}\boldsymbol{J}_{eq}(k_x,k_y)\boldsymbol{G}^{ej}(k_x,k_y,z,z')e^{-jk_x x}e^{-jk_y y}dk_x dk_y\,. \tag{2.33}$$

As shown in section 2.1.2 the equivalent current distribution of dipoles oriented along x, can be expressed as:

$$\boldsymbol{J}_{eq}(k_x,k_y) = i_{n'}B_{n'}(k_x)J_t(k_y)\hat{\boldsymbol{x}}\,. \tag{2.34}$$

The total electric field due to all basis functions can be expressed as the sum of the individual contributions from every basis function. The total electric field in (x_0, y_0, z_0) due to a current centered in $(z_{n'}, y_{n'}, z_{n'})$ can be found, by applying the stationary phase point approximation, as:

$$\begin{aligned} \boldsymbol{E}(x_0,y_0,z_0) \approx jk_{z0}\frac{1}{2\pi r}\sum_{n'=1}^{N} & i_{n'}B_{n'}(k_{x0})J_t(k_{y0})\hat{\boldsymbol{x}}\boldsymbol{G}^{ej}(k_{x0},k_{y0}) \\ & e^{-jk_{x0}(x_0-x_{n'})}e^{-jk_{y0}(y_0-y_{n'})}e^{-jk_{z0}(z_0-z_{n'})}\,. \end{aligned} \tag{2.35}$$

From the electric field strength the radiation intensity can be found as:

$$U(\theta,\phi) = r^2\frac{1}{2\zeta}\left(|E_\theta|^2 + |E_\phi|^2\right) \tag{2.36}$$

where $E_\theta = E_x\cos\theta\cos\phi + E_y\cos\theta\sin\phi - E_z\sin\theta$ and $E_\phi = -E_x\sin\phi + E_y\cos\phi$ are the θ- and ϕ-components of the electric field, and ζ is the free-space impedance. The directivity is defined as the ratio of the radiation intensity in a direction (θ, ϕ) to the radiation intensity of an isotropic antenna radiating the same amount of power. The radiation intensity of an isotropic antenna is $U_0 = P_{rad}/4\pi$, where P_{rad} is the total radiated power and can be found by integrating the radiation intensity over the entire sphere:

$$P_{rad} = \int_0^{2\pi}\int_0^{\pi} U(\theta,\phi)\sin\theta d\theta d\phi\,. \tag{2.37}$$

The directivity in every direction θ, ϕ is therefore:

$$D(\theta,\phi) = \frac{U(\theta,\phi)}{U_0} = 4\pi\frac{U(\theta,\phi)}{P_{rad}} \tag{2.38}$$

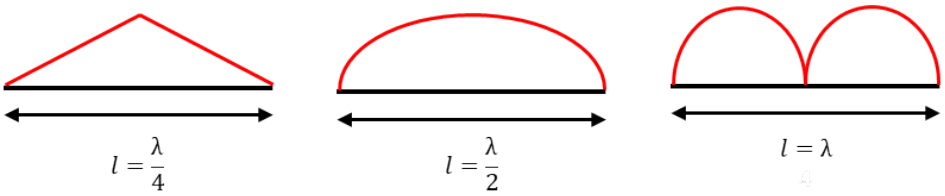

(a) (b) (c)

Figure 2.4: Current distribution on dipoles with finite length. a) $l = \frac{\lambda}{4}$. b) $l = \frac{\lambda}{2}$. c) $l = \lambda$

.

2.2 Entire domain basis functions

In the calculations of the previous sections a certain basis function, $b_{n',x}(x - x_{n'})$, is used to describe the equivalent current distribution over the dipole. The basis function is chosen in such a way that it resembles the current distribution over a dipole. Since the shape of the equivalent current distribution is known to be triangular for electrically short dipoles and sinusoidal for resonant dipoles, it is possible to define only one basis function on the entire dipole (entire domain basis function).

Figure 2.4 shows three dipoles with different length oriented along x and the expected current distribution [10]. The current distribution can be written as $i(x - x_{n'}) = i_{n'} b_{n',x}(x - x_{n'})$, where $i_{n'}$ is a certain weighting factor, l is the length of the dipole and $x_{n'}$ is the x-coordinate of the center of the dipole. The basis function is chosen to be piecewise sinusoidal, thus defined as:

$$b_{n',x}(x - x_{n'}) = \frac{\sin\left(k_0\left(\frac{l}{2} - |x - x_{n'}|\right)\right)}{\sin\left(k_0 \frac{l}{2}\right)} \operatorname{rect}_l(x - x_{n'}) \tag{2.39}$$

or in the spectral domain:

$$\begin{aligned} B_{n',x}(k_x) &= \int_{-\infty}^{\infty} \frac{\sin\left(k_0\left(\frac{l}{2} - |x - x_{n'}|\right)\right)}{\sin\left(k_0 \frac{l}{2}\right)} \operatorname{rect}_l(x - x_{n'}) e^{jk_x x} dx \\ &= \frac{2k_0\left(\cos\left(\frac{k_x l}{2}\right) - \cos\left(\frac{k_0 l}{2}\right)\right)}{(k_0^2 - k_x^2)\sin\left(k_0 \frac{l}{2}\right)} . \end{aligned} \tag{2.40}$$

The projection of the electric field in the gap on the basis function can be expressed as

$$p_n = \frac{1}{\delta} \int_{-\infty}^{\infty} \operatorname{rect}_\delta(x - x_m) b^*_{n,x}(x - x_n) dx \approx \begin{cases} 0 & \text{if } x_n \neq x_m \\ 1 & \text{if } x_n = x_m \end{cases} \tag{2.41}$$

where it is assumed that the gap size is small compared to the total length of the dipole. Therefore, the matrix $\boldsymbol{P}$ in equation (2.14) becomes the identity matrix.

2.2.1 Validation of impedances and current

As described in section 2.1 the method of moments is based on the calculation of the impedances of the dipoles and the mutual impedance between dipoles. These impedances are stored in a matrix which must be inverted and multiplied by the forcing term $\boldsymbol{v}$, in order to find the current weighting vector $\boldsymbol{i}$. If an entire domain basis function is used to approximate the current

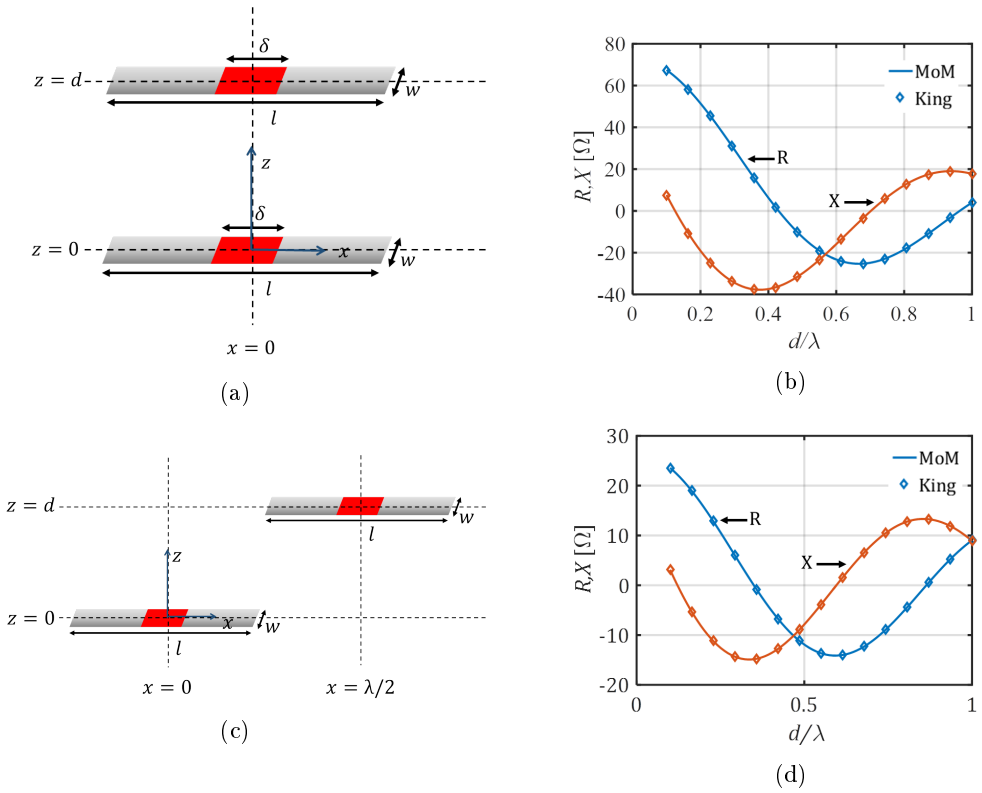

Figure 2.5: Comparison of the calculated mutual impedance between two dipoles. a) Two half-wavelength dipoles centered around $x = 0$ and displaced in the z-direction by a distance d. b) Mutual impedance between the two dipoles as a function of distance d. c) Two half-wavelength dipoles displaced in the x-direction by a distance of $\frac{\lambda}{2}$ and in the z-direction by a distance d. d) Mutual impedance between the two dipoles as a function of distance d.

distribution on the dipoles, this matrix will consist of $M \times M$ elements, where M is the number of dipoles.

In order to verify the values calculated for the mutual impedances, the results from the Matlab code of the method of moments is compared to the results found by the analytical expression for parallel dipoles in free space given in [11]. Two examples are presented in figure 2.5, comparing both methods. Figure 2.5a shows two dipoles with length $l = \frac{\lambda}{2}$ and width $w = \frac{\lambda}{10}$. Both dipoles are centered around the line $x = 0$ and the distance between them in the z-directions is varied from $z = \frac{\lambda}{10}$ to $z = \lambda$. The real part of the impedance R and the imaginary part X are shown in figure 2.5b. It can be seen that the values calculated using the two methods perfectly overlap. Figure 2.5c shows the same two dipoles however displaced in the x-direction by a distance of $\frac{\lambda}{2}$. As shown in figure 2.5d, again a perfect agreement is found.

Let us now consider a finite number of dipoles oriented along x as shown in figure 2.6. The figure shows four dipoles, however any finite amount of dipoles oriented along x can be considered. Let us consider four identical dipoles with length $l_1 = l_2 = l_3 = l_4 = \frac{\lambda}{2}$, width $w = 0.1\lambda$, port length $\delta = 0.1\lambda$ and port impedance $z_0 = 50\,\Omega$. The first dipole is located in the origin, $x_1 = 0, z_1 = 0$. The other dipoles are displaced in x and z such that $x_2 = \frac{\lambda}{2}, z_2 = \frac{\lambda}{2}$, $x_3 = \lambda, z_3 = \frac{\lambda}{4}$ and $x_4 = \frac{3\lambda}{2}, z_4 = -\frac{\lambda}{2}$. Calculating the impedances gives the following impedance

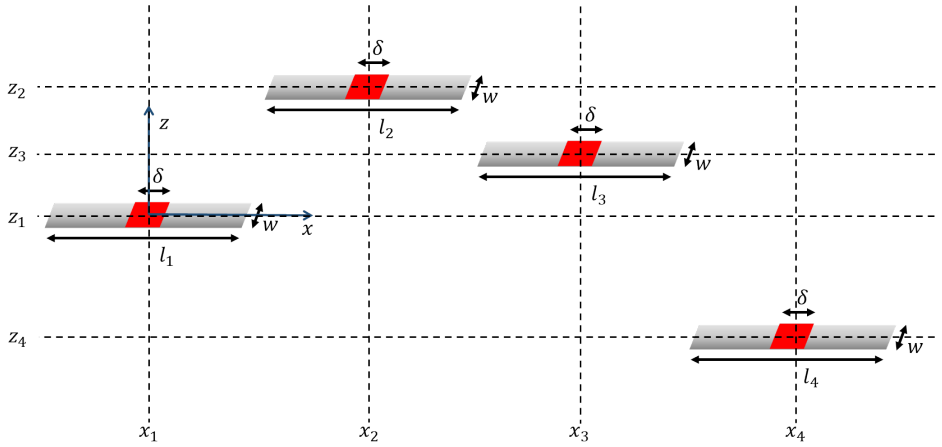

Figure 2.6: Four dipoles with lengths l_1, l_2, l_3 and l_4 and width w oriented along x, centered at $y = 0$ displaced in x and z. The excitation ports have a length δ.

matrix:

$$\boldsymbol{Z} = \begin{bmatrix} 72.7 + 30.9j & -11.9 - 7.9j & -3.8 + 1.1j & 1.1 - 1.4j \\ -11.9 - 7.9j & 72.7 + 30.9j & 10.6 - 12.5j & 4.1 - 4.2j \\ -3.8 + 1.1j & 10.6 - 12.5j & 72.7 + 30.9j & -8.4 + 10.8j \\ 1.1 - 1.4j & 4.1 - 4.2j & -8.4 + 10.8j & 72.7 + 30.9j \end{bmatrix} \Omega$$

It can be seen that all four of the self impedances are the same, since the four dipoles are identical. Also the matrix is symmetrical around the diagonal due to the reciprocity as explained in appendix A. Comparing the values of the mutual impedances to the values found using the analytical expressions from [11] one finds that they are equal. However, the values for the impedances are different from the values found in CST. This can be explained by noting that the impedances calculated using an entire domain basis function are calculated over the entire dipole, while CST calculates the active impedance by integrating the current only over the port of the dipole. Therefore the sinusoidal approximation for the current distribution fails to describe the real current, especially the reactive energy associated with the feeding gap. However, the radiation patterns can be still calculated accurately with this approximation.

The current distribution on the dipoles are of the same shape as the sinusoidal expression of equation (2.39) multiplied by a complex weight factor $i_{n'}$. The real and imaginary parts of the normalized current on the dipole located in the origin are shown in figure 2.7.

2.2.2 Validation of radiation patterns

Once the current vector $\boldsymbol{i}$ is calculated the radiation pattern of the dipoles can be calculated using the method described in section 2.1.3. In this section the same four dipoles are considered as in section 2.2.1, which are shown in figure 2.6. Figure 2.8a shows the radiation pattern in the plane $\phi = 0$ of the four dipoles without a phase difference in the excitation between the dipoles. A good match with CST is found. Figure 2.8b shows the radiation pattern for the case where only the first and the third dipole are excited while the second and the fourth dipole are passive ($v_2 = v_4 = 0$). Again a good agreement is found between CST and the Matlab simulation.

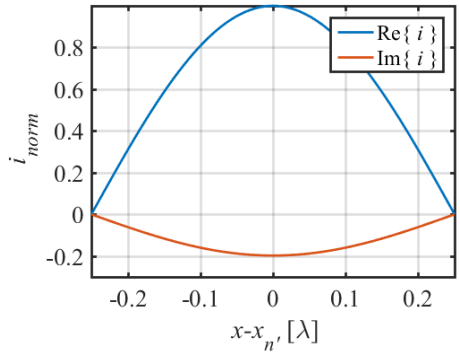

Figure 2.7: The normalized current calculated using an entire domain basis function on the half wavelength dipole located in the origin.

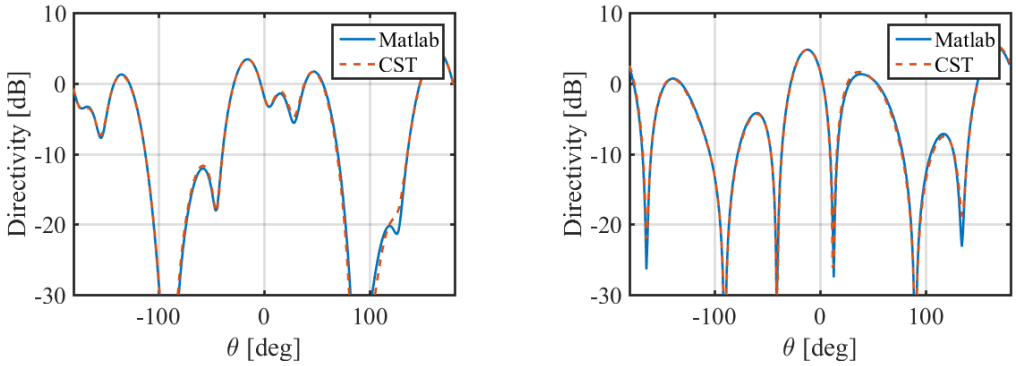

Figure 2.8: Radiation patterns in the $\phi = 0$-plane of the four dipoles as shown in figure 2.6 calculated using the Method of Moments using entire domain basis functions compared to CST for four different cases: a) all four dipoles are active and there is no phase difference between the dipoles. b) only the first and the third dipole are active and there is no phase difference between the dipoles.

2.3 Subdomain basis functions

In the previous section a sinusoidal entire domain basis function was used. Although this basis function describes well the real part of current distribution, for more generic current distributions and to account for the reactance of the feed, a larger number of basis functions defined on smaller domains can be employed. This section focuses on piecewise linear sub-domain basis functions. On every subdomain with a length l_t, a triangular basis function is placed, as is shown in figure 2.9. The weighted sum of all triangles will describe the current distribution over the dipole:

$$i(x) = \sum_{n'=1}^{N} i_{n'} b_{n',x}(x - x_{n'}) \tag{2.42}$$

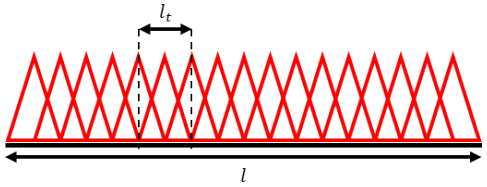

Figure 2.9: Piecewise sinusoidal subdomain basis functions.

where N is the total number of triangles, $i_{n'}$ is a weighting factor and $x_{n'}$ is the x-coordinate of the center of the subdomain. The basis functions $b_{n',x}$ are triangular, i.e.:

$$b_{n',x}(x - x_{n'}) = \left(1 - |x - x_{n'}| \frac{2}{l_t}\right) \mathrm{rect}_{l_t}(x - x_{n'}) \tag{2.43}$$

or in the spectral domain:

$$\begin{aligned} B_{n',x}(k_x) &= \int_{-\infty}^{\infty} \left(1 - |x - x_{n'}| \frac{2}{l_t}\right) \mathrm{rect}_{l_t}(x - x_{n'}) e^{jk_x x} dx \\ &= \frac{l_t}{2} \mathrm{sinc}^2\left(\frac{k_x l_t}{4}\right). \end{aligned} \tag{2.44}$$

For small domain basis functions, the terms p_n can be expressed as:

$$p_n = \frac{1}{\delta} \int_{-\infty}^{\infty} \mathrm{rect}_{\delta}(x - x_m) b^*_{n,x}(x - x_n) dx = \begin{cases} 0 & \text{if } n^{th} \text{ basis function and } m^{th} \text{ gap do not overlap} \\ c_n & \text{if } n^{th} \text{ basis function and } m^{th} \text{ gap do overlap} \end{cases} \tag{2.45}$$

where it is assumed that the gap size is small compared to the total length of the dipole and c_n is a constant indicating the fraction of the area of the triangular basis function that overlaps with the gap.

2.3.1 Validation of impedances and current

The impedance matrix calculated using a subdomain basis function will consist of $N \times N$ elements. The voltage vector $\boldsymbol{v}$ and the port impedance matrix $z_0\boldsymbol{P}$ are different from 0, only for the subdomains which lie in the dipole feed region. The sum of the elements of $z_0\boldsymbol{P}$ corresponding to the same port is equal to the port impedance z_0. Let us consider a single dipole located in the origin. The dipole is identical to the dipoles described in section 2.2.1, with length $l = \frac{\lambda}{2}$, width $w = 0.1\lambda$, port length $\delta = 0.1\lambda$ and port impedance $z_0 = 50\,\Omega$. The number of subdomains on the dipole is chosen to be 37. The input impedance of the dipole is found as:

$$Z_{in} = \sum_{n=1}^{N} \frac{v_n}{i_n} - z_0 \tag{2.46}$$

where v_n and i_n are the weights of the voltage and the current for the n^{th}-triangle. Since $\boldsymbol{v}$ is 0 everywhere, except for the triangles which lie in the port, the active impedance is in this case calculated only on the port which is similar to the way CST calculates the impedance. The

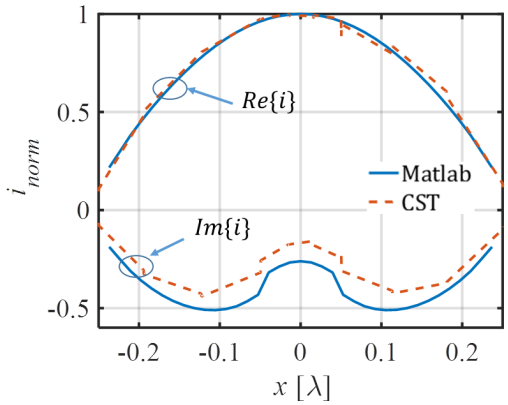

Figure 2.10: The normalized current along a dipole on the half wavelength dipole located in the origin exported from CST compared to the current calculated using a piece wise linear subdomain basis function in Matlab.

impedances calculated with the developed code and CST are:

$$Z_{in,MoM} = (105.2 + 30.5\text{j})\,\Omega$$
$$Z_{in,CST} = (106.9 + 35.1\text{j})\,\Omega$$

As expected, their values are very similar.

Figure 2.10 shows the normalized current on the dipole exported from CST and calculated using Matlab. It can be seen that the real part of the current shows a sinusoidal behaviour while the imaginary part of the current behaves differently in the port of the dipole. The current calculated in Matlab is very similar to the current exported from CST.

2.3.2 Validation of radiation patterns

Let us consider the same four dipoles as in section 2.2.1, with length $l_1 = l_2 = l_3 = l_4 = \frac{\lambda}{2}$, width $w = 0.1\lambda$, port length $\delta = 0.1\lambda$ and port impedance $z_0 = 50\,\Omega$. The first dipole is located in the origin, $x_1 = 0, z_1 = 0$. The other dipoles are displaced in x and z such that $x_2 = \frac{\lambda}{2}, z_2 = \frac{\lambda}{2}$, $x_3 = \lambda, z_3 = \frac{\lambda}{4}$ and $x_4 = \frac{3\lambda}{2}, z_4 = -\frac{\lambda}{2}$. The number of subdomains on every dipole is chosen to be 37. Figure 2.11a shows the radiation pattern in the plane $\phi = 0$ of the four dipoles without a phase difference between the dipoles. A good match with CST is found. Figure 2.11b shows the radiation pattern for the case where only the first and the third dipole are excited while the second and the fourth dipole are passive ($v_2 = v_4 = 0$). Again a good agreement is found between CST and the Matlab simulation.

2.4 Conclusion

A method of moments code is implemented in order to calculate the radiation pattern of a finite number of dipoles in free space, oriented along x. The expressions for the mutual impedance and the forcing terms are found both in the spatial and the spectral domain. Two types of basis functions, an entire domain basis function and piecewise linear basis functions, are considered and implemented. The impedances calculated with the entire domain basis function correspond to the impedances found in [11]. The current distribution on the dipole consists of a complex current weighting factor multiplied by a sinusoidal basis function. The radiation patterns of

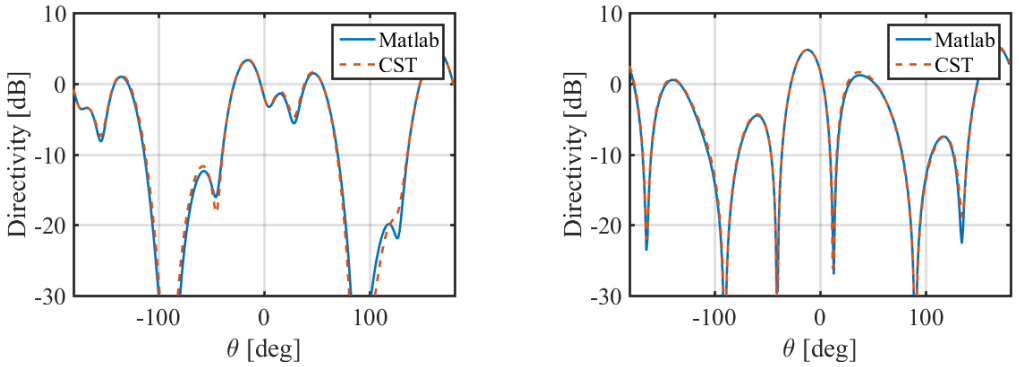

Figure 2.11: Radiation patterns in the plane $\phi = 0$ of the four dipoles as shown in figure 2.6 calculated using the method of moments using subdomain basis functions compared to CST for two different cases: a) all four dipoles are active. b) only the first and the third dipole are active.

.

multiple dipoles while all are active or when some are passive are calculated. Both patterns show a good agreement with CST.

When the piecewise linear basis function is used the self impedance calculated in Matlab is similar to the impedance found using CST. The current distribution along x shows a good agreement with CST and the radiation patterns for the same two cases of excitation are again a good match.

Chapter 3

MoM for arrays of non-parallel dipoles

This chapter describes the implementation of a method of moments code for non-parallel dipoles. First dipoles oriented along x and z will be discussed. Hereafter the dipoles will be skewed with respect to each other by an arbitrary angle. The ability to simulate dipoles which are placed under a skew angle with respect to each other allows to investigate the radiation properties of tilted elements above a ground plane. From the image theorem it is known that an electric current source in the vicinity of an infinite ground plane may be represented as the original current and its image. The image is equal in amplitude to the original current. The orientation of the image is such that the component normal to the ground plane is the same, while the tangential component changes sign. The distance between the image and the ground plane is equal to the distance between the original current and the ground plane. An electric current above an infinite ground plane and the equivalent model found using the image theorem are shown in figure 3.1.

Appendix B describes an example showing that the equivalent model of figure 3.1 satisfies the boundary condition at the ground plane.

3.1 Dipoles oriented along x and z

3.1.1 Spatial domain expressions

Chapter 2 describes the derivation of the method of moments expressions for dipoles oriented along x. When dipoles along z are added, the expressions become longer, but most of the steps are very similar. A complete derivation of all expressions can be found in appendix C. This sections describes the most important differences between the expressions found for dipoles along x and the expressions for dipoles along both x and z.

First the boundary conditions for the electric field on a perfect electric conductor are written separately for dipoles along x and z:

$$\begin{aligned} -\hat{\boldsymbol{z}} \times \boldsymbol{e}_{scat} + z_0 \boldsymbol{j}_x &= \hat{\boldsymbol{z}} \times \boldsymbol{e}_{inc} \\ -\hat{\boldsymbol{x}} \times \boldsymbol{e}_{scat} + z_0 \boldsymbol{j}_z &= \hat{\boldsymbol{x}} \times \boldsymbol{e}_{inc} \end{aligned} \tag{3.1}$$

The equivalent current along x and z are written as an unknown weighting terms $i_{n'_x}$ and $i_{n'_z}$ multiplied by known basis functions $\boldsymbol{b}_{n'_x}$ and $\boldsymbol{b}_{n'_z}$. Once the weighting terms $i_{n'_x}$ and $i_{n'_z}$ are

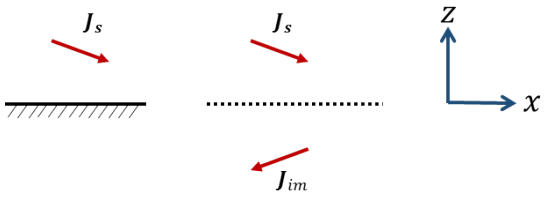

Figure 3.1: Original problem consisting of an electric current above a ground plane and its equivalent problem consisting of the current and its image.

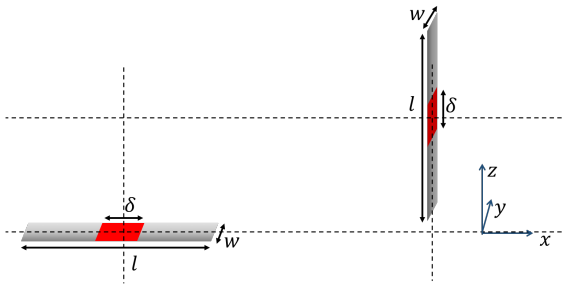

Figure 3.2: Two identical dipoles with length l and width w oriented along x and z, centered at $y = 0$ displaced in x and z. The excitation port has a length δ.

calculated the current distributions over the dipoles are known. Rewritting the scattered field as the convolution between the Green's function and the equivalent current gives:

$$\begin{aligned}
-\hat{\boldsymbol{z}} \times \int_{-\infty}^{\infty}\int_{-\infty}^{\infty}\int_{-\infty}^{\infty} \left(\sum_{n'_x=1}^{N_x} i_{n'_x} \boldsymbol{b}_{n'_x}(\boldsymbol{r}')\hat{\boldsymbol{x}} + \sum_{n',z=1}^{N_z} i_{n'_z} \boldsymbol{b}_{n'_z}(\boldsymbol{r}')\hat{\boldsymbol{z}} \right) \boldsymbol{g}^{ej}(\boldsymbol{r},\boldsymbol{r}')d\boldsymbol{r}' + z_0 \boldsymbol{j}_x(\boldsymbol{r}) = \hat{\boldsymbol{z}} \times \boldsymbol{e}_{inc}(\boldsymbol{r}) \\
-\hat{\boldsymbol{x}} \times \int_{-\infty}^{\infty}\int_{-\infty}^{\infty}\int_{-\infty}^{\infty} \left(\sum_{n'_x=1}^{N_x} i_{n'_x} \boldsymbol{b}_{n'_x}(\boldsymbol{r}')\hat{\boldsymbol{x}} + \sum_{n'_z=1}^{N_z} i_{n'_z} \boldsymbol{b}_{n'_z}(\boldsymbol{r}')\hat{\boldsymbol{z}} \right) \boldsymbol{g}^{ej}(\boldsymbol{r},\boldsymbol{r}')d\boldsymbol{r}' + z_0 \boldsymbol{j}_z(\boldsymbol{r}) = \hat{\boldsymbol{x}} \times \boldsymbol{e}_{inc}(\boldsymbol{r})\,.
\end{aligned} \tag{3.2}$$

Note that the equations are coupled via $i_{n'_x}$ and $i_{n'_z}$, representing the coupling between basis functions oriented along x and along z.

Let us consider a finite number of infinitely thin dipoles oriented along x and z. The elements are placed along the y-axis and can be displaced in x and z. Figure 3.2 shows an example of such an array consisting of two elements. We define x_{n_x}, z_{n_x}, $x_{n'_x}$, $z_{n'_x}$ to be the x- and z-coordinates of the center of the observation domain and the center of the source domain for dipoles along x. In a similar way x_{n_z}, z_{n_z}, $x_{n'_z}$, $z_{n'_z}$ to be the x- and z-coordinates of the center of the observation domain and the center of the source domain for dipoles along z.

The equivalent current will be oriented along the dipole. The basis functions can thus be written as:

$$\begin{aligned}
\boldsymbol{b}_{n'_x}(\boldsymbol{r}') &= b_{n'_x}(x' - x_{n'_x}) j_t(y') \delta(z' - z_{n'_x}) \hat{\boldsymbol{x}} \\
\boldsymbol{b}_{n'_z}(\boldsymbol{r}') &= b_{n'_z}(z' - z_{n'_z}) j_t(y') \delta(x' - x_{n'_z}) \hat{\boldsymbol{z}}
\end{aligned} \tag{3.3}$$

where $j_t(y')$ is the same edge-singular distribution as found in equation (2.16). The test functions are chosen to be equal to the basis function in the longitudinal direction. The observation domain is chosen to be along the dipole axes, $y = 0$.

Substituting the expressions for the basis functions in equation (3.2), projecting both sides

on the test function and performing similar steps as in the case of the dipoles along x, four expressions for the active impedance are defined:

$$
\begin{aligned}
Z_{x_{n'_x},x_{n_x}} &= \int_{x_{n'_x}-\frac{l_b}{2}}^{x_{n'_x}+\frac{l_b}{2}} \int_{-\frac{w}{2}}^{\frac{w}{2}} \int_{x_{n_x}-\frac{l_b}{2}}^{x_{n_x}+\frac{l_b}{2}} b_{n'_x}(x'-x_{n'_x}) j_t(y') b^*_{n_x}(x-x_{n_x}) g^{ej}_{xx}(x-x', y', z_{n_x}-z_{n'_x}) dx dy' dx' \\
Z_{z_{n'_z},x_{n_x}} &= \int_{z_{n'_z}-\frac{l_b}{2}}^{z_{n'_z}+\frac{l_b}{2}} \int_{-\frac{w}{2}}^{\frac{w}{2}} \int_{x_{n_x}-\frac{l_b}{2}}^{x_{n_x}+\frac{l_b}{2}} b_{n'_z}(z'-z_{n'_z}) j_t(y') b^*_{n_x}(x-x_{n_x}) g^{ej}_{xz}(x-x_{n'_z}, y', z_{n_x}-z') dx dy' dz' \\
Z_{x_{n'_x},z_{n_z}} &= \int_{x_{n'_x}-\frac{l_b}{2}}^{x_{n'_x}+\frac{l_b}{2}} \int_{-\frac{w}{2}}^{\frac{w}{2}} \int_{z_{n_z}-\frac{l_b}{2}}^{z_{n_z}+\frac{l_b}{2}} b_{n'_x}(x'-x_{n'_x}) j_t(y') b^*_{n_z}(z-z_{n_z}) g^{ej}_{zx}(x_{n_z}-x', y', z-z_{n'_x}) dz dy' dx' \\
Z_{z_{n'_z},z_{n_z}} &= \int_{z_{n'_z}-\frac{l_b}{2}}^{z_{n'_z}+\frac{l_b}{2}} \int_{-\frac{w}{2}}^{\frac{w}{2}} \int_{z_{n_z}-\frac{l_b}{2}}^{z_{n_z}+\frac{l_b}{2}} b_{n'_z}(z'-z_{n'_z}) j_t(y') b^*_{n_z}(z-z_{n_z}) g^{ej}_{zz}(x_{n_z}-x_{n'_z}, y', z-z') dz dy' dz' .
\end{aligned}
\tag{3.4}
$$

The forcing terms on dipoles along x and z are defined as:

$$
\begin{aligned}
v_{xn} &= \frac{v_{m_x}}{\delta} \int_{x_{n_x}-\frac{l_b}{2}}^{x_{n_x}+\frac{l_b}{2}} \mathrm{rect}_\delta(x-x_{n_x}) b^*_{n_x}(x-x_{n_x}) dx \\
v_{zn} &= \frac{v_{m_z}}{\delta} \int_{z_{n_z}-\frac{l_b}{2}}^{z_{n_z}+\frac{l_b}{2}} \mathrm{rect}_\delta(z-z_{n_z}) b^*_{n_z}(z-z_{n_z}) dz
\end{aligned}
\tag{3.5}
$$

such that:

$$
\begin{aligned}
\sum_{n'_x=1}^{N_x} i_{n'_x} Z_{x_{n'_x},x_{n_x}} + \sum_{n'_z=1}^{N_z} i_{n'_z} Z_{z_{n'_z},x_{n_x}} + z_0 p_{nx} i_{n_x} &= v_{xn} \\
\sum_{n'_z=1}^{N_z} i_{n'_z} Z_{z_{n'_z},z_{n_z}} + \sum_{n'_x=1}^{N_x} i_{n'_x} Z_{x_{n'_x},z_{n_z}} + z_0 p_{nz} i_{n_z} &= v_{zn} .
\end{aligned}
\tag{3.6}
$$

Equation (3.6) can be written in matrix notation as:

$$
\left(\begin{bmatrix} \boldsymbol{Z}_{x'x} & \boldsymbol{Z}_{z'x} \\ \boldsymbol{Z}_{x'z} & \boldsymbol{Z}_{z'z} \end{bmatrix} + z_0 \begin{bmatrix} \boldsymbol{P}_x & \boldsymbol{0} \\ \boldsymbol{0} & \boldsymbol{P}_z \end{bmatrix} \right) \begin{bmatrix} \boldsymbol{i}_x \\ \boldsymbol{i}_z \end{bmatrix} = \begin{bmatrix} \boldsymbol{v}_x \\ \boldsymbol{v}_z \end{bmatrix}
\tag{3.7}
$$

where $\boldsymbol{Z}_{x'x}$ is a matrix containing the terms $Z_{x_{n'_x},x_{n_x}}$, $\boldsymbol{Z}_{z'x}$ is a matrix containing the terms $Z_{z_{n'_z},x_{n_x}}$, et cetera. $\boldsymbol{P}_x$ and $\boldsymbol{P}_z$ are diagonal matrices $\boldsymbol{P}_x = diag(p_{nx})$ and $\boldsymbol{P}_z = diag(p_{nz})$, whose terms are zero if if the n^{th} basis function is defined on the metal and different from zero if the basis function overlaps with the feeding gap region of a dipole along x or a dipole along z respectively.

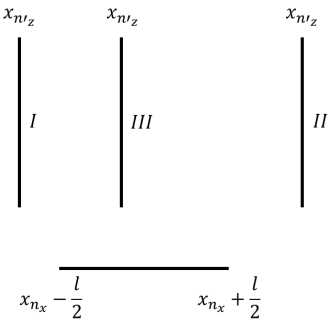

Figure 3.3: Three cases of for $|x_{n_x} - x_{n'_z}|$.

3.1.2 Spectral domain expressions

The spectral expressions for $Z_{x_{n'_x},x_{n_x}}$ and $Z_{z_{n'_z},z_{n_z}}$ can be found following the steps described in section 2.1.2. The derivations for $Z_{z_{n'_z},z_{n_z}}$ are very similar to that of $Z_{x_{n'_x},x_{n_x}}$ because the dipoles are assumed to be in free space. The expressions for the mutual impedance between a dipole along x and a dipole along z require more attention.

Let us first consider $Z_{z_{n'_z},x_{n_x}}$. Substituting the spectral expression for the xz-component of the Green's function:

$$g_{xz}^{ej}(\boldsymbol{r}-\boldsymbol{r}') = j\frac{\zeta}{k_0}\frac{1}{(2\pi)^3}\int_{-\infty}^{\infty}\int_{-\infty}^{\infty}\int_{-\infty}^{\infty}(-k_x k_z)\frac{e^{-jk_x(x-x')}e^{-jk_y(y-y')}e^{-jk_z(z-z')}}{k_0^2-k_x^2-k_y^2-k_z^2}dk_x dk_y dk_z \quad (3.8)$$

in the expression for $Z_{z_{n'_z},x_{n_x}}$ found in equation (3.4) and evaluating the integrals along z' and y' as the integrals in x' and y' in chapter 2 gives:

$$\begin{aligned} Z_{z_{n'_z},x_{n_x}} = j\frac{\zeta}{k_0}\frac{1}{(2\pi)^3}\int_{x_{n_x}-\frac{l_b}{2}}^{x_{n_x}+\frac{l_b}{2}} b_{n_x}^*(x-x_{n_x})\int_{-\infty}^{\infty}\int_{-\infty}^{\infty}\int_{-\infty}^{\infty}(-k_x k_z) \\ B_{n'_z}(k_z)J_t(k_y)\frac{e^{-jk_x(x-x_{n'_z})}e^{-jk_z(z_{n_x}-z_{n'_z})}}{k_0^2-k_x^2-k_y^2-k_z^2}dk_x dk_y dk_z dx\,. \end{aligned} \quad (3.9)$$

Three cases must be considered, as is shown in figure 3.3:

1. $x_{n'_z} < x_{n_x} - \frac{l_b}{2}$

2. $x_{n'_z} > x_{n_x} + \frac{l_b}{2}$

3. $x_{n_x} - \frac{l_b}{2} < x_{n'_z} < x_{n_x} + \frac{l_b}{2}$

Case I ($x_{n'_z} < x_{n_x} - \frac{l_b}{2}$)

Since $x - x_{n'_z} > 0$ for all x, the integration contour for the integration along k_x can be closed counter clockwise around $k_x = \sqrt{k_0^2 - k_y^2 - k_z^2}$.

$$\begin{aligned}
&\int_{-\infty}^{\infty} k_x \frac{e^{-jk_x(x-x_{n'_z})}}{k_0^2 - k_x^2 - k_y^2 - k_z^2} dk_x \\
&= -\int_{-\infty}^{\infty} k_x \frac{e^{-jk_x(x-x_{n'_z})}}{\left(k_x - \sqrt{k_0^2 - k_y^2 - k_z^2}\right)\left(k_x + \sqrt{k_0^2 - k_y^2 - k_x^2}\right)} dk_x \\
&= -2\pi j \sqrt{k_0^2 - k_y^2 - k_z^2} \frac{e^{-j\sqrt{k_0^2 - k_y^2 - k_z^2}(x-x_{n'_z})}}{2\sqrt{k_0^2 - k_y^2 - k_z^2}} \\
&= -\pi j e^{-j\sqrt{k_0^2 - k_y^2 - k_z^2}|x-x_{n'_z}|} .
\end{aligned} \tag{3.10}$$

The integral along x can now be solved to be:

$$\int_{x_{n_x} - \frac{l_b}{2}}^{x_{n_x} + \frac{l_b}{2}} b^*_{n_x}(x - x_{n_x}) e^{-j\sqrt{k_0^2 - k_y^2 - k_z^2}x} dx = B^*_{n_x}\left(-\sqrt{k_0^2 - k_y^2 - k_z^2}\right) e^{-j\sqrt{k_0^2 - k_y^2 - k_z^2}x_{n_x}} . \tag{3.11}$$

Substituting equations (3.10) and (3.11) into (3.9):

$$\begin{aligned}
Z_{z_{n'_z}, x_{n_x}} = -\frac{\zeta}{k_0}\frac{1}{8\pi^2} \int_{-\infty}^{\infty}\int_{-\infty}^{\infty} k_z \\
B_{n'_z}(k_z) J_t(k_y) B^*_{n_x}\left(-\sqrt{k_0^2 - k_y^2 - k_z^2}\right) \frac{e^{-j\sqrt{k_0^2 - k_y^2 - k_z^2}|x_{n_x} - x_{n'_z}|} e^{-jk_z(z_{n_x} - z_{n'_z})}}{k_0^2 - k_y^2 - k_z^2} dk_y dk_z .
\end{aligned} \tag{3.12}$$

Case II ($x_{n'_z} > x_{n_x} + \frac{l_b}{2}$)

Since $x - x_{n'_z} < 0$ for all x the integration contour for the integration along k_x can be closed clockwise around $k_x = -\sqrt{k_0^2 - k_y^2 - k_z^2}$.

$$\begin{aligned}
&\int_{-\infty}^{\infty} k_x \frac{e^{-jk_x(x-x_{n'_z})}}{k_0^2 - k_x^2 - k_y^2 - k_z^2} dk_x \\
&= -\int_{-\infty}^{\infty} k_x \frac{e^{-jk_x(x-x_{n'_z})}}{\left(k_x - \sqrt{k_0^2 - k_y^2 - k_z^2}\right)\left(k_x + \sqrt{k_0^2 - k_y^2 - k_x^2}\right)} dk_x \\
&= -2\pi j \sqrt{k_0^2 - k_y^2 - k_z^2} \frac{e^{j\sqrt{k_0^2 - k_y^2 - k_z^2}(x-x_{n'_z})}}{-2\sqrt{k_0^2 - k_y^2 - k_z^2}} \\
&= \pi j e^{-j\sqrt{k_0^2 - k_y^2 - k_z^2}|x-x_{n'_z}|} .
\end{aligned} \tag{3.13}$$

The integral along x can now be solved to be:

$$\int_{x_{n_x}-\frac{l_b}{2}}^{x_{n_x}+\frac{l_b}{2}} b^*_{n_x}(x-x_{n_x})e^{-j\sqrt{k_0^2-k_y^2-k_z^2}x}dx = B^*_{n_x}(-\sqrt{k_0^2-k_y^2-k_z^2})e^{-j\sqrt{k_0^2-k_y^2-k_z^2}x_{n_x}}\,. \tag{3.14}$$

Substituting equations (3.13) and (3.14) into (3.9):

$$Z_{z_{n'_z},x_{n_x}} = \frac{\zeta}{k_0}\frac{1}{8\pi^2}\int_{-\infty}^{\infty}\int_{-\infty}^{\infty} k_z \\ B_{n'_z}(k_z)J_t(k_y)B^*_{n_x}(-\sqrt{k_0^2-k_y^2-k_z^2})\frac{e^{-j\sqrt{k_0^2-k_y^2-k_z^2}|x_{n_x}-x_{n'_z}|}e^{-jk_z(z_{n_x}-z_{n'_z})}}{k_0^2-k_y^2-k_z^2}dk_ydk_z\,. \tag{3.15}$$

Case III ($x_{n_x}-\frac{l_b}{2} < x_{n'_z} < x_{n_x}+\frac{l_b}{2}$)

The integration domain along x is split in two: $x-x_{n'_z}>0$ and $x-x_{n'_z}<0$. The integral along k_x is closed counter clockwise for the values for x corresponding to $x-x_{n'_z}>0$ and clockwise for the values of x corresponding to $x-x_{n'_z}<0$ in the same way as shown for cases I and II. The integral along x is calculated in two parts:

$$\int_{x_{n_x}-\frac{l_b}{2}}^{x_{n_z}} b^*_{n_x}(x-x_{n_x})e^{-j\sqrt{k_0^2-k_y^2-k_z^2}x}dx \tag{3.16}$$

and

$$\int_{x_{n_z}}^{x_{n_x}+\frac{l_b}{2}} b^*_{n_x}(x-x_{n_x})e^{-j\sqrt{k_0^2-k_y^2-k_z^2}x}dx\,. \tag{3.17}$$

The expression for the active impedance $Z_{z_{n'_z},x_{n_x}}$ can now be found to be:

$$Z_{z_{n'_z},x_{n_x}} = \frac{\zeta}{k_0}\frac{1}{8\pi^2}\int_{-\infty}^{\infty}\int_{-\infty}^{\infty} B_{n'_z}(k_z)J_t(k_y)\Bigg(-k_z\int_{x_{n_x}-\frac{l_b}{2}}^{x_{n_z}} b^*_{n_x}(x-x_{n_x})e^{-j\sqrt{k_0^2-k_y^2-k_z^2}|x-x_{n'_z}|}dx \\ +k_z\int_{x_{n_z}}^{x_{n_x}+\frac{l_b}{2}} b^*_{n_x}(x-x_{n_x})e^{-j\sqrt{k_0^2-k_y^2-k_z^2}|x-x_{n'_z}|}dx\Bigg)\frac{e^{-jk_z(z_{n_x}-z_{n'_z})}}{k_0^2-k_y^2-k_z^2}dk_ydk_z\,. \tag{3.18}$$

The expressions for $Z_{x_{n'_x},z_{n_z}}$ are derived in a similar manner.

3.1.3 Validation of radiation patterns

Let us consider the four dipoles as shown in figure 3.4a. The dipoles are identical with $l=0.5\lambda$, $w=0.1\lambda$, port length $\delta=0.1\lambda$ and port impedance $z_0=50\,\Omega$. Figures 3.4b and 3.4c show the radiation patterns calculated using the method of moments code compared to CST for the cases when all dipoles are active and when only the first and the fourth are active ($v_2=v_3=0$). An

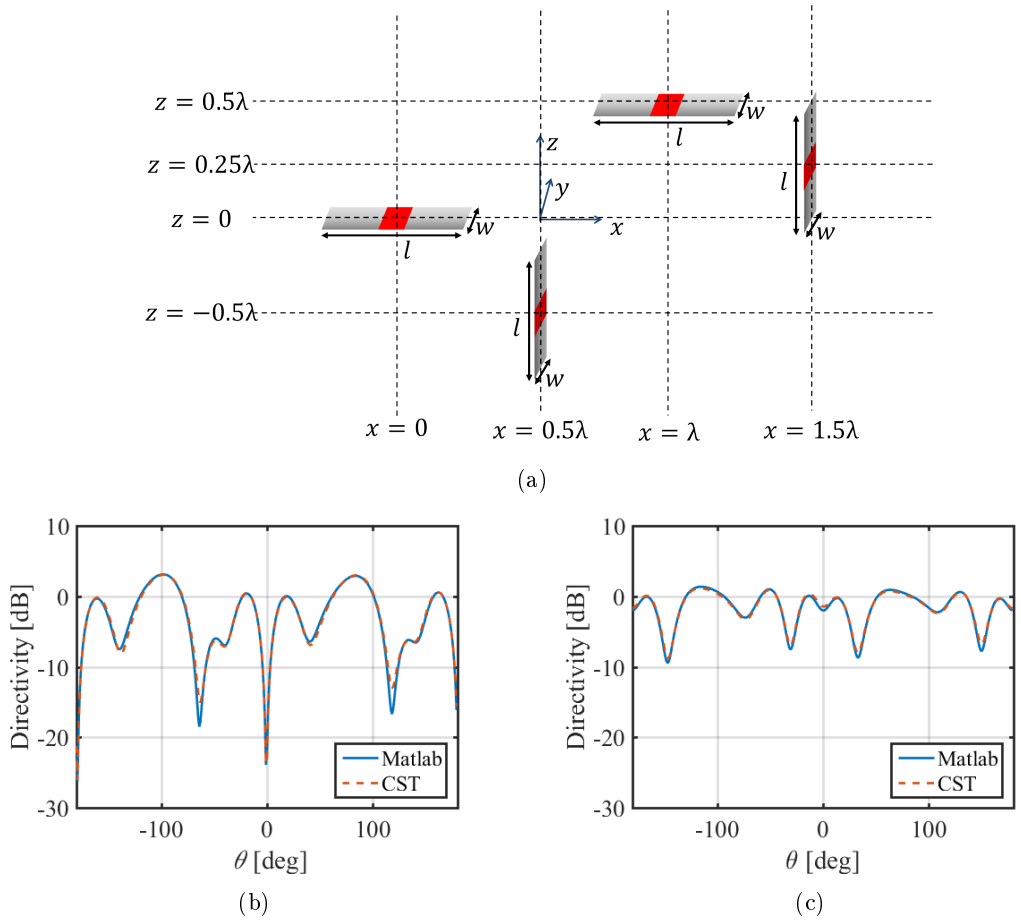

Figure 3.4: Radiation patterns in the $\phi = 0$-plane of four dipoles calculated using the Method of Moments using entire domain basis functions compared to CST. a) Geometry of the dipoles. b) Pattern when all four dipoles are active. c) Pattern when only the first and the fourth dipole are active.

entire domain basis function is used to approximate the current distribution along the dipoles. A good agreement is found.

Figure 3.5a shows two dipoles, one along x and one along z. It can be seen that the dipole along z is above the dipole along x, i.e. $x_{n_x} - \frac{l}{2} < x_{n'_z} < x_{n_x} + \frac{l}{2}$. The mutual impedance, $Z_{z_{n'_z}, x_{n_x}}$, between the dipoles is calculated using the equations from the third case as described in the previous section. Figure 3.5b shows the pattern calculated in Matlab compared to CST. A good agreement is found.

3.2 Dipoles with arbitrary skew angle

3.2.1 Mutual impedance

Let us consider dipoles skewed by an arbitrary angle above a ground plane. It is shown above that the dipoles above a ground plane can be represented using the image theorem as real dipoles and virtual dipoles or images. In order to be able to use the method of moments, the mutual

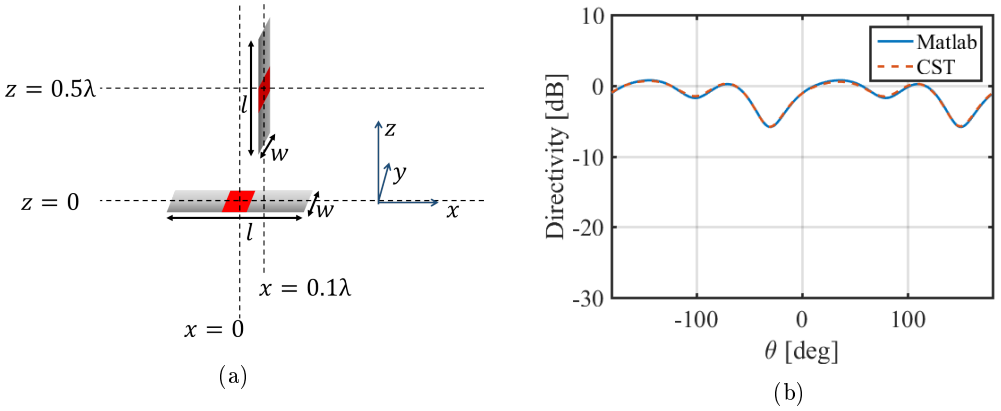

Figure 3.5: Two dipoles above each other. a) Geometry under consideration. b) Radiation pattern in the $\phi = 0$-plane.

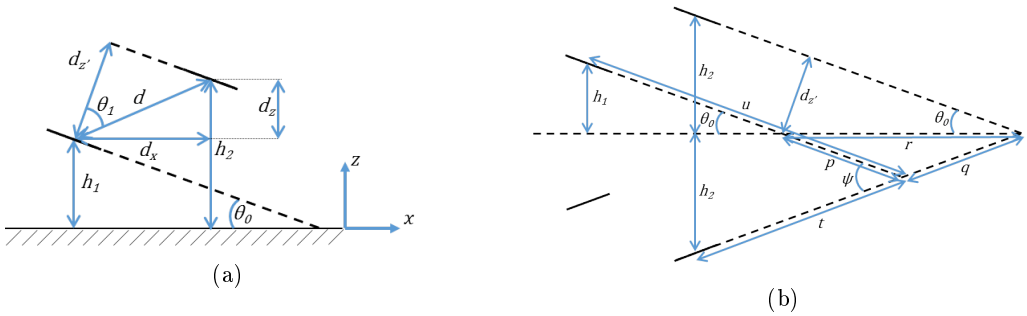

Figure 3.6: Two dipoles above a ground plane. a) Original system. b) Equivalent system with images.

impedance between dipoles and their images must be calculated. Since the dipoles and their images are skewed with respect to each other, the numerical method described in chapter 2 cannot be used. The mutual impedance between two dipoles of arbitrary length placed at an angle can be calculated analytically using the method described in [12]. Note that in [12] the reference system is defined in terms of z and t. In order to avoid confusion with the original xz-reference system in which the dipoles will be placed, the name of the z-axis in [12] will be changed to the u-axis.

Consider two dipoles above a ground plane as shown in figure 3.6a. The original problem is expressed as the equivalent problem shown in figure 3.6b. We decide the location of the dipoles in the xz-reference system, where the ground plane is in the xy-plane and z is oriented normal to the ground plane, as shown in figure 3.6a. Therefore h_1, h_2, θ_{elev} and d_x are known. From figure 3.6a it can be seen that $d_z = h_2 - h_1$. The distance between the dipoles, d, can be found using the Pythagorean theorem, $d = \sqrt{d_x^2 + d_z^2}$. d'_z is found to be $d'_z = \cos(\theta_1)d$, where $\theta_1 = 90 - \theta_{elev} - \arctan(\frac{d_z}{d_x})$.

The u- and t-coordinates can be found from figure 3.6b. First the length r is found as $r = \frac{d'_z}{\sin\theta_{elev}}$. Using the law of sines the lengths of p and q can be found to be $p = q = r\frac{\sin\theta_{elev}}{\sin(180-2\theta_{elev})}$. From here it can be seen that $u = \frac{h}{\sin\theta_{elev}} + p$ and $t = \frac{h_2}{\sin\theta_{elev}} - q$. The angle between the u- and t-axes $\psi = -2\theta_{elev}$. Performing all these steps leads to the final expressions for the u- and

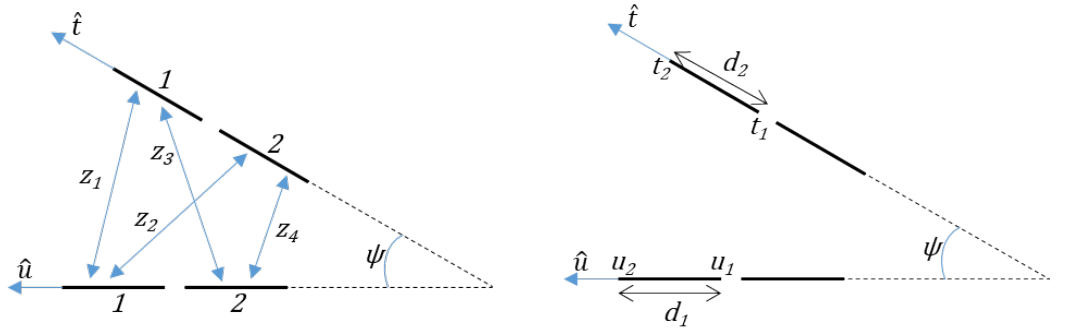

(a) (b)

Figure 3.7: Two dipoles, both split into two monopoles, placed at an angle ψ. a) The mutual impedances Z_1, Z_2, Z_3 and Z_4. b) ut-coordinates and monopole dimensions.

t-coordinates and the angle ψ as functions of known terms:

$$u = \frac{h}{\sin\theta_{elev}} + \frac{\cos(90-\theta_{elev}-\arctan(\frac{h_2-h_1}{d_x})\sqrt{d_x^2+(h_2-h_1)^2}}{\sin\theta_{elev}}\frac{\sin\theta_{elev}}{\sin(180-2\theta_{elev})} \tag{3.19}$$

$$t = \frac{h_2}{\sin\theta_{elev}} - \frac{\cos(90-\theta_{elev}-\arctan(\frac{h_2-h_1}{d_x})\sqrt{d_x^2+(h_2-h_1)^2}}{\sin\theta_{elev}}\frac{\sin\theta_{elev}}{\sin(180-2\theta_{elev})} \tag{3.20}$$

$$\psi = -2\theta_{elev} \tag{3.21}$$

To calculate the mutual impedance between two dipoles, they are divided in two monopoles, as shown in figure 3.7. The mutual impedance between the two dipoles is the sum of the mutual impedance between the monopoles:

$$Z_{mutual} = Z_1 + Z_2 + Z_3 + Z_4 \tag{3.22}$$

where Z_1, Z_2, Z_3 and Z_4 are the mutual impedances between the monopoles, defined as shown in figure 3.7a.

The mutual impedance between two monopoles can be calculated as [12]:

$$Z_{ij} = (-1)^{i+j}B\left(e^{\gamma t_n}\left(F_{i1} - e^{-\gamma u_m}G_{12} + e^{\gamma u_m}G_{22}\right) - e^{-\gamma t_n}\left(F_{i2} - e^{-\gamma u_m}G_{11} + e^{\gamma u_m}G_{21}\right)\right) \tag{3.23}$$

$$B = \frac{\eta}{16\pi\sinh(\gamma d_1)\sinh(\gamma d_2)} \tag{3.24}$$

where $\gamma = jk_0$, $m = 2/i$ and $n = 2/j$. The functions F_{ik} and G_{kl} are defined as:

$$F_{ik} = 2\sinh(\gamma d_1)e^{(-1)^k u_i\cos(\psi)}E(R_i + (-1)^k\cos(\psi) - (-1)^k t) \tag{3.25}$$

$$G_{kl} = 2E(R_2 + (-1)^k u_2 + (-1)^l t) + 2E(R_1 + (-1)^k u_1 + (-1)^l t) \tag{3.26}$$

R_i is defined as the distance between u_i and the point along d_2 under consideration. The functions E are defined as:

$$E(\alpha) = \int_{\alpha_1}^{\alpha_2}\frac{e^{-\gamma w}dw}{w} \tag{3.27}$$

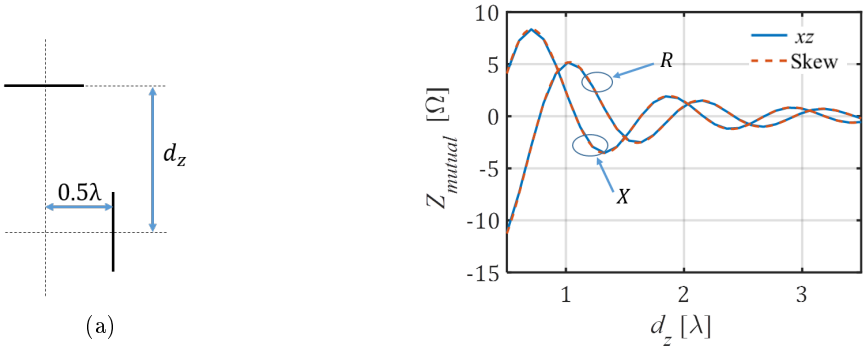

(a) (b)

Figure 3.8: Z_{mutual} between a dipole oriented along x and a dipole oriented along z. a) The two dipoles under consideration. b) Comparison of Z_{mutual} as function of d_z calculated using the method described in [12] (Skew) and using the MoM from appendix C.

where α is a function of t, $\alpha_1 = \alpha(t_1)$ and $\alpha_2 = \alpha(t_2)$. For example, if F_{11} is considered it can be seen that the argument of the E-function is equal to $R_1 - \cos(\psi) + t$. α_1 and α_2 from equation (3.27) are then:

$$\alpha_1 = \sqrt{(u_1 - t_1\cos(\psi))^2 + (t_1\sin(\psi))^2} - \cos(\psi) + t_1 \tag{3.28a}$$

$$\alpha_2 = \sqrt{(u_1 - t_2\cos(\psi))^2 + (t_2\sin(\psi))^2} - \cos(\psi) + t_2 \tag{3.28b}$$

Figure 3.8 shows a comparison between the real part, R, and the imaginary part, X, of the calculated mutual impedance between two half-wavelength dipoles using the theory described above and the method of moments for dipoles along x and z as discussed in section 3.1. In order to use the method of moments code, the angle between the elements is $\psi = 90°$ so that the dipoles can be represented by a dipole along x and a dipole along z. The displacement along x equals $d_x = 0.5\lambda$ and the displacement along z, d_z, is varied. The width of the dipoles is $w = 0.12\lambda$. A perfect agreement is found.

3.2.2 Electric field in original reference system

As the impedances between the dipoles and the images can now be calculated, it is possible to calculate the electric far field and the directivity. The calculation of the electric far field is split in three steps:

1. The field while only the original dipoles are excited, E_r.
2. The field while only the virtual dipoles are excited, E_i .
3. The total electric field by superimposing these results, E_{tot}.

The calculation of the electric field while only the original dipoles or only the virtual dipoles are excited is similar to that described in section 2.1.3. However, care must be taken to rotate the reference system to line up with the dipoles under consideration. As shown in figure 3.9 three reference systems can be distinguished:

1. $x'z'$-reference system. This reference system lines up with the real dipoles above the ground plane.

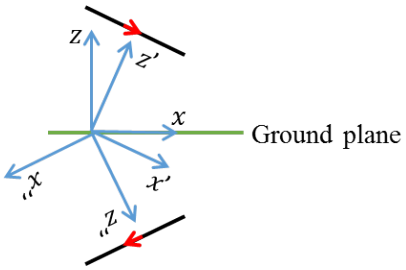

Figure 3.9: The original reference system xz, a reference system lined up with the real dipoles $x'z'$, and a reference system lined up with the virtual dipoles $x''z''$

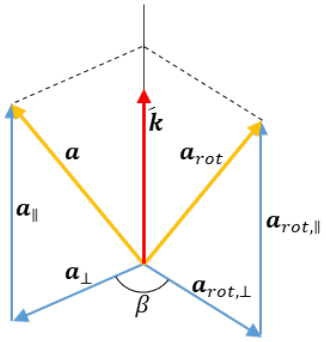

Figure 3.10: Vector $\mathbf{a}$ to be rotated around $\hat{\mathbf{k}}$ by an angle β

2. $x''z''$-reference system. This reference system lines up with the virtual dipoles beneath the ground plane.

3. xz-reference system. This is the original reference system which lines up with the ground plane and the given positions of the dipoles.

The electric far fields will be calculated on a unit sphere, S', described by θ' and ϕ' for the $x'z'$-reference system, and S", described by θ'' and ϕ'' for the $x''z''$-reference system. These spheres are co-centered with the unit sphere S, described by the angles θ and ϕ from the original xz-reference system. To be able to sum the fields calculated on the surface of the spheres S' and S" these spheres should be mapped on the original sphere S.

In order to understand the mapping of these rotated spheres on the original sphere one can imagine every point on the surface of this sphere to be found as a vector $\mathbf{a} = (\sin\theta\cos\phi, \sin\theta\sin\phi, \cos\theta)$ where $0 < \theta < \pi$ and $-\pi < \phi < \pi$. The change from the xz- to $x'z'$-reference system can be described as a rotation of these vectors around the y-axis. The rotation of a vector around an arbitrary axis can be performed using Rodrigues' formula. Figure 3.10 shows a vector $\mathbf{a}$ and a rotation axis $\hat{\mathbf{k}}$. Let us say we would like to rotate $\mathbf{a}$ around $\hat{\mathbf{k}}$ by an angle β. First the vector $\mathbf{a}$ can be decomposed in a component parallel to $\hat{\mathbf{k}}$ and a component perpendicular to $\hat{\mathbf{k}}$, $\mathbf{a}_\parallel$ and $\mathbf{a}_\perp$ respectively:

$$\mathbf{a} = \mathbf{a}_\parallel + \mathbf{a}_\perp \tag{3.29}$$

where

$$\begin{aligned} \mathbf{a}_\parallel &= \left(\mathbf{a}\cdot\hat{\mathbf{k}}\right)\hat{\mathbf{k}} \\ \mathbf{a}_\perp &= \mathbf{a} - \mathbf{a}_\parallel = \mathbf{a} - \left(\mathbf{a}\cdot\hat{\mathbf{k}}\right)\hat{\mathbf{k}} \end{aligned} \tag{3.30}$$

Rotating the vector $\mathbf{a}$ around $\hat{\mathbf{k}}$ by an angle β results in a new vector $\mathbf{a_{rot}} = \mathbf{a_{rot\parallel}} + \mathbf{a_{rot\perp}}$. As can be seen from figure 3.10 the component parallel to the rotation axis does not change: $\mathbf{a_{rot\parallel}} = \mathbf{a_\parallel}$. The perpendicular component can be found as: $\mathbf{a_{rot\perp}} = \cos\beta\mathbf{a}_\perp + \sin\beta\left(\hat{\mathbf{k}} \times \mathbf{a}_\perp\right)$. Substituting $\mathbf{a}_\perp = \mathbf{a} - \mathbf{a}_\parallel$ this results into $\mathbf{a_{rot\perp}} = \cos\beta\mathbf{a}_\perp + \sin\beta\left(\hat{\mathbf{k}} \times \mathbf{a}\right)$, since $\hat{\mathbf{k}} \times \mathbf{a}_\parallel = \mathbf{0}$. The rotated vector $\mathbf{a_{rot}}$ can therefore be written as:

$$\begin{aligned}
\mathbf{a_{rot}} &= \mathbf{a_{rot\parallel}} + \mathbf{a_{rot\perp}} \\
&= \mathbf{a}_\parallel + \cos\beta\mathbf{a}_\perp + \sin\beta\left(\hat{\mathbf{k}} \times \mathbf{a}\right) \\
&= \left(\mathbf{a} \cdot \hat{\mathbf{k}}\right)\hat{\mathbf{k}} + \cos\beta\left(\mathbf{a} - \left(\mathbf{a} \cdot \hat{\mathbf{k}}\right)\hat{\mathbf{k}}\right) + \sin\beta\left(\hat{\mathbf{k}} \times \mathbf{a}\right) \\
&= (1 - \cos\beta)\left(\mathbf{a} \cdot \hat{\mathbf{k}}\right)\hat{\mathbf{k}} + \cos\beta\mathbf{a} + \sin\beta\left(\hat{\mathbf{k}} \times \mathbf{a}\right)
\end{aligned} \tag{3.31}$$

The final expression for the rotated vector $\mathbf{a_{rot}}$ is known as Rodrigues' rotation formula. The angles in the rotated reference system, θ' and ϕ' can be found as:

$$\begin{aligned}
\theta' &= \arctan\left(\frac{\mathbf{a_{rot,y}}}{\mathbf{a_{rot,x}}}\right) \\
\phi' &= \arctan\left(\frac{\sqrt{\mathbf{a_{rot,x}^2} + \mathbf{a_{rot,y}^2}}}{\mathbf{a_{rot,z}}}\right)
\end{aligned} \tag{3.32}$$

Figure 3.11 shows values for θ and ϕ on the original sphere and the values for θ' and ϕ' mapped on the original sphere for a skew angle $\beta = 20°$. It can be seen that the sphere is correctly rotated by 20° around the y-axis.

Besides mapping the rotated spheres on the original sphere the electric field components should also be mapped in the original reference system before they can be summed together. Since the axis of rotation is the y-axis the y-components of the fields do not change. The x'- and z'-components of the electric field however should be mapped into the xz-components defined in the original system. This can be done by multiplying the electric field vector with the rotation matrix:

$$\begin{bmatrix} E_x \\ E_y \\ E_z \end{bmatrix} = \begin{bmatrix} \cos -\beta & 0 & -\sin -\beta \\ 0 & 1 & 0 \\ \sin -\beta & 0 & \cos -\beta \end{bmatrix} \begin{bmatrix} E_{x'} \\ E_{y'} \\ E_{z'} \end{bmatrix} \tag{3.33}$$

From figure 3.9 it can be seen that, in case the real dipoles are considered to be active ($x'z'$-reference system), β is equal to the elevation angle of the dipoles θ_{elev}. When the virtual dipoles are considered to be excited ($x''z''$-reference system), β is equal to $\pi - \theta_{elev}$.

3.2.3 Validation of radiation patterns

Let us consider two skewed dipoles above a ground plane as shown in figure 3.12. The lengths of the two dipoles is $l = \frac{\lambda}{2}$, the width $w = 0.12\lambda$ and the length of the port is $\delta = 0.1\lambda$. The first dipole is centered in the point $x = 0, z = z_1$ and the second dipole is centered around $x = x_2, z = z_2$. The ground plane is infinite in x- and y-direction and located in the plane $z = 0$. The two dipoles are skewed by an angle of $\theta_{elev} = 20°$.

Figure 3.13a shows the radiation pattern ($\phi = 0°$) for $z_1 = z_2 = 0.7\lambda$ and $x_2 = 0.75\lambda$. Both an entire domain basis function and a piecewise linear basis function are used. The number of triangles per dipole for the sub domain basis function is chosen to be 11, since that is the smallest number of triangles for which the radiation patterns did not change when the number of triangles is increased. Figure 3.13b shows the radiation pattern ($\phi = 0°$) for $z_1 = 0.7\lambda$, $z_2 = 0.9\lambda$

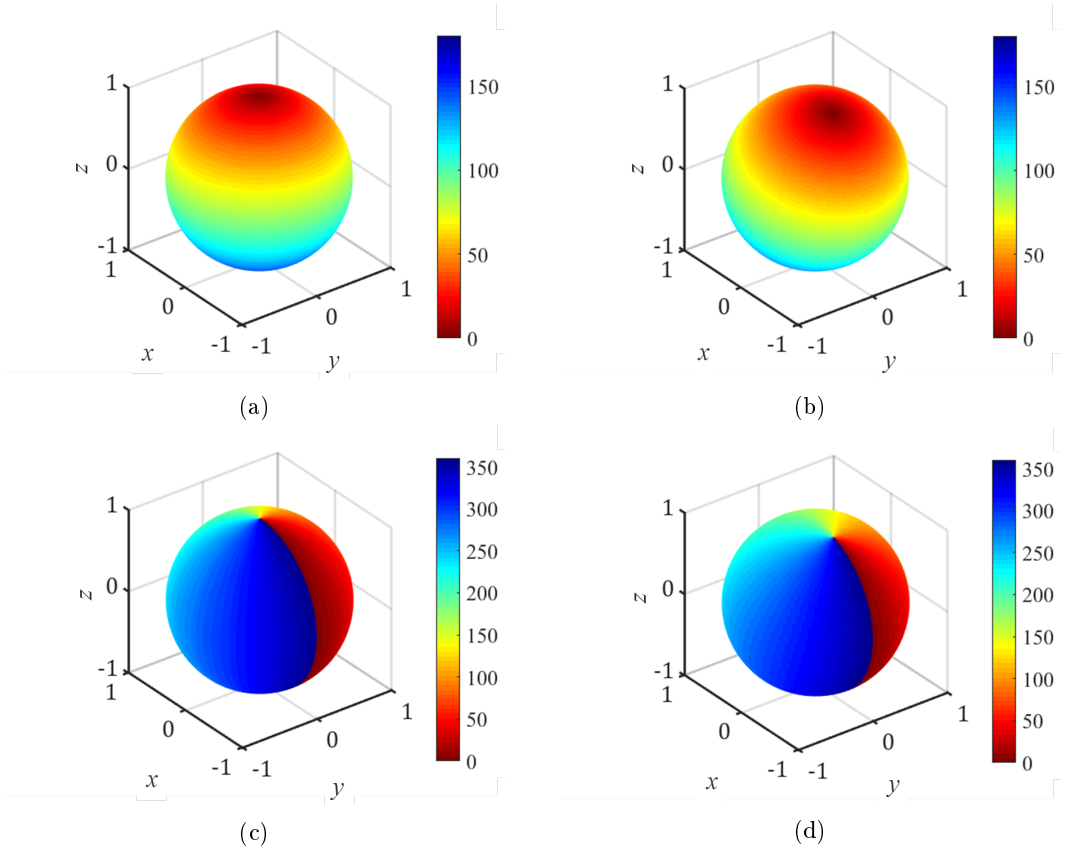

Figure 3.11: Visual representation of angular values mapped on a unit sphere. a) Values of θ of the original sphere. b) Values of θ' of a sphere, rotated by 20° around the y-axis, mapped on the original sphere. c) Values of ϕ of the original sphere. b) Values of ϕ' of a sphere, rotated by 20° around the y-axis, mapped on the original sphere.

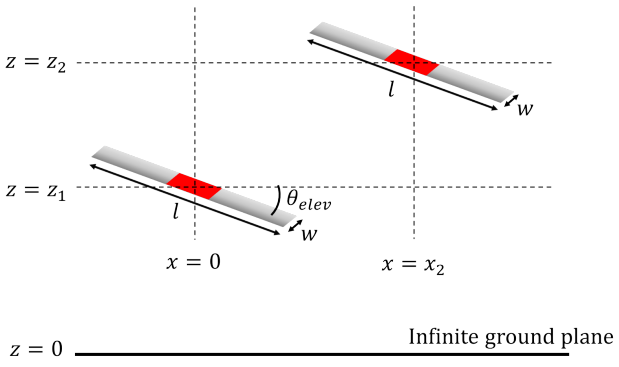

Figure 3.12: Two identical dipoles, skewed by and angle of θ_{elev} around the y-axis, above an infinite ground plane.

and $x_2 = 0.75\lambda$. Both the patterns shown in figure 3.13 show a good agreement with the results from CST.

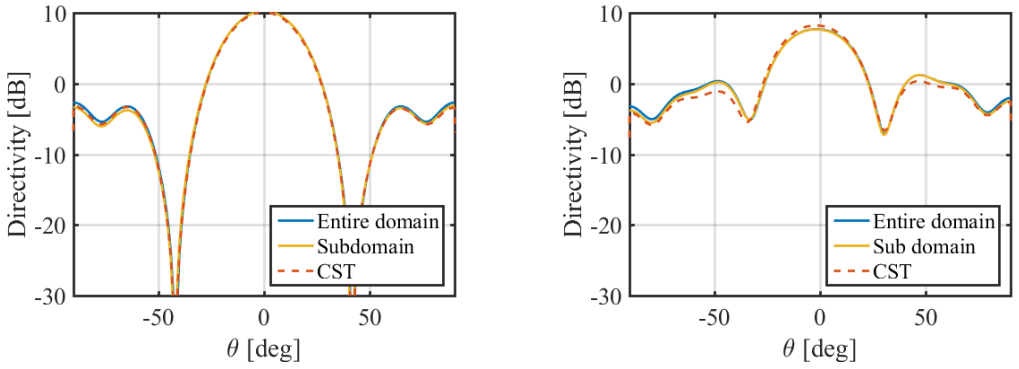

Figure 3.13: Radiation patterns ($\phi = 0°$) of two skewed halfwavelength dipoles above an infinite ground plane. The dipoles have a width of $w = 0.12\lambda$, a port length of $\delta = 0.1\lambda$ and the port impedance $z_0 = 50\,\Omega$. The dipoles are skewed by an angle of $\theta_{elev} = 20°$. The ground plane lies in the plane $z = 0$ and the dipoles are centered at $x_1 = 0$ and $x_2 = 0.75\lambda$ and: a) $z_1 = z_2 = 0.7\lambda$. b) $z_1 = 0.7\lambda$ and $z_2 = 0.9\lambda$.

3.3 Conclusion

The method of moments code is extended to simulate dipoles oriented along x and z. The expressions are shown to be very similar to that of dipoles only oriented along x. This is because the dipoles are assumed to be located in free space. Special care is taken for the cases when perpendicularly oriented dipoles are in line with each other. The method is validated by comparing the calculated radiation patterns to CST, in which a good agreement is found.

Another method is implemented to simulate dipoles skewed by an arbitrary angle above a ground plane. The original dipoles above a ground plane are represented dipoles and their images. The original dipoles and their images are under a skew angle with respect to each other. The locations of the dipoles are rewritten in a ut-reference system and the mutual impedances are calculated using the method described in [12].

The electric fields due to the original dipoles and due to the images are calculated separately in their own reference systems. The reference systems are rotated to align with the original reference system and the fields are summed together, after which the radiation pattern is calculated. The radiation patterns show a good comparison with CST.

Chapter 4

Study on asymmetry

This chapter will focus on the analysis of the active element patterns of different configurations of arrays of skewed dipoles. First a linear array of skewed dipoles above a ground plane is considered. Subsequently a directive element consisting of two dipoles, one excited and one passive, is introduced, referred to as stacked dipole. The asymmetry of linear arrays of both skewed dipoles and skewed stacked dipoles above a ground plane is studied.

4.1 Linear array of skewed dipoles

Let us consider a linear array of dipoles skewed by an angle θ_{elev} above a ground plane. The distance between adjacent elements in the x-direction is d_x. All elements are centered in $y = 0$, and the distance to the ground plane is h. Figure 4.1 shows such an array of dipoles above a ground plane and the equivalent array of dipoles and their images. The dipoles are excited with a phase difference between adjacent dipoles:

$$v_m = v_{m-1} e^{-jk_x d_x} \tag{4.1}$$

where $k_x = k_0 \sin\theta_{scan}$ and the main lobe of the radiation pattern will be pointing towards θ_{scan}. From figures 4.2a and 4.2b a symmetry about the ground plane can be seen, considering the dipoles and their images while scanning towards θ_{scan} and $-\theta_{scan}$. Because of this symmetry the radiation pattern while scanning to θ_{scan} will be a mirror of the pattern while scanning towards $-\theta_{scan}$. Therefore the active element pattern of a periodic linear array of dipoles above a ground plane will always be symmetric. Figure 4.3 shows the active element pattern of a linear array of dipoles for different skew angles. The dipoles are located at a distance $h = \frac{\lambda}{4}$ from the ground plane and the distance between adjacent dipoles in the x-direction is $d_x = 0.6\lambda$. The width of the dipoles equals $w = 0.12\lambda$, the length of the port is $\delta = 0.1\lambda$ and the port impedance is $z_0 = 50\,\Omega$. It can be seen from the figure that the active element pattern for different numbers of dipoles is indeed symmetric.

4.2 Linear array of skewed directive elements

4.2.1 Stacked dipoles

In order to increase the symmetry between the real dipoles and the images, directive element can be used. The directive element considered in this thesis is a stacked dipole structure. This configuration is chosen since it could be implemented in Matlab by making relatively small adjustments from the original code with single dipoles. The, non-tilted, structure consists of two

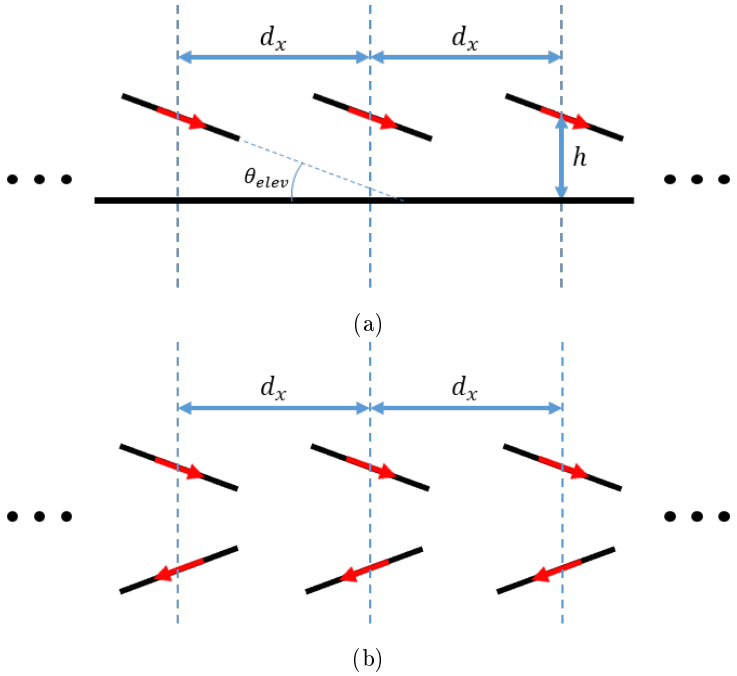

Figure 4.1: Linear array of skewed dipoles above an infinite ground plane. The displacement in x-direction between the dipoles is d_x and the distance between the center of the dipoles and the ground plane is h. a) The real geometry. b) The equivalent geometry using the image theorem.

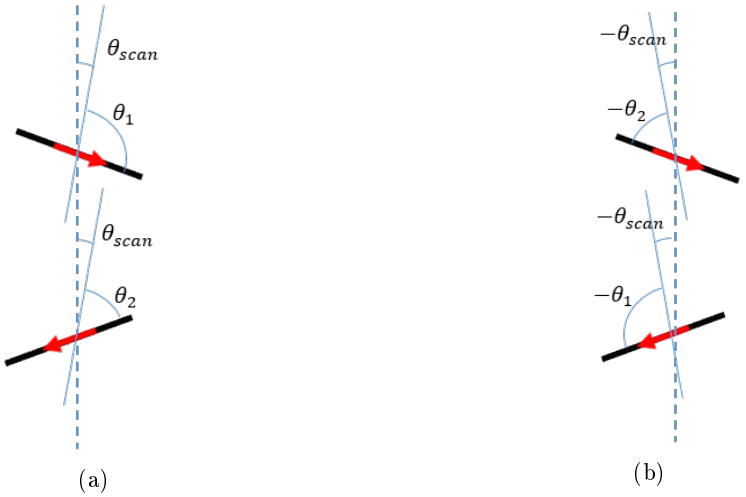

Figure 4.2: Symmetry of angles between scanning direction and the dipoles and the images. a) scanning towards θ_{scan}. b) scanning towards $-\theta_{scan}$.

dipoles of different length oriented along x and displaced by a small distance in the z-direction, as shown in figure 4.4. If the structure is dimensioned correctly the active dipole will induce a large current on the metal strip in such a way that the majority of the power is radiated upwards. This type of two element array is considered to be a superdirective structure [10].

Let us consider the two dipoles as shown in figure 4.4, with $l_1 = 0.5\lambda$, $l_2 = 0.42\lambda$ and

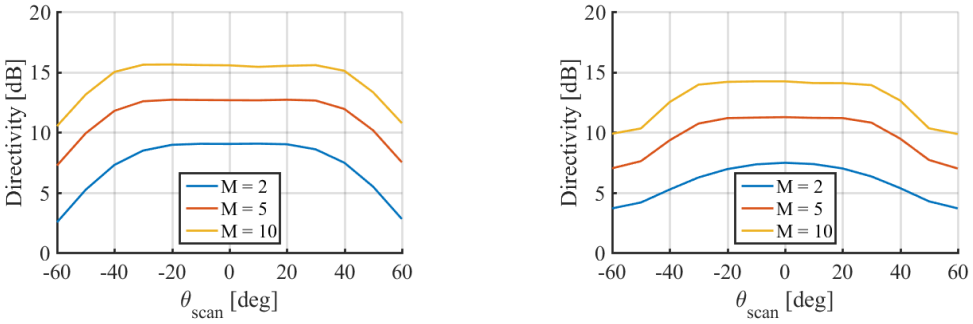

Figure 4.3: Average active element pattern of a linear array of M skewed dipoles above a ground plane. a) $\theta_{elev} = 20°$. b) $\theta_{elev} = 40°$.

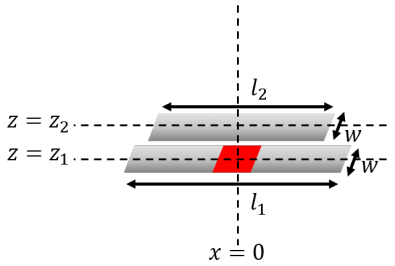

Figure 4.4: Stacked dipole element. Two dipoles with different length oriented along x, centered around the same x-coordinate and displaced in z. The short dipole is a metal strip without a port.

$d_z = z_2 - z_1 = 0.07\lambda$. The width $w = 0.12\lambda$, the length of the port $\delta = 0.1\lambda$ and the port impedance $z_0 = 50\,\Omega$. These numbers follow from an optimization using CST, in order to get a sufficient front-to-back ratio. By using the spectral expressions for the method of moments, as explained in section 2.1.2, a problem arises. In section 2.1.2 two expressions were given for approximations for the integral in k_y which hold when $|z_n - z_{n'}| = 0$ or $|z_n - z_{n'}| \gg w$. However, the distance between the two dipoles comprising the stacked dipole pair is small compared to the width. Therefore, while calculating the mutual impedances in the spectral domain, the integrals in both k_x and k_y need to be calculated resulting in a slow code.

Figure 4.5a shows the radiation pattern calculated using an entire domain basis function for the above mentioned structure. It is clear that the entire domain basis function does not represent the current distribution on the dipoles in an accurate manner, because of the reactive coupling between the dipoles and the reactance of the feed. Using the piecewise linear subdomain basis functions more accurate results are found, as is shown in figure 4.5b. It can be seen a sufficient amount of triangles need to be chosen on each dipole in order to get accurate results.

The large amount of triangles needed on each dipole in combination with the need for calculating the integrals in both k_x and k_y results in a very slow code. In order to increase the speed of the code it is noted that the integral in k_y only depends on the distance between the dipoles in the z-direction:

$$A(k_x) = \int_{-\infty}^{\infty} J_0\left(\frac{k_y w}{2}\right) \frac{e^{-j\sqrt{k_0^2 - k_x^2 - k_y^2}|z_n - z_{n'}|}}{\sqrt{k_0^2 - k_x^2 - k_y^2}} dk_y \tag{4.2}$$

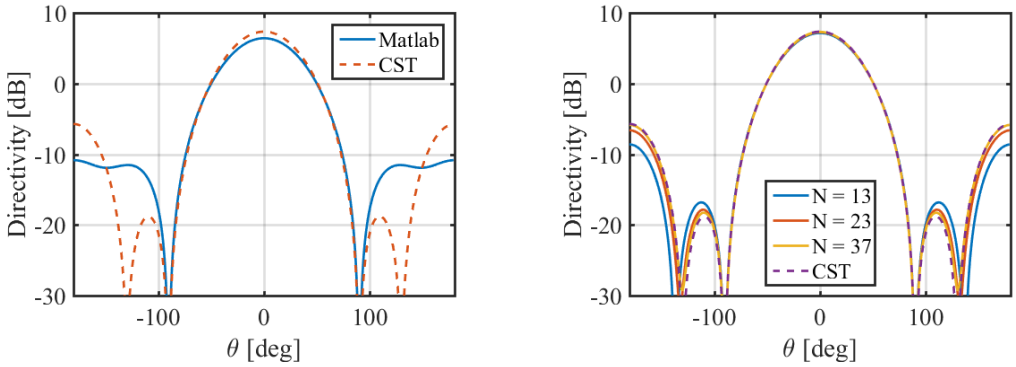

(a) (b)

Figure 4.5: Radiation pattern of a stacked dipole structure, with $l_1 = 0.5\lambda$, $l_2 = 0.42\lambda$ and $d_z = 0.07\lambda$. The width $w = 0.12\lambda$, the length of the port $\delta = 0.1\lambda$ and the port impedance $z_0 = 50\,\Omega$. a) An entire domain basis function is used. b) Piecewise linear subdomain basis functions are used. N is the number of triangles on each of the dipoles.

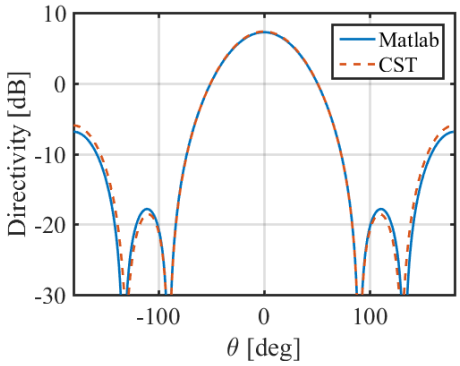

Figure 4.6: Radiation pattern of the stacked dipole structure, using 37 piecewise linear basis functions per dipole. The integral in k_y considering the mutual impedance between the two dipoles is calculated once, and approximated using a fitted function.

Therefore the function $A(k_x)$ will be the same for every combination of triangles on the two different dipoles. This makes it possible to calculated the integral only once, as a function of k_x, and use this function for further calculations. The function is found by calculating the integral for a set number of values for k_x and using a cubic interpolation to fit the function through these points. This fitted function is used in the calculation of the impedance matrix. Figure 4.6 shows the radiation pattern calculated using this fitted function. 37 triangles are used per dipole. A good agreement with CST is shown.

4.2.2 Linear array of skewed stacked dipoles

A linear array, as described in section 4.1, is again considered. The skewed dipoles are replaced by skewed stacked dipole structures, which were introduced in the previous section. Such an array, and the equivalent array of the dipoles and their images, are shown in figure 4.7.

The impedance matrix for such an array will consist of $4 \cdot M \cdot N \times 4 \cdot M \cdot N$ elements, where

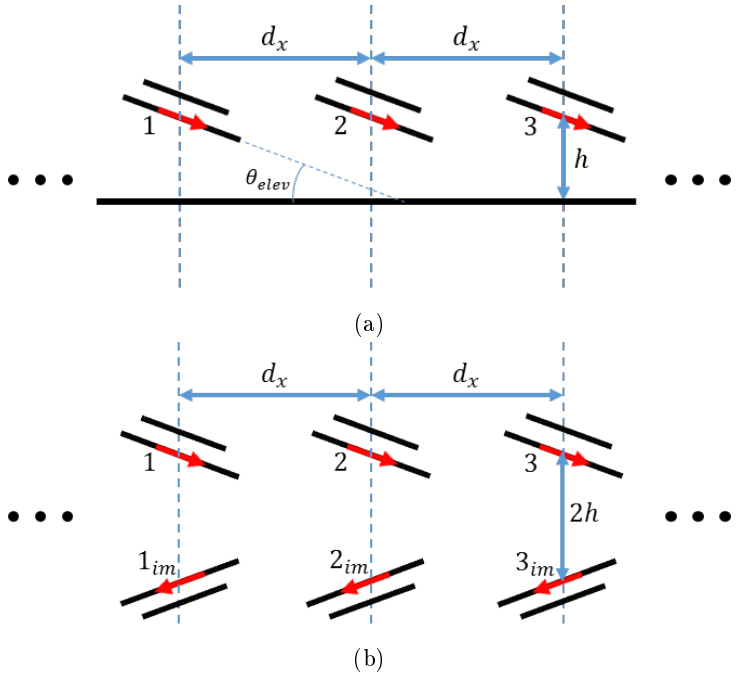

Figure 4.7: Linear array of skewed stacked dipoles above an infinite ground plane and their images. The displacement in x-direction between the dipoles is d_x and the distance between the center of the dipoles and the ground plane is h. a) The real geometry. b) The equivalent geometry using the image theorem.

M is the number of stacked dipole pairs and N is the number of triangles per dipole. The factor 4 comes from the two dipoles per stacked dipole pair and the images. Therefore an array of 2 elements with, for example, 37 triangles per dipole will consist of $296^2 = 87616$ elements. However, since the elements are identical and placed periodically along a line, the number of elements which need to be calculated can be reduced drastically using the periodicity of the array.

Let us consider the array with three elements as shown in figure 4.7. The entire impedance matrix is divided in smaller matrices such that:

$$\boldsymbol{Z}_{MoM} = \begin{bmatrix} \boldsymbol{Z}_{1,1} & \boldsymbol{Z}_{1,2} & \boldsymbol{Z}_{1,3} & \boldsymbol{Z}_{1,1_{im}} & \boldsymbol{Z}_{1,2_{im}} & \boldsymbol{Z}_{1,3_{im}} \\ \boldsymbol{Z}_{2,1} & \boldsymbol{Z}_{2,2} & \boldsymbol{Z}_{2,3} & \boldsymbol{Z}_{2,1_{im}} & \boldsymbol{Z}_{2,2_{im}} & \boldsymbol{Z}_{2,3_{im}} \\ \boldsymbol{Z}_{3,1} & \boldsymbol{Z}_{3,2} & \boldsymbol{Z}_{3,3} & \boldsymbol{Z}_{3,1_{im}} & \boldsymbol{Z}_{3,2_{im}} & \boldsymbol{Z}_{3,3_{im}} \\ \boldsymbol{Z}_{1_{im},1} & \boldsymbol{Z}_{1_{im},2} & \boldsymbol{Z}_{1_{im},3} & \boldsymbol{Z}_{1_{im},1_{im}} & \boldsymbol{Z}_{1_{im},2_{im}} & \boldsymbol{Z}_{1_{im},3_{im}} \\ \boldsymbol{Z}_{2_{im},1} & \boldsymbol{Z}_{2_{im},2} & \boldsymbol{Z}_{2_{im},3} & \boldsymbol{Z}_{2_{im},1_{im}} & \boldsymbol{Z}_{2_{im},2_{im}} & \boldsymbol{Z}_{2_{im},3_{im}} \\ \boldsymbol{Z}_{3_{im},1} & \boldsymbol{Z}_{3_{im},2} & \boldsymbol{Z}_{3_{im},3} & \boldsymbol{Z}_{3_{im},1_{im}} & \boldsymbol{Z}_{3_{im},2_{im}} & \boldsymbol{Z}_{3_{im},3_{im}} \end{bmatrix} \tag{4.3}$$

where the subscript 'im' indicates the image dipoles and each element is also a matrix given by

$$\boldsymbol{Z}_{i,j} = \begin{bmatrix} \boldsymbol{Z}_{ex_i,ex_j} & \boldsymbol{Z}_{ex_i,pas_j} \\ \boldsymbol{Z}_{pas_i,ex_j} & \boldsymbol{Z}_{pas_i,pas_j} \end{bmatrix} \tag{4.4}$$

The subscripts 'ex' and 'pas' refer to the excited dipole and the passive dipole of a stacked dipole pair respectively. Due to the reciprocity, as explained in appendix A, it is known that $\boldsymbol{Z}_{i,j} = \boldsymbol{Z}_{j,i}^T$ where the superscript T represents the transpose of the matrix. Because the antenna elements are identical and using the periodicity of the array the impedance matrix from equation (4.3) can

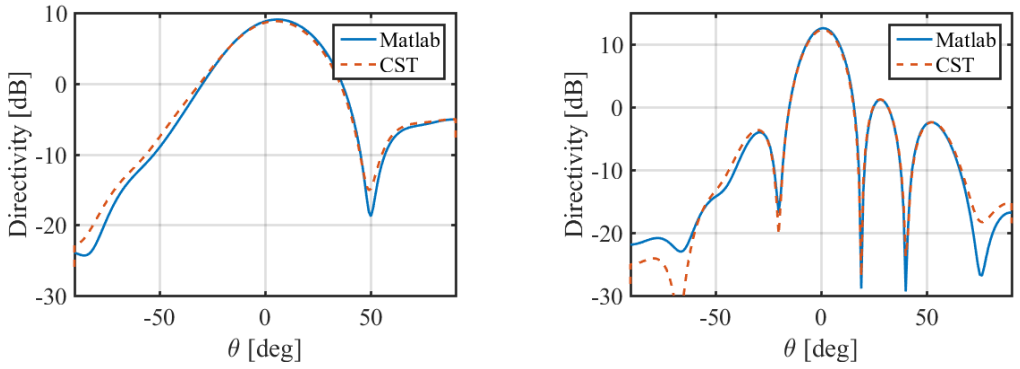

Figure 4.8: Radiation pattern of an array of stacked dipoles, with $l_1 = 0.5\lambda$, $l_2 = 0.42\lambda$ and $d_{z'} = 0.07\lambda$. The width $w = 0.12\lambda$, the length of the port $\delta = 0.1\lambda$ and the port impedance $z_0 = 50\,\Omega$. The periodicity in the x-direction is $d_x = 0.6\lambda$ and the distance between the center of the excited dipoles and the ground plane is $h = 0.25\lambda$. The scan angle of the array is $\theta_{scan} = 0°$. a) Array of two elements above a ground plane. b) Array of five elements above a ground plane.

be simplified to a block matrix consisting of four Toeplitz matrices of which the two non-diagonal blocks are symmetric:

$$\boldsymbol{Z}_{MoM} = \begin{bmatrix} \boldsymbol{Z}_{1,1} & \boldsymbol{Z}_{1,2} & \boldsymbol{Z}_{1,3} & \boldsymbol{Z}_{1,1_{im}} & \boldsymbol{Z}_{1,2_{im}} & \boldsymbol{Z}_{1,3_{im}} \\ \boldsymbol{Z}_{1,2}^T & \boldsymbol{Z}_{1,1} & \boldsymbol{Z}_{1,2} & \boldsymbol{Z}_{1,2_{im}} & \boldsymbol{Z}_{1,1_{im}} & \boldsymbol{Z}_{1,2_{im}} \\ \boldsymbol{Z}_{1,3}^T & \boldsymbol{Z}_{1,2}^T & \boldsymbol{Z}_{1,1} & \boldsymbol{Z}_{1,3_{im}} & \boldsymbol{Z}_{1,2_{im}} & \boldsymbol{Z}_{1,1_{im}} \\ \boldsymbol{Z}_{1,1_{im}}^T & \boldsymbol{Z}_{1,2_{im}}^T & \boldsymbol{Z}_{1,3_{im}}^T & \boldsymbol{Z}_{1,1} & \boldsymbol{Z}_{1,2} & \boldsymbol{Z}_{1,3} \\ \boldsymbol{Z}_{1,2_{im}}^T & \boldsymbol{Z}_{1,1_{im}}^T & \boldsymbol{Z}_{1,2_{im}}^T & \boldsymbol{Z}_{1,2}^T & \boldsymbol{Z}_{1,1} & \boldsymbol{Z}_{1,2} \\ \boldsymbol{Z}_{1,3_{im}}^T & \boldsymbol{Z}_{1,2_{im}}^T & \boldsymbol{Z}_{1,1_{im}}^T & \boldsymbol{Z}_{1,3}^T & \boldsymbol{Z}_{1,2}^T & \boldsymbol{Z}_{1,1} \end{bmatrix} \tag{4.5}$$

From equation (4.5) it can be seen that only the impedances from the first stacked dipole pair to all other stacked dipole pairs need to be calculated. The rest of the matrix can be filled reusing these parameters. Therefore, adding one element to the array will result in the calculation of two extra matrices: $\boldsymbol{Z}_{1,m}$ and $\boldsymbol{Z}_{1,m_{im}}$.

4.2.3 Validation of radiation patterns

Figures 4.8a and 4.8b show the radiation patterns of an array of stacked dipoles with two and five elements respectively. The stacked dipole structures are the same as introduced in section 4.2.1, with $l_1 = 0.5\lambda$, $l_2 = 0.42\lambda$ and $d_{z'} = 0.07\lambda$. The width $w = 0.12\lambda$, the length of the port $\delta = 0.1\lambda$ and the port impedance $z_0 = 50\,\Omega$. The periodicity in the x-direction is $d_x = 0.6\lambda$ and the distance between the center of the excited dipoles and the ground plane is $h = 0.25\lambda$. The stacked dipoles are rotated around the y-axis by an angle of $\theta_{elev} = 20°$. The pattern calculation is validated by comparison with CST, showing good agreement.

4.2.4 Analysis on asymmetry of a linear array of skewed stacked dipoles

All examples in this section will consider an array as shown in figure 4.9. Because the stacked dipole structure is highly resonant, the operational bandwidth of the stacked dipole structure is narrow (5% around 10 GHz). The geometrical parameters of the stacked dipoles are slightly

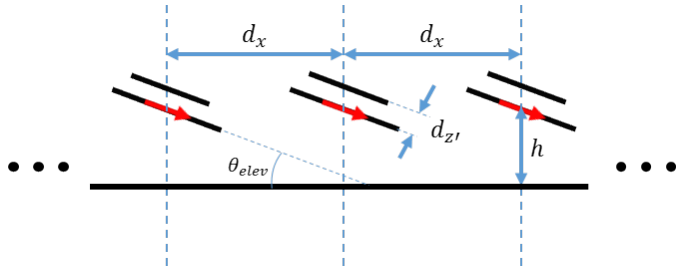

Figure 4.9: Linear array of M skewed stacked dipoles above an infinite ground plane and their images. The displacement in x-direction between the dipoles is d_x and the skew angle is θ_{elev}.

different from the structure introduced in the previous section, so that the array is matched while scanning from $-60°$ to $60°$ at 10 GHz. The geometrical parameters of the stacked dipole structures will not be changed throughout this section:

- $l_1 = 0.5\lambda$
- $l_2 = 0.4\lambda$
- $d_{z'} = 0.07\lambda$
- $h = 0.25\lambda$
- $w = 0.12\lambda$
- $\delta = 0.1\lambda$
- $z_0 = 25\,\Omega$

The variables under consideration are:

- number of elements in the array: M
- spacing between the elements in x-direction: d_x
- skew angle of the stacked dipoles: θ_{elev}

Figure 4.10a shows the radiation patterns for different scanning angles of an array of five elements with a spacing between the elements of $d_x = 0.6\lambda$. The skew angle of the array is $\theta_{elev} = 20°$. The grating lobe free region, for $d_x = 0.6\lambda$, can be found as:

$$|\theta_{scan}| \leq \arcsin\left(1 - \frac{2\pi}{d_x k_0}\right) = 41.8° \tag{4.6}$$

Figure 4.10b shows the active element pattern for this array of stacked dipoles. A clear asymmetry can be seen for large scanning angles. Since the comparison with CST shows a good agreement, the code is considered to be validated. It can be seen that, by introducing the grating lobes the directivity decreases 7 dB while scanning to $-60°$ and only 1.5 dB while scanning to $60°$. By using fewer elements and creating more space between the elements, the loss in directivity while scanning between $-20°$ and $50°$ is less than 0.5 dB. The asymmetry is defined as the difference in directivity while scanning towards θ_{scan} and $-\theta_{scan}$. The asymmetry shown in figure 4.10b is for example for $\theta_{scan} = \pm 60°$ equal to $D(60) - D(-60) = 10.4 - 1.9 = 8.5$ dB.

Figure 4.11 shows the asymmetry for different θ_{scan} of the active element pattern as a function of the number of elements in the array. The distance between the elements in the x-direction,

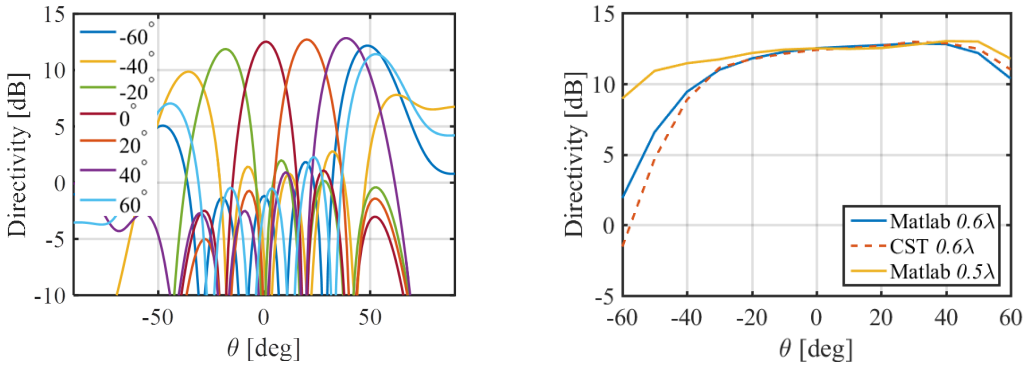

(a) (b)

Figure 4.10: Simulation results of an array consisting of five elements with a periodicity of $d_x = 0.6\lambda$ and a skew angle equal to $\theta_{elev} = 20°$. a) Radiation patterns while scanning towards different angles θ_{scan}. b) Comparison of the average active element pattern calculated in Matlab and CST. Also compared to an array of six elements with an inter-element distance of 0.5λ.

d_x, is changed ranging from 0.5λ to 0.75λ and the skew angle θ_{skew} is equal to 20°. It can be seen that for smaller inter-element spacing the asymmetry in the active element pattern is lower than for larger inter-element spacing. If the array is large (at least ten elements), the asymmetry of the scan angles outside of the grating lobe free region does not depend on the number of elements.

Figure 4.12 shows the asymmetry of the active element pattern as a function of the number of elements in the array for a skew angle $\theta_{elev} = 40°$. The same behaviour of the asymmetry can be seen when the number of elements is increased both inside and outside the grating lobe free region. Figure 4.12b shows a much higher asymmetry while scanning towards the larger angles outside the grating lobe free region. If the inter-element spacing is increased to $d_x = 0.75\lambda$, as shown in figure 4.12c, it can be seen that the asymmetry while scanning to ±60° is lower than the asymmetry for smaller scan angles. The asymmetry while scanning towards ±40° is increased significantly.

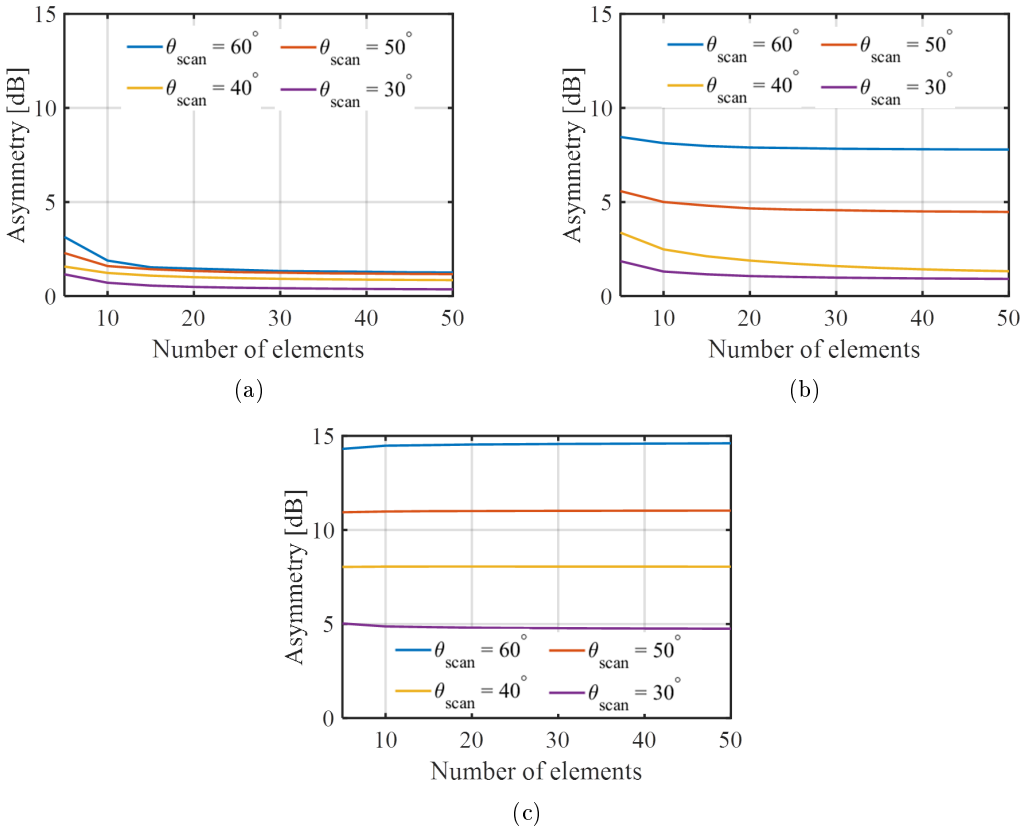

Figure 4.11: Asymmetry as a function of the number of element for a linear array of skewed stacked dipole elements above a ground plan. The skew angle $\theta_{elev} = 20°$ and the distance between the elements is: a) $d_x = 0.5\lambda$ (no grating lobes). b) $d_x = 0.6\lambda$ ($\theta_{GL} = 41.8°$). c) $d_x = 0.75\lambda$ ($\theta_{GL} = 19.6°$).

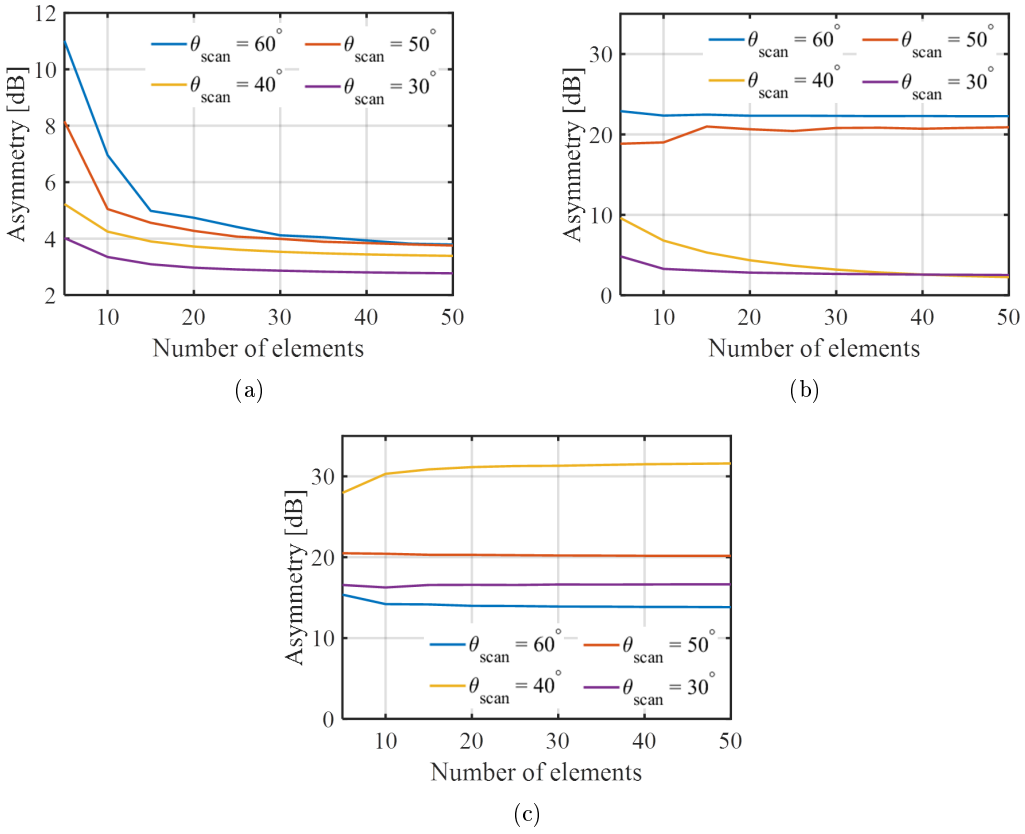

Figure 4.12: Asymmetry as a function of the number of element for a linear array of skewed stacked dipole elements above a ground plan. The skew angle $\theta_{elev} = 40°$ and the distance between the elements is: a) $d_x = 0.5\lambda$ (no grating lobes). b) $d_x = 0.6\lambda$ ($\theta_{GL} = 41.8°$). c) $d_x = 0.75\lambda$ ($\theta_{GL} = 19.6°$).

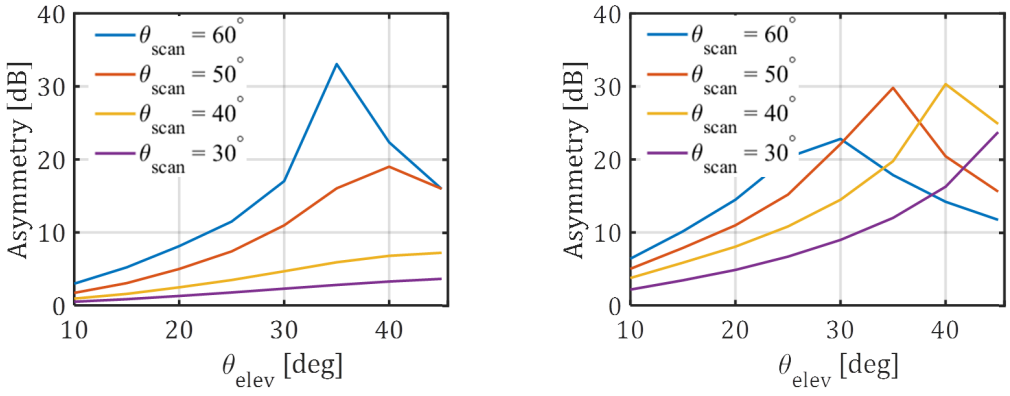

Figure 4.13: Asymmetry as a function of the skew angle for a linear array of skewed stacked dipole elements above a ground plan. The number of elements is ten and the distance between the elements is: a) $d_x = 0.6\lambda$ ($\theta_{GL} = 41.8°$). b) $d_x = 0.75\lambda$ ($\theta_{GL} = 19.6°$).

Figure 4.13 shows the asymmetry of the active element pattern for different scan angles, as a function of the skew angle θ_{elev} for different inter-element distances. The number of elements is ten. It can be seen that the asymmetry increases for increasing skew angle until a certain maximum, after which it starts decreasing. The maximum is found to be at lower skew angles for higher scan angles. The maxima occur at smaller skew angles for a larger inter-element distance.

Figure 4.14 shows the asymmetry of the active element pattern in dB for different scan angles, as a function of both the skew angle θ_{elev} and the inter-element distances d_x. The number of elements is ten. The skew angle is increased in steps of 5° and the inter-element distance in steps of 0.05λ. The results are interpolated to increase the readability of the images. The maxima in the asymmetry are clearly visible and it can be seen that the maxima indeed move to lower inter-element distance and skew angles for larger scan angles. Using these figures one can find the optimal inter-element distance and skew angle to achieve the desired asymmetry for different scan angles. Figure 4.15 shows a comparison of the active element pattern calculated in Matlab and CST of the case with the highest asymmetry while scanning to $\pm 60°$ as found in figure 4.14d. A good comparison can be seen, except for the point while scanning towards $-60°$. The asymmetry is still very high (22 dB), but not as high as calculated in Matlab (33 dB).

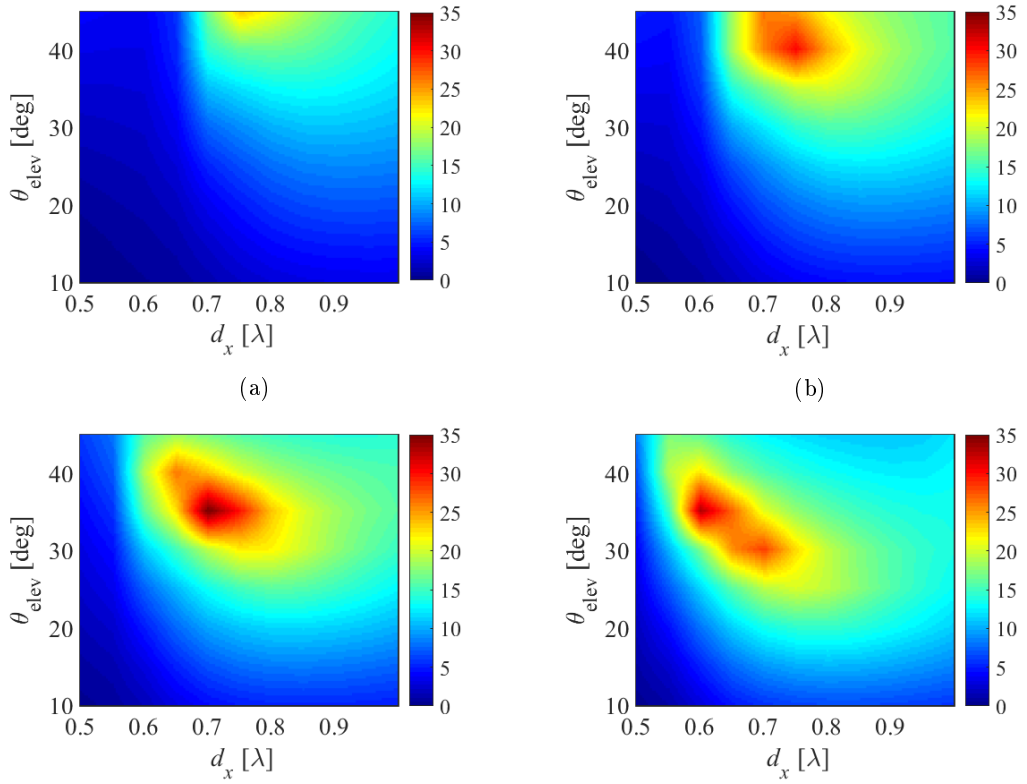

Figure 4.14: Asymmetry of the active element pattern in dB of an array of ten elements as a function of inter-element distance and skew angle. The results are interpolated to improve the readability of the images. The asymmetry is shown for: a) $\theta_{scan} = \pm 30°$. b) $\theta_{scan} = \pm 40°$. c) $\theta_{scan} = \pm 50°$. d) $\theta_{scan} = \pm 60°$.

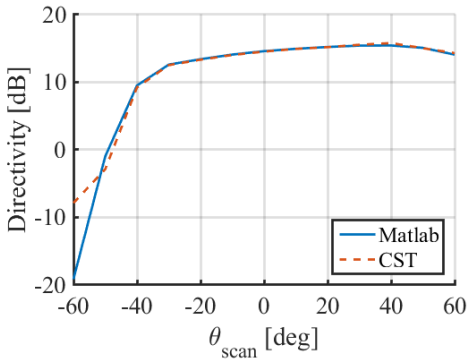

Figure 4.15: Comparison of the active element pattern for an array of ten elements skewed by 35°. The inter-element distance $d_x = 0.6\lambda$.

4.3 Conclusion

It is found that the active element pattern of skewed dipoles above a ground plane is highly symmetric. This is because of the symmetry between the real dipoles and the images about the ground plane. This symmetry is broken by introducing a directive element. Most power is directed in the upper half space and only a small portion is radiated backward and is reflected specularly by the ground plane. The directive element is implemented as a stacked dipole pair. If the stacked dipoles are dimensioned correctly, the element will radiate most power upwards, away from the ground plane. Asymmetry in the active element pattern can be achieved, for scan angles outside of the grating lobe free region. The asymmetry does not depend on the number of elements for arrays larger than ten elements. It is found that, by varying the inter-element distance and the skew angle of the elements, maxima in the asymmetry occur. The maxima occur at lower skew angle for larger scan angles. Also, for larger inter-element distance the skew angle at which a maximum in the asymmetry is found is smaller. Given the requirements on the asymmetry of the active element pattern, an optimum geometry exists.

Chapter 5

MoM for Z-shaped dipoles

In the previous chapters skewed dipoles were considered. Such elements are not convenient for fabrication purposes. A more convenient angular directive structure would be a Z-shaped dipole. An example of such a Z-shaped dipole can be found in figure 5.1. Such a structure can be implemented in planar PCB technology by printing the two horizontal metallizations and connect them with a via. The total length of the dipole is $l = l_x + l_z$ and the width is w. It can be seen that the dipole is oriented partly along x and partly along z. The dipole is fed in the center of the vertical part of the dipole. The Z-shaped dipole is proposed as an alternative for the skewed dipole and it is shown that the radiation pattern of a Z-shaped dipole is similar to a skewed dipole.

The Z-shaped dipole is analyzed using the expression for the method of moments to analyse dipoles oriented along x and z, which can be found in section 3.1.

5.1 Truncated sinusoidal basis functions

Let us consider a single Z-shaped dipole. The total length of the dipole is chosen to be $l = 0.5\lambda$ and the current is assumed to be sinusoidal over the whole dipole. The sinusoidal shape is truncated at the junctions, as is shown in figure 5.2.

The basis functions, similar to the entire domain basis function for dipoles along x as found in equation (2.39), are chosen to be:

$$\begin{aligned}
b_{up,n'}(x - x_{n'}) &= \frac{\sin\left(k_0\left(\frac{l}{2} - \frac{l_z}{2} - |x - x_{n'}|\right)\right)}{\sin\left(k_0\frac{l}{2}\right)} \operatorname{rect}_{l_x/2}(x - x_{n'} + l_x/4)\delta(z - z_{n'} - l_z/2) \\
b_{mid,n'}(z - z_{n'}) &= \frac{\sin\left(k_0\left(\frac{l}{2} - |z - z_{n'}|\right)\right)}{\sin\left(k_0\frac{l}{2}\right)} \operatorname{rect}_{l_z}(z - z_{n'})\delta(x - x_{n'}) \\
b_{down,n'}(x - x_{n'}) &= \frac{\sin\left(k_0\left(\frac{l}{2} - \frac{l_z}{2} - |x - x_{n'}|\right)\right)}{\sin\left(k_0\frac{l}{2}\right)} \operatorname{rect}_{l_x/2}(x - x_{n'} - l_x/4)\delta(z - z_{n'} + l_z/2)
\end{aligned} \tag{5.1}$$

where $x_{n'}$ and $z_{n'}$ are the x- and z-coordinates of the center of the part of the dipole along z.

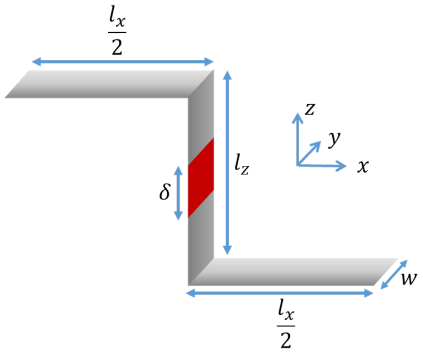

Figure 5.1: Z-shaped dipole with length $l = l_x + l_z$, width w. The length of the port is δ and the port impedance is z_0.

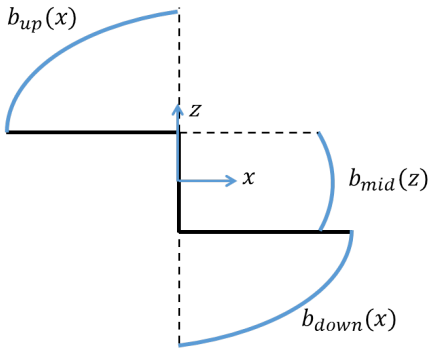

Figure 5.2: Truncated sinusoidal basis function on the Z-shaped dipole. The sinusoidal basis function is cut in three parts: b_{up}, b_{mid} and b_{down}.

Transforming the basis functions from equation (5.1) to the spectral domain gives:

$$
\begin{aligned}
B_{up,n'}(k_x) &= \frac{-e^{jk_x\frac{l_x}{4}}}{2\sin\left(k_0\frac{l}{2}\right)}\left(e^{jk_0\left(\frac{l}{2}-\frac{l_z}{2}\right)}\frac{1-e^{-j\frac{l_x}{2}(k_0+k_x)}}{k_0+k_x}+e^{-jk_0\left(\frac{l}{2}-\frac{l_z}{2}\right)}\frac{1-e^{j\frac{l_x}{2}(k_0-k_x)}}{k_0-k_x}\right)\\
B_{mid,n'}(k_z) &= \frac{1}{2\sin\left(k_0\frac{l}{2}\right)}\left(\frac{\cos(k_0\frac{l}{2})-\cos(k_0\frac{l}{2}-\frac{l_z}{2}(k_0-k_z))}{k_0-k_z}+\frac{\cos(k_0\frac{l}{2})-\cos(k_0\frac{l}{2}-\frac{l_z}{2}(k_0+k_z))}{k_0+k_z}\right)\\
B_{down,n'}(k_x) &= \frac{-e^{-jk_x\frac{l_x}{4}}}{2\sin\left(k_0\frac{l}{2}\right)}\left(e^{jk_0\left(\frac{l}{2}-\frac{l_z}{2}\right)}\frac{1-e^{-j\frac{l_x}{2}(k_0-k_x)}}{k_0-k_x}+e^{-jk_0\left(\frac{l}{2}-\frac{l_z}{2}\right)}\frac{1-e^{j\frac{l_x}{2}(k_0+k_x)}}{k_0+k_x}\right)
\end{aligned}
\tag{5.2}
$$

Care must be taken to ensure the continuity of the current at the junctions. Therefore the unknown weight factor i will be the same for the three parts of the dipole along x and z. This is done by calculating the input impedance of the dipole as a whole by summing the individual components of the impedance:

$$Z_{in} = Z_{x_1,x_1} + Z_{x_1,z} + Z_{x_1,x_2} + Z_{z,x_1} + Z_{z,z} + Z_{z,x_2} + Z_{x_2,x_1} + Z_{x_2,z} + Z_{x_2,x_2} \tag{5.3}$$

where Z_{x_1,x_1} is the impedance from the top part of the dipole to itself, $Z_{x_1,z}$ is the impedance from the top part of the dipole to the part along z, et cetera. The weight factor of the current i

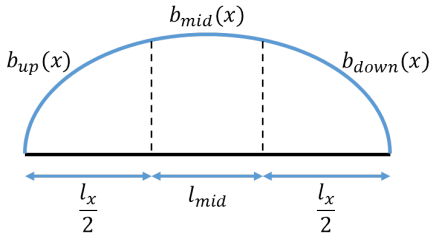

Figure 5.3: Truncated sinusoidal basis function on a planar dipole. The sinusoidal basis function is cut in three parts: b_{up}, b_{mid} and b_{down}.

is now calculated as:

$$i = \frac{v}{(Z_{in} + z_0)} \tag{5.4}$$

Once the weighting factor i is calculated, the electric field radiated by the different parts of the dipole is calculated as described in appendix C and summed together to calculate the radiation pattern.

5.1.1 Validation using planar dipole

In order to check whether or not the truncated basis function from equation (5.1) can be used to approximate the current, a planar half wavelength dipole as shown in figure 5.3 is considered. The three basis functions for a planar dipole become:

$$\begin{aligned}
b_{up,n'}(x - x_{n'}) &= \frac{\sin\left(k_0\left(\frac{l}{2} - |x - x_{n'}|\right)\right)}{\sin\left(k_0\frac{l}{2}\right)} \operatorname{rect}_{l_x/2}(x - x_{n'} + l_{mid}/2 + l_x/4)\delta(z - z_{n'}) \\
b_{mid,n'}(x - x_{n'}) &= \frac{\sin\left(k_0\left(\frac{l}{2} - |x - x_{n'}|\right)\right)}{\sin\left(k_0\frac{l}{2}\right)} \operatorname{rect}_{l_{mid}}(x - x_{n'})\delta(z - z_{n'}) \\
b_{down,n'}(x - x_{n'}) &= \frac{\sin\left(k_0\left(\frac{l}{2} - |x - x_{n'}|\right)\right)}{\sin\left(k_0\frac{l}{2}\right)} \operatorname{rect}_{l_x/2}(x - x_{n'} - l_{mid}/2 - l_x/4)\delta(z - z_{n'})
\end{aligned} \tag{5.5}$$

where $l = l_x + l_{mid}$ is the total length of the dipole. Transforming these basis functions to the spectral domain gives:

$$\begin{aligned}
B_{up}(k_x) &= \frac{-e^{jk_x\frac{l_{mid}+l}{4}}}{2\sin\left(k_0\frac{l}{2}\right)}\left(e^{-jk_0\frac{l}{2}}\frac{e^{j\frac{l_{mid}}{2}(k_0-k_x)} - e^{j\frac{l}{2}(k_0-k_x)}}{k_0 - k_x} + e^{jk_0\frac{l}{2}}\frac{e^{-j\frac{l_{mid}}{2}(k_0+k_x)} - e^{-j\frac{l}{2}(k_0+k_x)}}{k_0 + k_x}\right) \\
B_{mid}(k_x) &= 2\sin\left(k_0\frac{l}{2}\right)\left(\frac{2\cos\left(k_0\frac{l}{2}\right)}{k_0 + k_x} + \frac{2\cos\left(k_0\frac{l}{2}\right)}{k_0 - k_x}\right. \\
&\quad \left. - e^{-jk_0\frac{l}{2}}\frac{e^{j\frac{l_{mid}}{2}(k_0-k_x)}}{k_0 - k_x} - e^{jk_0\frac{l}{2}}\frac{e^{-j\frac{l_{mid}}{2}(k_0-k_x)}}{k_0 - k_x} - e^{jk_0\frac{l}{2}}\frac{e^{-j\frac{l_{mid}}{2}(k_0+k_x)}}{k_0 + k_x} - e^{-jk_0\frac{l}{2}}\frac{e^{j\frac{l_{mid}}{2}(k_0+k_x)}}{k_0 + k_x}\right) \\
B_{down}(k_x) &= \frac{e^{-jk_x\frac{l+l_{mid}}{4}}}{2\sin\left(k_0\frac{l}{2}\right)}\left(e^{jk_0\frac{l}{2}}\frac{e^{-j\frac{l}{2}(k_0-k_x)} - e^{-j\frac{l_{mid}}{2}(k_0-k_x)}}{k_0 - k_x} + e^{-jk_0\frac{l}{2}}\frac{e^{j\frac{l}{2}(k_0+k_x)} - e^{j\frac{l_{mid}}{2}(k_0+k_x)}}{k_0 + k_x}\right)
\end{aligned} \tag{5.6}$$

The transverse basis function is chosen to be edge-singular, as described in chapter 2. Calculating the impedance matrix using the method described in section 2.1.2 the imaginary parts of the individual elements in the impedance matrix do not converge. Let us consider a dipole oriented

along x with total length $l = 0.5\lambda$, $l_{mid} = 0.15\lambda$ and a width equal to $w = 0.12\lambda$. The integration limits for the numerical calculation of the integral in Matlab are $-k_{lim}$ and k_{lim}. The impedance matrix calculated with integration limits equal to $k_{lim} = 300k_0$ gives:

$$Z_{MoM} = \begin{bmatrix} 5.8 - 229j & 9.0 + 236j & 4.3 + 6.4j \\ 9.0 + 236j & 16.0 - 472j & 9.0 + 236j \\ 4.3 + 6.4j & 9.0 + 236j & 5.8 - 229j \end{bmatrix} \Omega$$

while the impedance matrix with integration limits equal to $k_{lim} = 500k_0$ gives:

$$Z_{MoM} = \begin{bmatrix} 5.8 - 249j & 9.0 + 257j & 4.3 + 6.4j \\ 9.0 + 257j & 16.0 - 513j & 9.0 + 257j \\ 4.3 + 6.4j & 9.0 + 257j & 5.8 - 249j \end{bmatrix} \Omega$$

Increasing the integration limits further gives higher values of the absolute values of the imaginary part of the elements of the impedance matrix. Appendix D gives a step by step calculation to find the asymtotic expression for the impedance in the limit $|k_x| \gg k_0$ and shows that the integral indeed does not converge.

Calculating the total input impedance of the dipole by summing the elements of the matrix, as found in equation (5.3), does give a constant value in both cases: $Z_{in} = (72.1 + 28.6\text{j})\,\Omega$. This input impedance is the same as the impedance found using a single entire domain basis function as described in chapter 2. Therefore it can be concluded that the imaginary parts of the impedance of the individual dipole parts do not converge, but compensate each other and summing them together gives the correct result.

5.1.2 Results on Z-shaped dipole

In order to see whether or not the same compensating behaviour happens for the Z-shaped dipole, the basis functions found in equation (5.2) are used in a method of moments code. The dimensions of the dipole are similar to the planar dipole of the previous section. The total length is $l = 0.5\lambda$ and $l_z = 0.15\lambda$. The width of the dipole is $w = 0.12\lambda$. The length of the port is $\delta = 0.1\lambda$ and the port impedance is $z_0 = 50\,\Omega$.

Because, for the mutual impedances between a dipole along x and a dipole along z, the integral in k_y cannot be closed analytically, as described in section 3.1, the mutual impedance between the dipole parts along x and the dipole part along z are calculated in Matlab using a double integral function. The integration limits for the integral in k_x and the integral in k_y are $k_{x,lim}$ and $k_{y,lim}$ respectively. It is found that, similar to the case of the planar dipole, the imaginary parts of the individual components of the impedance matrix do not converge. The impedance matrix calculated with integration limits equal to $k_{x,lim} = 300k_0$ and $k_{y,lim} = 300k_0$ gives:

$$Z_{MoM} = \begin{bmatrix} 5.8 - 229j & 0.17 + 227j & 4.8 - 2.6j \\ 0.17 + 227j & 16.0 - 472j & 0.17 + 227j \\ 4.8 - 2.6j & 0.17 + 227j & 5.8 - 229j \end{bmatrix} \Omega$$

while the impedance matrix with integration limits equal to $k_{x,lim} = 500k_0$ and $k_{y,lim} = 300k_0$ gives:

$$Z_{MoM} = \begin{bmatrix} 5.8 - 249j & 0.17 + 247j & 4.8 - 2.6j \\ 0.17 + 247j & 16.0 - 513j & 0.17 + 247j \\ 4.8 - 2.6j & 0.17 + 247j & 5.8 - 249j \end{bmatrix} \Omega$$

It can be seen that the self impedances of the dipole parts are equal for the Z-shaped dipole as for the planar dipole. This is as expected since the dipoles are in free space and the location and orientation of the dipole parts should not influence the self impedance. It can also be

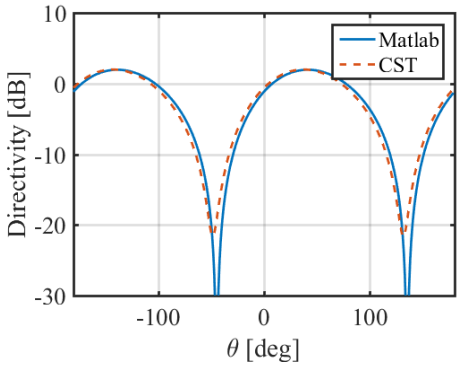

Figure 5.4: Radiation pattern of a Z-shaped dipole. $l = 0.5\lambda$ and $l_z = 0.15\lambda$. The width of the dipole is $w = 0.12\lambda$. The length of the port is $\delta = 0.1\lambda$ and the port impedance is $z_0 = 50\,\Omega$.

found that, as opposed to the case of the planar dipole, the total input impedances of the Z-shaped dipole are very similar, but not completely converged: $Z_{in,300k_0} = (37.9 - 24.4\text{j})\,\Omega$ and $Z_{in,500k_0} = (37.9 - 28.0\text{j})\,\Omega$. Due to numerical limitations in Matlab the integration limits cannot be increased further.

Figure 5.4 shows the radiation pattern for this Z-shaped dipole calculated using the method of moments code compared to CST. A good agreement is found.

Let us now consider three identical Z-shaped dipoles, located at $x_1 = z_1 = 0$, $x_2 = \lambda, z_2 = 0$ and $x_3 = 2\lambda, z_3 = \lambda$, as shown in figure 5.5a. The radiation pattern ($\phi = 0°$) calculated using the matlab code for these three dipoles is calculated and compared to CST. It can be seen from figure 5.5b that, when all the dipoles are active, a good agreement is found. Also when one or more of the dipoles are passive the comparison between Matlab and CST is good, as shown in figures 5.5c ($v_2 = 0$) and 5.5d ($v_1 = v_3 = 0$).

Although the calculations show good agreement with CST for the considered cases, problems arise as the width of the dipole is decreased. Changing the width of the dipoles to $w = 0.025\lambda$ shows the dependency on the integration limits in k_y. For a single Z-shaped dipole the impedance calculated using $k_{y,lim} = 250k_0$ is found to be $Z_{in} = (38.3 - 31.4\text{j})\,\Omega$, while the impedance of the same dipole using $k_{y,lim} = 300k_0$ is found to be $Z_{in} = (38.3 - 95.7\text{j})\,\Omega$. Figure 5.6 shows the imaginary part of the input impedance as a function of the integration limits in k_y. The integration limit in k_x, $k_{x,lim} = 400k_0$. It can be seen that for the dipole with a width equal to $w = 0.12\lambda$ the imaginary part of the impedance is not converged, but the amplitude of the oscillations is low and does not significantly affect the results. When the width is decreased, the amplitude of the oscilations increases and the results become inaccurate.

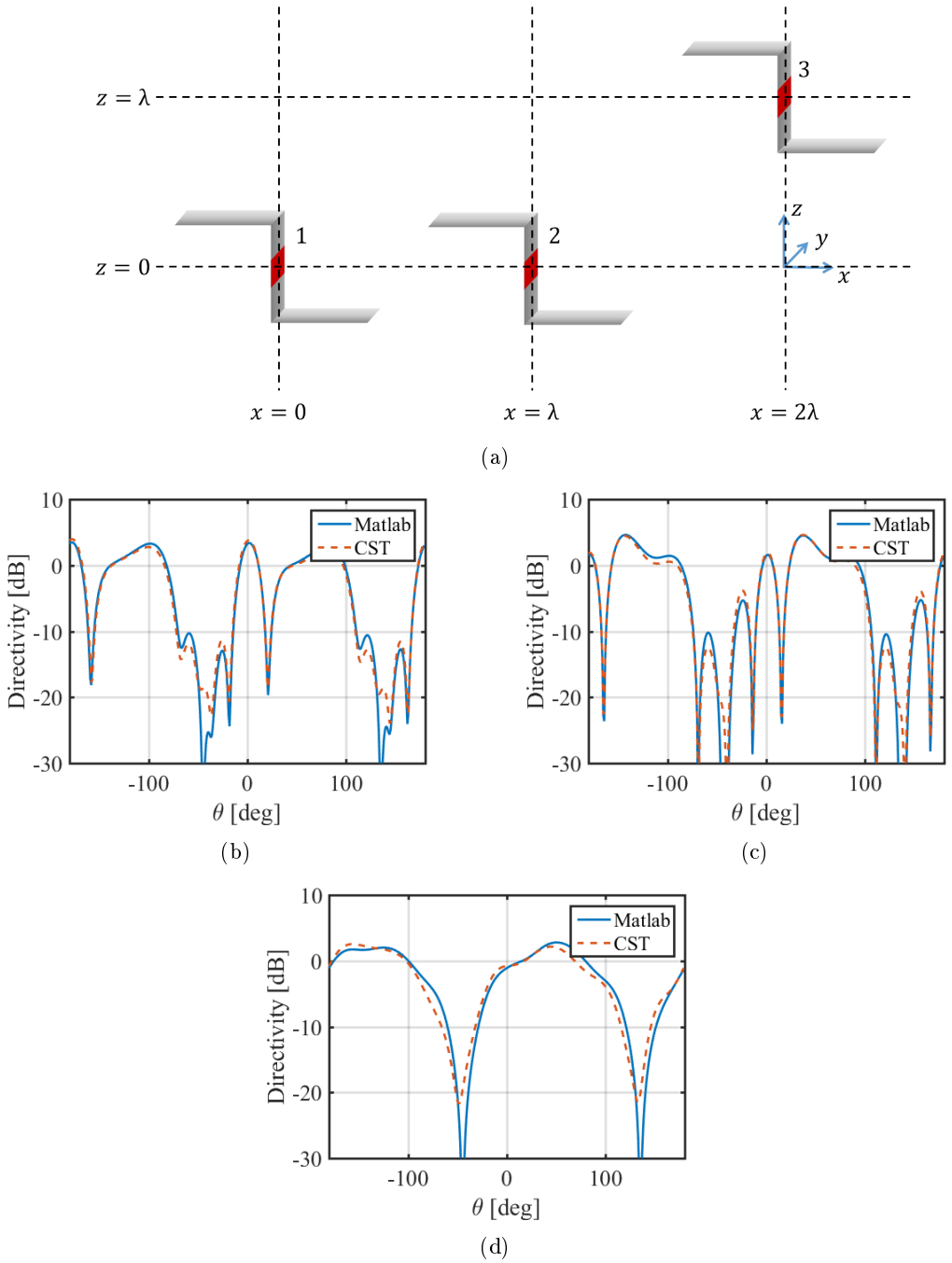

Figure 5.5: Simulation results of three identical Z-shaped dipoles. The total length of the dipoles is $l = 0.5\lambda$, $l_z = 0.15\lambda$, $w = 0.12\lambda$. The length of the port is 0.1λ and the port impedance is $z_0 = 50\,\Omega$. a) The geometry of the entire structure under consideration. b) Radiation patterns when all three dipoles are active. c) Radiation pattern when the second dipole is passive. d) Radiation pattern when the first and the third dipoles are passive.

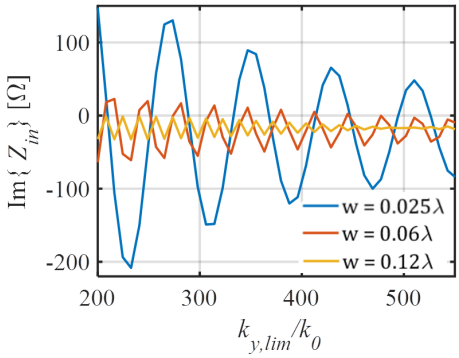

Figure 5.6: Imaginary part of the input impedance of a Z-shaped dipole as a function of the integration limits in k_y, calculated using truncated sinusoidal basis functions. The width of the dipole is decreased from $w = 0.12\lambda$ to $w = 0.025\lambda$. The integration limits in $k_x = 400k_0$. The total lenght of the dipole is $l = 0.5\lambda$ and $l_z = 0.15\lambda$.

5.2 Conclusion

A Z-shaped dipole is analized, as it is more convenient for fabrication purposes than skewed dipoles. A method of moments code is written to calculate the input impedance and the radiation patterns of these dipoles. It is found that the imaginary parts of the elements of the impedance matrix do not converge if a truncated sinusoidal basis function is used. However, when the width of the dipole is sufficiently large, the total input impedance does converge. The radiation patterns calculated using the truncated sinusoidal are in good agreement with CST.

Chapter 6

Conclusions and future work

6.1 Summary and conclusions

In this thesis we aimed to find design rules to shape the active element pattern of a linear array of dipoles above a ground plane to be asymmetric. An asymmetric active element pattern can be advantageous for the design of a low-profile steerable beam antenna. The radiation to high elevation angles can be increased, reducing the radiation for low elevation. A method of moments solution is implemented in Matlab to find the active element pattern of such linear arrays.

The mathematical expressions for the method of moments for horizontal dipoles are derived in both the spatial and the spectral domain. Since the spectral domain representation requires fewer integrals to solve, the spectral domain expressions are used throughout the thesis to calculate the radiation patterns. Two types of basis functions are implemented to describe the current distribution along the dipoles: an entire domain basis function and piecewise linear sub domain basis functions. Both basis functions are found to provide accurate radiation patterns. Piecewise linear basis functions are more accurate to find the input impedance of the dipoles as they describe the reactance of the feed better.

Similar expressions are derived for the case of dipoles both along x and z. Care is taken for the mutual impedance between a dipole along x and a dipole along z. The sign of the mutual impedance depends on the relative location of these dipoles. A special case exists when the dipoles are in line with each other. For this case the observation domain is split in two and the integrals are evaluated separately with their own respective signs.

The method of moments code is extended to be able to simulate skewed dipoles. The method described in [12] is implemented to calculate the mutual impedance between dipoles under an arbitrary skew angle with respect to each other. This method is used to simulate skewed dipoles above a ground plane. Using the image theorem the real dipoles above a ground plane are represented as an equivalent problem of the real dipoles and virtual dipoles. The electric field contributions due to the real dipoles and the virtual dipoles are calculated in separate reference systems and mapped onto the original reference system. It is found that a periodic array of skewed dipoles above a ground plane will result in a highly symmetric active element pattern. This is due to the symmetry of these dipoles about the ground plane.

To break the symmetry, a directive structure is introduced, in the form of stacked dipoles. It is found that the entire domain basis function does not give accurate results for this type of directive element. Therefore the piecewise linear basis functions are used. Using the periodicity of the array, the number of calculations necessary to find the mutual impedance between all the dipoles is reduced drastically. Only the mutual impedance between the first stacked dipole pair and the other stacked dipole pairs needs to be calculated. These numbers can be reused as the

mutual impedance between the other elements. The time needed to calculated the radiation pattern of a linear array of 30 skewed stacked dipole pairs above a ground plane is found to be 1189 seconds ($\approx$ 20 minutes) using the Matlab code, while CST needs 4229 seconds ($\approx$ 70 minutes) to simulate the same array.

A second method of moments code is implemented to simulate a dipole bent into a Z-shape. The radiation pattern of such a dipole is shown to be similar to the radiation pattern of a skewed dipole. Using standard PCB technology a Z-shaped dipole can be implemented by printing horizontal metalizations and connecting them using vias. A truncated sinusoidal basis function is implemented to approximate the current on the dipole. Mathematical expressions are derived for the method of moments of horizontal and vertical dipoles.

The asymmetry in the active element pattern for a linear array of skewed dipoles and directive elements is investigated and design rules are derived. Asymmetry in the active element pattern can be achieved by an under-sampled array of skewed directive element. It is found that for arrays larger than ten elements the asymmetry does not depend on the number of array elements. The asymmetry for different scan angles depends on the inter-element distance and the skew angle of the elements. Maxima exist for the asymmetry for varying skew angles and a fixed inter-element distance. These maxima occur at lower skew angles for larger scan angles. Also for larger inter-element distances the maxima are found to be at lower skew angles than for smaller inter-element distances.

It can be concluded that the truncated sinusoidal basis functions can be used to calculate radiation pattern of a Z-shaped dipole, however the dipole must have a sufficient width in order for the input impedance to converge within the numerical limitations of Matlab.

6.2 Future work

The Z-shaped dipole can be analyzed to a certain extend using the truncated sinusoidal basis function. However, when the width of the dipoles is reduced, the impedance does not converge before Matlab reaches a numerical limitation. It can be looked into to rewrite the expressions in such a way that the numerical limitation is avoided. Also one can consider another basis function to make the impedances converge.

We have derived the expressions for a finite linear array of skewed dipoles above a ground plane. The work done in this thesis was a theoretical study in order to find design rules for shaping the active element pattern to be asymmetric. The array used in this work consisted on infinitely thin skewed dipoles fed by a delta gap excitation. The design rules proposed in this thesis can be used to make a realistic design, for example using Z-shaped dipoles, for an array with an asymmetric active element pattern.

Although this thesis considered periodic arrays, where all the dipoles were tilted by the same skew angle, this does not have to be the case. One can imagine a linear array where the skew angle of the elements is reduced until the dipole is planar in the center of the array after which the skew of the dipoles would be reversed. The radiation characteristics of such arrays, or other configurations of skewed dipoles can be analyzed using the theory described in this thesis.

Appendix A

Reciprocity theorem

While calculating the impedance matrix $\boldsymbol{Z}$ one can reduce the number of calculations necessary by using the property of the $\boldsymbol{Z}$-matrix that it must be symetric around the diagonal. This can be explained using the reciprocity theorem.

If one considers two sets of sources: $\boldsymbol{J}_1$,$\boldsymbol{J}_{m1}$ and $\boldsymbol{J}_2$,$\boldsymbol{J}_{m2}$, where $\boldsymbol{J}$ is an electric current and $\boldsymbol{J}_m$ is a magnetic current. If both sets of sources operate at the same frequency they will generate two sets of fields: $\boldsymbol{E}_1$,$\boldsymbol{H}_1$ and $\boldsymbol{E}_2$, $\boldsymbol{H}_2$. Using Ampères law and Faradays law from the Maxwell's equations,

$$\nabla \times \boldsymbol{H} = j\omega\epsilon\boldsymbol{E} + \boldsymbol{J} \tag{A.1}$$

and

$$\nabla \times \boldsymbol{E} = -j\omega\mu\boldsymbol{H} - \boldsymbol{J}_m \tag{A.2}$$

respectively, it can be shown that:

$$-\nabla \cdot (\boldsymbol{E}_1 \times \boldsymbol{H}_2 - \boldsymbol{E}_2 \times \boldsymbol{H}_1) = \boldsymbol{E}_1 \cdot \boldsymbol{J}_2 + \boldsymbol{H}_2 \cdot \boldsymbol{J}_{m1} - \boldsymbol{E}_2 \cdot \boldsymbol{J}_1 - \boldsymbol{H}_1 \cdot \boldsymbol{J}_{m2}$$

If both sides are integrated over a volume V and the divergence theorem is applied to the left hand side the general form of the reciprocity theorem is found:

$$-\oiint_S (\boldsymbol{E}_1 \times \boldsymbol{H}_2 - \boldsymbol{E}_2 \times \boldsymbol{H}_1)\, ds = \iiint_V \boldsymbol{E}_1 \cdot \boldsymbol{J}_2 + \boldsymbol{H}_2 \cdot \boldsymbol{J}_{m1} - \boldsymbol{E}_2 \cdot \boldsymbol{J}_1 - \boldsymbol{H}_1 \cdot \boldsymbol{J}_{m2} dV \tag{A.3}$$

For S and V going to infinity the integrand of left hand side of equation(A.3) becomes:

$$\begin{aligned}
&\boldsymbol{E}_1 \times \boldsymbol{H}_2 - \boldsymbol{E}_2 \times \boldsymbol{H}_1 = \\
&\boldsymbol{E}_1 \times \hat{\boldsymbol{r}} \times \frac{\boldsymbol{E}_2}{\zeta} - \boldsymbol{E}_2 \times \hat{\boldsymbol{r}} \times \frac{\boldsymbol{E}_1}{\zeta} = \\
&\hat{\boldsymbol{r}}\,(\boldsymbol{E}_1 \cdot \boldsymbol{E}_2)\,\frac{1}{\zeta} - \hat{\boldsymbol{r}}\,(\boldsymbol{E}_2 \cdot \boldsymbol{E}_1)\,\frac{1}{\zeta} = 0
\end{aligned}$$

Therefore

$$\iiint_V \boldsymbol{E}_1 \cdot \boldsymbol{J}_2 - \boldsymbol{H}_1 \cdot \boldsymbol{J}_{m2} dV = \iiint_V \boldsymbol{E}_2 \cdot \boldsymbol{J}_1 - \boldsymbol{H}_2 \cdot \boldsymbol{J}_{m1} dV \tag{A.4}$$

Since in this case there are no magnetic currents equation (A.4) simplyfies to:

$$\iiint_V \boldsymbol{E}_1 \cdot \boldsymbol{J}_2 dV = \iiint_V \boldsymbol{E}_2 \cdot \boldsymbol{J}_1 dV \tag{A.5}$$

One can rewrite $\boldsymbol{E}_1$ as the convolution integral between the equivalent current $\boldsymbol{J}_1$ and the Green's function $\boldsymbol{g}^{ej}(\boldsymbol{r}, \boldsymbol{r'})$ and $\boldsymbol{E}_2$ as the convolution integral between the equivalent current $\boldsymbol{J}_2$ and the Green's function $\boldsymbol{g}^{ej}(\boldsymbol{r}, \boldsymbol{r'})$. Substituting the basis function and the test function for the equivalent currents, one recognises equation (2.19) and finds:

$$Z_{xn',xn} = Z_{xn,xn'} \tag{A.6}$$

Appendix B

Image theorem

The image theorem states that a source in the vicinity of an infinite ground plane can be respresented by the source itself and a virtual source beneath the ground plane. The electromagnetic fields calculated by this equivalent problem are equal in the region above the ground plane as those of the original problem. From the boundary conditions it is known that the electric field tangential to a perfect electric conductor equals 0:

$$\hat{\boldsymbol{n}} \times \boldsymbol{E} = 0 \tag{B.1}$$

In case of electric currents this is achieved when the virtual source is located at the same distance from the ground plane and its perpendicular orientation remains the same while its tangential orientation is reversed. According to the uniqueness theorem this solution is unique. The original problem and the equivalent problem from the image theorem is shown in figure B.1.

Let us consider an elementary electric current source above an infinite plane of perfect electric conductor. The electric field at any point in freespace due to an elementary electric current source can be found as:

$$\boldsymbol{E}(\boldsymbol{r}) = \zeta_0 \frac{e^{-jkr}}{4\pi r}\left(\cos\theta\left(\frac{2}{r^2} - \frac{2j}{kr^3}\right)\hat{r} + \sin\theta\left(\frac{jk}{r} + \frac{1}{r^2} - \frac{j}{kr^3}\right)\hat{\boldsymbol{\theta}}\right) \tag{B.2}$$

This equation can be rewritten to a Cartesian reference system using:

$$\begin{aligned} \hat{\boldsymbol{r}} &= \sin\theta\cos\phi\hat{\boldsymbol{x}} + \sin\theta\sin\phi\hat{\boldsymbol{y}} + \cos\theta\hat{\boldsymbol{z}} \\ \hat{\boldsymbol{\theta}} &= \cos\theta\cos\phi\hat{\boldsymbol{x}} + \cos\theta\sin\phi\hat{\boldsymbol{y}} - \sin\theta\hat{\boldsymbol{z}} \\ \hat{\boldsymbol{\phi}} &= -\sin\phi\hat{\boldsymbol{x}} + \cos\phi\hat{\boldsymbol{y}} \end{aligned} \tag{B.3}$$

Equation (B.2) now becomes:

$$\begin{aligned} \boldsymbol{E}(\boldsymbol{r}) = \zeta_0 \frac{e^{-jkr}}{4\pi r}\Bigg(&\left(\cos\theta\sin\theta\cos\phi\left(\frac{2}{r^2} - \frac{2j}{kr^3}\right) + \sin\theta\cos\theta\cos\phi\left(\frac{jk}{r} + \frac{1}{r^2} - \frac{j}{kr^3}\right)\right)\hat{\boldsymbol{x}} + \\ &\left(\cos\theta\sin\theta\sin\phi\left(\frac{2}{r^2} - \frac{2j}{kr^3}\right) + \sin\theta\cos\theta\sin\phi\left(\frac{jk}{r} + \frac{1}{r^2} - \frac{j}{kr^3}\right)\right)\hat{\boldsymbol{y}} + \\ &\left(\cos^2\theta\left(\frac{2}{r^2} - \frac{2j}{kr^3}\right) - \sin^2\theta\left(\frac{jk}{r} + \frac{1}{r^2} - \frac{j}{kr^3}\right)\right)\hat{\boldsymbol{z}}\Bigg) \end{aligned} \tag{B.4}$$

We can now use equation (B.4) to determine the electric field on every point on the ground

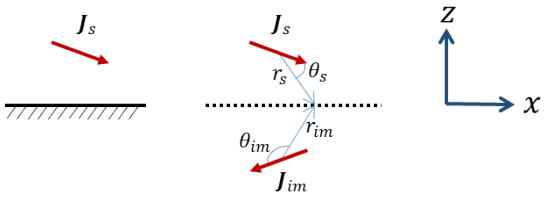

Figure B.1: Real system consisting of an electric current above a ground plane and its equivelent system consisting of the current and its image.

plane given the electric current source shown in figure B.1 and its image. It can be seen that $r_{im} = r_s = r$, $\theta_{im} = \pi - \theta_s$ and $\phi_{im} = \phi_s = \phi$. The field due to the original current equals:

$$\begin{aligned}\boldsymbol{E_1}(\boldsymbol{r}) = \zeta_0 \frac{e^{-jkr}}{4\pi r}\Bigg(&\left(\cos\theta_s \sin\theta_s \cos\phi \left(\frac{2}{r^2} - \frac{2j}{kr^3}\right) + \sin\theta_s \cos\theta_s \cos\phi \left(\frac{jk}{r} + \frac{1}{r^2} - \frac{j}{kr^3}\right)\right)\hat{\boldsymbol{x}} + \\ &\left(\cos\theta_s \sin\theta_s \sin\phi \left(\frac{2}{r^2} - \frac{2j}{kr^3}\right) + \sin\theta_s \cos\theta_s \sin\phi \left(\frac{jk}{r} + \frac{1}{r^2} - \frac{j}{kr^3}\right)\right)\hat{\boldsymbol{y}} + \\ &\left(\cos^2\theta_s \left(\frac{2}{r^2} - \frac{2j}{kr^3}\right) - \sin^2\theta_s \left(\frac{jk}{r} + \frac{1}{r^2} - \frac{j}{kr^3}\right)\right)\hat{\boldsymbol{z}}\Bigg)\end{aligned} \tag{B.5}$$

and since $\cos(\pi - \theta) = -\cos\theta$ the field due to the image of the source is simply:

$$\begin{aligned}\boldsymbol{E_2}(\boldsymbol{r}) = \zeta_0 \frac{e^{-jkr}}{4\pi r}\Bigg(&-\left(\cos\theta_s \sin\theta_s \cos\phi \left(\frac{2}{r^2} - \frac{2j}{kr^3}\right) + \sin\theta_s \cos\theta_s \cos\phi \left(\frac{jk}{r} + \frac{1}{r^2} - \frac{j}{kr^3}\right)\right)\hat{\boldsymbol{x}} + \\ &-\left(\cos\theta_s \sin\theta_s \sin\phi \left(\frac{2}{r^2} - \frac{2j}{kr^3}\right) + \sin\theta_s \cos\theta_s \sin\phi \left(\frac{jk}{r} + \frac{1}{r^2} - \frac{j}{kr^3}\right)\right)\hat{\boldsymbol{y}} + \\ &\left(\cos^2\theta_s \left(\frac{2}{r^2} - \frac{2j}{kr^3}\right) - \sin^2\theta_s \left(\frac{jk}{r} + \frac{1}{r^2} - \frac{j}{kr^3}\right)\right)\hat{\boldsymbol{z}}\Bigg)\end{aligned} \tag{B.6}$$

Summing these two fields using superposition gives:

$$\boldsymbol{E_{tot}}(\boldsymbol{r}) = \boldsymbol{E_1}(\boldsymbol{r}) + \boldsymbol{E_2}(\boldsymbol{r}) = \zeta_0 \frac{e^{-jkr}}{4\pi r}\left(\cos^2\theta_s \left(\frac{2}{r^2} - \frac{2j}{kr^3}\right) - \sin^2\theta_s \left(\frac{jk}{r} + \frac{1}{r^2} - \frac{j}{kr^3}\right)\right)\hat{\boldsymbol{z}} \tag{B.7}$$

As the perfect electric conductor is in the xy-plane and the electric field only has a normal component, this solution indeeed satisfies the boundary condition stated in equation (B.1).

Since the dipoles above a ground plane can be represented by an equivalent electric current along the dipoles, the same equivalent system can be used to represent dipoles above a ground plane.

Appendix C

MoM for dipoles oriented along x and z

Chapter 2 describes the method om moments for dipoles made of PEC oriented along x. In this appendix the expressions will be generalized to include elements along z.

$$\hat{\boldsymbol{n}} \times \boldsymbol{e}_{tot} = z_{surf}\boldsymbol{j} \tag{C.1}$$

where z_{surf} is the surface impedance on the dipoles, which is zero on the dipole arms and different from zero on the gap.

The total electric field can be decomposed in the incident field, $\boldsymbol{e}_{inc}$, and the scattered field, $\boldsymbol{e}_{scat}$, such that:

$$\begin{aligned} \hat{\boldsymbol{n}} \times (\boldsymbol{e}_{inc} + \boldsymbol{e}_{scat}) &= z_{surf}\boldsymbol{j} \\ -\hat{\boldsymbol{n}} \times \boldsymbol{e}_{scat} + z_{surf}\boldsymbol{j} &= \hat{\boldsymbol{n}} \times \boldsymbol{e}_{inc} \end{aligned} \tag{C.2}$$

The incident field is the field induced due to the voltage in the gap and is assumed constant:

$$\begin{aligned} \hat{\boldsymbol{n}} \times \boldsymbol{e}_{inc} &= \frac{v_{m_x}}{\delta}\,\mathrm{rect}_{w,\delta}(x,y) \\ \hat{\boldsymbol{n}} \times \boldsymbol{e}_{inc} &= \frac{v_{m_z}}{\delta}\,\mathrm{rect}_{w,\delta}(y,z) \end{aligned} \tag{C.3}$$

where v_m is the complex excitation voltage of the m^{th} dipole.

By using the equivalence theorem, the original problem of a dipole made of perfect electric conductor can be expressed as equivalent currents in free space. A surface S enclosing a volume V is defined just around the dipole, as shown in figure C.1a. The fields inside S, $\boldsymbol{e}_1$ and $\boldsymbol{h}_1$, are chosen to be 0. The equivalent currents need to satisfy the boundary conditions:

$$\boldsymbol{j}'_{eq} = \hat{\boldsymbol{n}} \times (\boldsymbol{h}_2 - \boldsymbol{h}_1) \tag{C.4}$$

$$\boldsymbol{m}'_{eq} = -\hat{\boldsymbol{n}} \times (\boldsymbol{e}_2 - \boldsymbol{e}_1) \tag{C.5}$$

where $\boldsymbol{h}_1$, $\boldsymbol{e}_1$ and $\boldsymbol{h}_2$, $\boldsymbol{e}_2$ are the magnetic and electric fields just inside and outside S, respectively. Since the fields outside the surface S must be equal to the original problem, we know from equation (2.1) that $\hat{\boldsymbol{n}} \times \boldsymbol{e}_2 = 0$ on the dipole arms. Therefore, the equivalent magnetic current $\boldsymbol{m}'_{eq}$ vanishes on the metal leaving only an equivalent electric current $\boldsymbol{j}'_{eq}$ as can be seen in figure C.1b. Due to the continuity of the field, i.e. the electric field below the gap $\boldsymbol{e}_2^-$ and the electric field above the gap $\boldsymbol{e}_2^+$ are equal, the magnetic current vanishes also in the gaps. For the dipole oriented along x, $\hat{\boldsymbol{n}} = \hat{\boldsymbol{z}}$ on top of the dipole and $\hat{\boldsymbol{n}} = -\hat{\boldsymbol{z}}$ on the bottom, while for the dipole

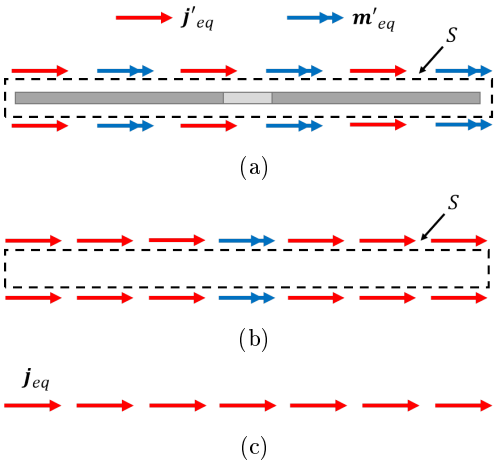

Figure C.1: Visual representation of the equivalence theorem considering a thin dipole made of perfect electric conductor. a) Defining a surface S around the dipole and the equivalent currents $\boldsymbol{j'}_{eq}$ and $\boldsymbol{m'}_{eq}$. b) Satisfying the boundary conditions the magnetic currents vanish everywhere except on the gap. c) Due to the continuity of the fields, the magnetic current in the gap vanishes and, assuming a thin dipole, an equivalent electric current $\boldsymbol{j}_{eq} = 2\boldsymbol{j'}_{eq}$ remains.

oriented along z, $\hat{\boldsymbol{n}} = \hat{\boldsymbol{x}}$ on right of the dipole and $\hat{\boldsymbol{n}} = -\hat{\boldsymbol{x}}$ on the left. Assuming the dipoles to be very thin and since the magnetic field on one side of the dipole, $\boldsymbol{h}_2^+$, is equal but opposite to the magnetic field on the other side of the dipole, $\boldsymbol{h}_2^-$, the total equivalent current can be expressed as:

$$\boldsymbol{j}_{eq} = \hat{\boldsymbol{z}} \times \boldsymbol{h}_2^+ - \hat{\boldsymbol{z}} \times \boldsymbol{h}_2^- = 2\boldsymbol{j}'_{eq} \tag{C.6}$$

in free space which is shown in figure C.1c.

The scattered field can be rewritten as a convolution between the Green's function and the equivalent electric current:

$$\boldsymbol{e}_{scat} = \int_{-\infty}^{\infty}\int_{-\infty}^{\infty}\int_{-\infty}^{\infty} \boldsymbol{j}_{eq}(\boldsymbol{r}')\boldsymbol{g}^{ej}(\boldsymbol{r},\boldsymbol{r}')d\boldsymbol{r}' \tag{C.7}$$

where $\boldsymbol{r}' \equiv (x', y', z')$ and $\boldsymbol{r} \equiv (x, y, z)$ are the source and observation points respectively. Writing the integral equations seperatly for the dipoles oriented along x and z results in:

$$\begin{aligned} -\hat{\boldsymbol{z}} \times \boldsymbol{e}_{scat} + z_{surf,x}\boldsymbol{j}_x &= \hat{\boldsymbol{z}} \times \boldsymbol{e}_{inc} \\ -\hat{\boldsymbol{x}} \times \boldsymbol{e}_{scat} + z_{surf,z}\boldsymbol{j}_z &= \hat{\boldsymbol{x}} \times \boldsymbol{e}_{inc} \end{aligned} \tag{C.8}$$

where

$$\begin{aligned} z_{surf,x}(x,y) &= \frac{z_0}{\delta}\,\mathrm{rect}_{w,\delta}(x,y) \\ z_{surf,z}(y,z) &= \frac{z_0}{\delta}\,\mathrm{rect}_{w,\delta}(y,z)\,. \end{aligned} \tag{C.9}$$

Substituting equation (C.7) in (C.8):

$$\begin{aligned} -\hat{\boldsymbol{z}} \times \int_{-\infty}^{\infty}\int_{-\infty}^{\infty}\int_{-\infty}^{\infty} \boldsymbol{j}_{eq}(\boldsymbol{r}')\boldsymbol{g}^{ej}(\boldsymbol{r},\boldsymbol{r}')d\boldsymbol{r}' + z_{surf,x}\boldsymbol{j}_x = \hat{\boldsymbol{z}} \times \boldsymbol{e}_{inc}(\boldsymbol{r}) \\ -\hat{\boldsymbol{x}} \times \int_{-\infty}^{\infty}\int_{-\infty}^{\infty}\int_{-\infty}^{\infty} \boldsymbol{j}_{eq}(\boldsymbol{r}')\boldsymbol{g}^{ej}(\boldsymbol{r},\boldsymbol{r}')d\boldsymbol{r}' + z_{surf,z}\boldsymbol{j}_z = \hat{\boldsymbol{x}} \times \boldsymbol{e}_{inc}(\boldsymbol{r}) \end{aligned} \tag{C.10}$$

The equivalent current along x and z are written as an unknown weighting terms i_{n_x} and i_{n_z} multiplied by known basis functions $\boldsymbol{b}_{n'_x}$ and $\boldsymbol{b}_{n'_z}$. Once the weighting terms i_{n_x} and i_{n_z} are calculated the current distributions over the dipoles are known. Substituting the expressions for the equivalent current in equation (C.10) gives:

$$\begin{aligned} -\hat{\boldsymbol{z}} \times \int_{-\infty}^{\infty}\int_{-\infty}^{\infty}\int_{-\infty}^{\infty} \left(\sum_{n'_x=1}^{N_x} i_{n'_x}\boldsymbol{b}_{n'_x}(\boldsymbol{r}')\hat{\boldsymbol{x}} + \sum_{n',z=1}^{N_z} i_{n'_z}\boldsymbol{b}_{n'_z}(\boldsymbol{r}')\hat{\boldsymbol{z}} \right) \boldsymbol{g}^{ej}(\boldsymbol{r},\boldsymbol{r}')d\boldsymbol{r}' + z_{surf,x}\boldsymbol{j}_x = \hat{\boldsymbol{z}} \times \boldsymbol{e}_{inc}(\boldsymbol{r}) \\ -\hat{\boldsymbol{x}} \times \int_{-\infty}^{\infty}\int_{-\infty}^{\infty}\int_{-\infty}^{\infty} \left(\sum_{n'_x=1}^{N_x} i_{n'_x}\boldsymbol{b}_{n'_x}(\boldsymbol{r}')\hat{\boldsymbol{x}} + \sum_{n'_z=1}^{N_z} i_{n'_z}\boldsymbol{b}_{n'_z}(\boldsymbol{r}')\hat{\boldsymbol{z}} \right) \boldsymbol{g}^{ej}(\boldsymbol{r},\boldsymbol{r}')d\boldsymbol{r}' + z_{surf,z}\boldsymbol{j}_x = \hat{\boldsymbol{x}} \times \boldsymbol{e}_{inc}(\boldsymbol{r}) \end{aligned} \tag{C.11}$$

Both sides of the integral equations are projected on the same known current distributions along x and z. These current distributiosn are called the test functions $\boldsymbol{t}_{n_x}$ and $\boldsymbol{t}_{n_z}$. Projecting both sides of the electric field integral equations on the test functions gives:

$$\begin{aligned} \langle -\hat{\boldsymbol{z}} \times \int_{-\infty}^{\infty}\int_{-\infty}^{\infty}\int_{-\infty}^{\infty} \left(\sum_{n'_x=1}^{N_x} i_{n'_x}\boldsymbol{b}_{n'_x}(\boldsymbol{r}')\hat{\boldsymbol{x}} + \sum_{n'_z=1}^{N_z} i_{n'_z}\boldsymbol{b}_{n'_z}(\boldsymbol{r}')\hat{\boldsymbol{z}} \right) \boldsymbol{g}^{ej}(\boldsymbol{r},\boldsymbol{r}')d\boldsymbol{r}', \boldsymbol{t}_{n_x}(\boldsymbol{r})\rangle \\ +\langle z_{surf,x}\boldsymbol{j}_x, \boldsymbol{t}_{n_x}\rangle = \langle \hat{\boldsymbol{z}} \times \boldsymbol{e}_{inc}(\boldsymbol{r}), \boldsymbol{t}_{n_x}(\boldsymbol{r})\rangle \\ \langle -\hat{\boldsymbol{x}} \times \int_{-\infty}^{\infty}\int_{-\infty}^{\infty}\int_{-\infty}^{\infty} \left(\sum_{n'_x=1}^{N_x} i_{n'_x}\boldsymbol{b}_{n'_x}(\boldsymbol{r}')\hat{\boldsymbol{x}} + \sum_{n'_z=1}^{N_z} i_{n'_z}\boldsymbol{b}_{n'_z}(\boldsymbol{r}')\hat{\boldsymbol{z}} \right) \boldsymbol{g}^{ej}(\boldsymbol{r},\boldsymbol{r}')d\boldsymbol{r}', \boldsymbol{t}_{n_z}(\boldsymbol{r})\rangle \\ +\langle z_{surf,z}\boldsymbol{j}_z, \boldsymbol{t}_{n_z}\rangle = \langle \hat{\boldsymbol{x}} \times \boldsymbol{e}_{inc}(\boldsymbol{r}), \boldsymbol{t}_{n_z}(\boldsymbol{r})\rangle \end{aligned} \tag{C.12}$$

where $\langle \boldsymbol{f}_1, \boldsymbol{f}_2 \rangle = \int_{-\infty}^{\infty}\int_{-\infty}^{\infty}\int_{-\infty}^{\infty} \boldsymbol{f}_1(\boldsymbol{r}) \cdot \boldsymbol{f}_2^*(\boldsymbol{r})d\boldsymbol{r}$, N_x and N_z are the number of basis functions along x and z respectively.

C.1 Spatial domain

Let us consider a finite number M_x of infinitely thin dipoles oriented along x and M_z along z. The elements are placed along the y-axis and can be displaced in x and z. Figure C.2 shows an example of such an array consisting of two elements. We define x_{n_x}, z_{n_x}, $x_{n'_x}$, $z_{n'_x}$ to be the x- and z-coordinates of the center of the observation domain and the center of the source domain for dipoles along x. In a similar way x_{n_z}, z_{n_z}, $x_{n'_z}$, $z_{n'_z}$ to be the x- and z-coordinates of the center of the observation domain and the center of the source domain for dipoles along z.

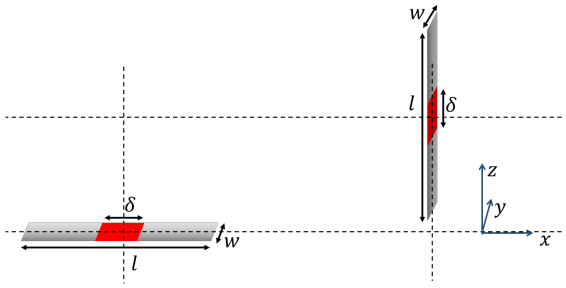

Figure C.2: Two identical dipoles with lenght l and width w oriented along x and z, centered at $y = 0$ displaced in x and z. The excitation port has a lenght δ

.

The equivalent current will be oriented along the dipole. For dipoles the transverse current distribution can be approximated to be edge-singular. The basis functions can thus be written as:

$$\begin{aligned} \boldsymbol{b}_{n'_x}(\boldsymbol{r}') &= b_{n'_x}(x' - x_{n'_x}) j_t(y') \delta(z' - z_{n'_x}) \hat{\boldsymbol{x}} \\ \boldsymbol{b}_{n'_z}(\boldsymbol{r}') &= b_{n'_z}(z' - z_{n'_z}) j_t(y') \delta(x' - x_{n'_z}) \hat{\boldsymbol{z}} \end{aligned} \tag{C.13}$$

where

$$j_t(y') = \frac{2}{w\pi} \frac{\mathrm{rect}_w(y')}{\sqrt{1 - \left(\frac{2y'}{w}\right)^2}} \tag{C.14}$$

The test function along x is chosen to be the same as the basis function. The observation domain is chosen to be along the line $y = 0$. Therefore the test functions can be written as:

$$\begin{aligned} \boldsymbol{t}_{n_x}(\boldsymbol{r}) &= b_{n_x}(x - x_{n_x}) \delta(y) \delta(z - z_n) \hat{\boldsymbol{x}} \\ \boldsymbol{t}_{n_z}(\boldsymbol{r}) &= b_{n_z}(z - z_{n_z}) \delta(y) \delta(x - x_n) \hat{\boldsymbol{z}} \end{aligned} \tag{C.15}$$

Let us define projection terms p_{nx} and p_{nz} as:

$$\begin{aligned} p_{n_x} &= \frac{1}{\delta} \langle \mathrm{rect}_{w,\delta}(x, y) \hat{\boldsymbol{x}}, \boldsymbol{t}_{n_x}(\boldsymbol{r}) \rangle \\ p_{n_z} &= \frac{1}{\delta} \langle \mathrm{rect}_{w,\delta}(y, z) \hat{\boldsymbol{z}}, \boldsymbol{t}_{n_z}(\boldsymbol{r}) \rangle \end{aligned} \tag{C.16}$$

such that

$$\begin{aligned} \langle z_{surf,x} \boldsymbol{j}_x, \boldsymbol{t}_{n_x} \rangle &= z_0 i_{n_x} p_{n_x} \\ \langle z_{surf,z} \boldsymbol{j}_z, \boldsymbol{t}_{n_z} \rangle &= z_0 i_{n_z} p_{n_z} \, . \end{aligned} \tag{C.17}$$

The projection of the electric field in the gap on an entire domain basis function can be expressed as:

$$\begin{aligned} p_{n_x} &= \frac{1}{\delta} \int_{-\infty}^{\infty} \mathrm{rect}_\delta(x - x_m) b^*_{n,x}(x - x_{n_x}) dx \approx \begin{cases} 0 & \text{if } x_{n_x} \neq x_m \\ 1 & \text{if } x_{n_x} = x_m \end{cases} \\ p_{n_z} &= \frac{1}{\delta} \int_{-\infty}^{\infty} \mathrm{rect}_\delta(z - z_m) b^*_{n,z}(z - z_{n_z}) dz \approx \begin{cases} 0 & \text{if } z_{n_z} \neq z_m \\ 1 & \text{if } z_{n_z} = z_m \end{cases} \end{aligned} \tag{C.18}$$

where it is assumed that the gap size is small compared to the total length of the dipole. For small domain basis functions, the terms p_{nx} and p_{nz} can be expressed, using the property of the

δ-function, $\int_{-\infty}^{\infty} f(x)\delta(x-x_0)dx = f(x_0)$, as:

$$p_{n_x} = \frac{1}{\delta}\int_{-\infty}^{\infty} \mathrm{rect}_\delta(x-x_m)b^*_{n,x}(x-x_{n_x})dx = \begin{cases} 0 & \text{if } n_x^{th} \text{ basis function and } m_x^{th} \text{ gap do not overlap} \\ c_n & \text{if } n_x^{th} \text{ basis function and } m_x^{th} \text{ gap do overlap} \end{cases}$$
$$p_{n_z} = \frac{1}{\delta}\int_{-\infty}^{\infty} \mathrm{rect}_\delta(z-z_m)b^*_{n,z}(z-z_{n_z})dz = \begin{cases} 0 & \text{if } n_z^{th} \text{ basis function and } m_z^{th} \text{ gap do not overlap} \\ c_n & \text{if } n_z^{th} \text{ basis function and } m_z^{th} \text{ gap do overlap} \end{cases} \tag{C.19}$$

where it is assumed that the gap size is small compared to the total length of the dipole and c_n is a constant indicating the fraction of the area of the triangular basis function that overlaps with the gap.

The left hand side of the integral equation (C.12) can now be written as:

$$\begin{aligned} &-\hat{\boldsymbol{z}} \times \int_{-\infty}^{\infty}\int_{-\infty}^{\infty}\int_{-\infty}^{\infty} \left(\int_{-\infty}^{\infty}\int_{-\infty}^{\infty}\int_{-\infty}^{\infty} \left(\sum_{n'_x=1}^{N_x} i_{n'_x} b_{n'_x}(x'-x_{n'_x}) j_t(y')\delta(z'-z_{n'_x}) b^*_{n_x}(x-x_{n_x})\delta(y)\delta(z-z_n)\hat{\boldsymbol{x}} + \right.\right. \\ &\left.\left. \sum_{n'_z=1}^{N_z} i_{n'_z} b_{n'_z}(z'-z_{n'_z}) j_t(y')\delta(x'-x_{n'_z}) b^*_{n_x}(x-x_{n_x})\delta(y)\delta(z-z_n)\hat{\boldsymbol{z}} \right) \boldsymbol{g}^{ej}(\boldsymbol{r},\boldsymbol{r}')d\boldsymbol{r}' \right) d\boldsymbol{r} + z_0 i_{n_x} p_{n_x} \\ &-\hat{\boldsymbol{x}} \times \int_{-\infty}^{\infty}\int_{-\infty}^{\infty}\int_{-\infty}^{\infty} \left(\int_{-\infty}^{\infty}\int_{-\infty}^{\infty}\int_{-\infty}^{\infty} \left(\sum_{n'_x=1}^{N_x} i_{n'_x} b_{n'_x}(x'-x_{n'_x}) j_t(y')\delta(z'-z_{n'_x}) b^*_{n_z}(z-z_{n_z})\delta(y)\delta(x-x_x)\hat{\boldsymbol{x}} + \right.\right. \\ &\left.\left. \sum_{n'_z=1}^{N_z} i_{n'_z} b_{n'_z}(z'-z_{n'_z}) j_t(y')\delta(x'-x_{n'_z}) b^*_{n_z}(z-z_{n_z})\delta(y)\delta(x-x_x)\hat{\boldsymbol{z}} \right) \boldsymbol{g}^{ej}(\boldsymbol{r},\boldsymbol{r}')d\boldsymbol{r}' \right) d\boldsymbol{r} + z_0 i_{n_z} p_{n_z}\,. \end{aligned} \tag{C.20}$$

The right hand side of the integral equation (C.12) can be written as:

$$\begin{aligned} &\sum_{n_{x'}=1}^{N_x} \frac{v_{m_x}}{\delta} \int_{-\infty}^{\infty}\int_{-\infty}^{\infty}\int_{-\infty}^{\infty} \mathrm{rect}_\delta(x-x_{m_x})\delta(z_{n_z}-z_{n'_z})\,\mathrm{rect}_w(y)\hat{\boldsymbol{x}} b^*_{n_x}(x-x_{n_x})\delta(y)\delta(z-z_n)d\boldsymbol{r} \\ &\sum_{n_{z'}=1}^{N_z} \frac{v_{m_z}}{\delta} \int_{-\infty}^{\infty}\int_{-\infty}^{\infty}\int_{-\infty}^{\infty} \mathrm{rect}_\delta(z-z_{m_z})\delta(x_{n_x}-x_{n_x})\,\mathrm{rect}_w(y)\hat{\boldsymbol{z}} b^*_{n_z}(z-z_{n_z})\delta(y)\delta(x-x_n)d\boldsymbol{r} \end{aligned} \tag{C.21}$$

We define the mutual impedances as:

$$
\begin{aligned}
Z_{x_{n'_x},x_{n_x}} &= \int_{x_{n'_x}-\frac{l_b}{2}}^{x_{n'_x}+\frac{l_b}{2}} \int_{-\frac{w}{2}}^{\frac{w}{2}} \int_{x_{n_x}-\frac{l_b}{2}}^{x_{n_x}+\frac{l_b}{2}} b_{n'_x}(x'-x_{n'_x}) j_t(y') b^*_{n_x}(x-x_{n_x}) g^{ej}_{xx}(x-x', y', z_{n_x}-z_{n'_x}) dx dy' dx' \\
Z_{z_{n'_z},x_{n_x}} &= \int_{z_{n'_z}-\frac{l_b}{2}}^{z_{n'_z}+\frac{l_b}{2}} \int_{-\frac{w}{2}}^{\frac{w}{2}} \int_{x_{n_x}-\frac{l_b}{2}}^{x_{n_x}+\frac{l_b}{2}} b_{n'_z}(z'-z_{n'_z}) j_t(y') b^*_{n_x}(x-x_{n_x}) g^{ej}_{xz}(x-x_{n'_z}, y', z_{n_x}-z') dx dy' dz' \\
Z_{x_{n'_x},z_{n_z}} &= \int_{x_{n'_x}-\frac{l_b}{2}}^{x_{n'_x}+\frac{l_b}{2}} \int_{-\frac{w}{2}}^{\frac{w}{2}} \int_{z_{n_z}-\frac{l_b}{2}}^{z_{n_z}+\frac{l_b}{2}} b_{n'_x}(x'-x_{n'_x}) j_t(y') b^*_{n_z}(z-z_{n_z}) g^{ej}_{zx}(x_{n_z}-x', y', z-z_{n'_x}) dz dy' dx' \\
Z_{z_{n'_z},z_{n_z}} &= \int_{z_{n'_z}-\frac{l_b}{2}}^{z_{n'_z}+\frac{l_b}{2}} \int_{-\frac{w}{2}}^{\frac{w}{2}} \int_{z_{n_z}-\frac{l_b}{2}}^{z_{n_z}+\frac{l_b}{2}} b_{n'_z}(z'-z_{n'_z}) j_t(y') b^*_{n_z}(z-z_{n_z}) g^{ej}_{zz}(x_{n_z}-x_{n'_z}, y', z-z') dz dy' dz'
\end{aligned}
\tag{C.22}
$$

and the forcing terms as:

$$
\begin{aligned}
v_{n_x} &= \frac{v_{m_x}}{\delta} \int_{x_{n_x}-\frac{l_b}{2}}^{x_{n_x}+\frac{l_b}{2}} \mathrm{rect}_\delta(x-x_{m_x}) b^*_{n_x}(x-x_{n_x}) dx \\
v_{n_z} &= \frac{v_{m_z}}{\delta} \int_{z_{n_z}-\frac{l_b}{2}}^{z_{n_z}+\frac{l_b}{2}} \mathrm{rect}_\delta(z-z_{m_z}) b^*_{n_z}(z-z_{n_z}) dz
\end{aligned}
\tag{C.23}
$$

such that:

$$
\begin{aligned}
\sum_{n'_x=1}^{N_x} i_{n'_x} Z_{x_{n'_x},x_{n_x}} + \sum_{n'_z=1}^{N_z} i_{n'_z} Z_{z_{n'_z},x_{n_x}} + z_0 i_{n_x} p_{n_x} &= v_{n_x} \\
\sum_{n'_z=1}^{N_z} i_{n'_z} Z_{z_{n'_z},z_{n_z}} + \sum_{n'_x=1}^{N_x} i_{n'_x} Z_{x_{n'_x},z_{n_z}} + z_0 i_{n_z} p_{n_z} &= v_{n_z}
\end{aligned}
\tag{C.24}
$$

or matrix notation as:

$$
\left(\begin{bmatrix} \boldsymbol{Z}_{x'x} & \boldsymbol{Z}_{z'x} \\ \boldsymbol{Z}_{x'z} & \boldsymbol{Z}_{z'z} \end{bmatrix} + z_0 \begin{bmatrix} \boldsymbol{P}_x & \boldsymbol{0} \\ \boldsymbol{0} & \boldsymbol{P}_z \end{bmatrix} \right) \begin{bmatrix} \boldsymbol{i}_x \\ \boldsymbol{i}_z \end{bmatrix} = \begin{bmatrix} \boldsymbol{v}_x \\ \boldsymbol{v}_z \end{bmatrix}
\tag{C.25}
$$

where $\boldsymbol{Z}_{x'x}$ is a matrix containing the terms $Z_{x_{n'_x},x_{n_x}}$, $\boldsymbol{Z}_{z'x}$ is a matrix containing the terms $Z_{z_{n'_z},x_{n_x}}$, et cetera. $\boldsymbol{P}_x$ and $\boldsymbol{P}_z$ are diagonal matrices $\boldsymbol{P}_x = diag(p_{n_x})$ and $\boldsymbol{P}_z = diag(p_{n_z})$, whose terms are zero if the n^{th} basis function is defined on the metal and different from zero if the basis function overlaps with the feeding gap region of a dipole along x or a dipole along z respectively.

C.2 Spectral domain

The spatial expressions from the previous section can be rewritten in the spectral domain. Using the spectral represenation of the Green's function:

$$
\begin{aligned}
g_{xx}^{ej}(\boldsymbol{r}-\boldsymbol{r}') &= j\frac{\zeta}{k_0}\frac{1}{(2\pi)^3}\int_{-\infty}^{\infty}\int_{-\infty}^{\infty}\int_{-\infty}^{\infty}\left(k_0^2-k_x^2\right)\frac{e^{-jk_x(x-x')}e^{-jk_y(y-y')}e^{-jk_z(z-z')}}{k_0^2-k_x^2-k_y^2-k_z^2}dk_xdk_ydk_z\\
g_{xz}^{ej}(\boldsymbol{r}-\boldsymbol{r}') &= j\frac{\zeta}{k_0}\frac{1}{(2\pi)^3}\int_{-\infty}^{\infty}\int_{-\infty}^{\infty}\int_{-\infty}^{\infty}\left(-k_xk_z\right)\frac{e^{-jk_x(x-x')}e^{-jk_y(y-y')}e^{-jk_z(z-z')}}{k_0^2-k_x^2-k_y^2-k_z^2}dk_xdk_ydk_z\\
g_{zx}^{ej}(\boldsymbol{r}-\boldsymbol{r}') &= j\frac{\zeta}{k_0}\frac{1}{(2\pi)^3}\int_{-\infty}^{\infty}\int_{-\infty}^{\infty}\int_{-\infty}^{\infty}\left(-k_xk_z\right)\frac{e^{-jk_x(x-x')}e^{-jk_y(y-y')}e^{-jk_z(z-z')}}{k_0^2-k_x^2-k_y^2-k_z^2}dk_xdk_ydk_z\\
g_{zz}^{ej}(\boldsymbol{r}-\boldsymbol{r}') &= j\frac{\zeta}{k_0}\frac{1}{(2\pi)^3}\int_{-\infty}^{\infty}\int_{-\infty}^{\infty}\int_{-\infty}^{\infty}\left(k_0^2-k_z^2\right)\frac{e^{-jk_x(x-x')}e^{-jk_y(y-y')}e^{-jk_z(z-z')}}{k_0^2-k_x^2-k_y^2-k_z^2}dk_xdk_ydk_z
\end{aligned}
\tag{C.26}
$$

Let us consider the four expressions for the active impedance seperately.

C.2.1 $Z_{x_{n'_x},x_{n_x}}$ in the spectral domain

Substituting the spectral expression for the xx-component of the Green's function in the expression for $Z_{x_{n'_x},x_{n_x}}$ found in equation (C.22) gives:

$$
\begin{aligned}
Z_{x_{n'_x},x_{n_x}} = &\int_{x_{n'_x}-\frac{l_b}{2}}^{x_{n'_x}+\frac{l_b}{2}}\int_{-\frac{w}{2}}^{\frac{w}{2}}\int_{x_{n_x}-\frac{l_b}{2}}^{x_{n_x}+\frac{l_b}{2}} b_{n'_x}(x'-x_{n'_x})j_t(y')b_{n_x}^*(x-x_{n_x})\\
&\left(j\frac{\zeta}{k_0}\frac{1}{(2\pi)^3}\int_{-\infty}^{\infty}\int_{-\infty}^{\infty}\int_{-\infty}^{\infty}\left(k_0^2-k_x^2\right)\frac{e^{-jk_x(x-x')}e^{jk_yy'}e^{-jk_z(z_{n_x}-z_{n'_x})}}{k_0^2-k_x^2-k_y^2-k_z^2}dk_xdk_ydk_z\right)dxdy'dx'
\end{aligned}
\tag{C.27}
$$

Let us consider the integral in k_z first. For $(z_{n_x}-z_{n'_x})>0$ the integration contour can be closed counter clockwise around the pole $k_z=\sqrt{k_0^2-k_x^2-k_y^2}$ and the integral can be solved using the residue theorem:

$$
\begin{aligned}
&\int_{-\infty}^{\infty}\frac{e^{-jk_z(z_{n_x}-z_{n'_x})}}{k_0^2-k_x^2-k_y^2-k_z^2}dk_z\\
&=-\int_{-\infty}^{\infty}\frac{e^{-jk_z(z_{n_x}-z_{n'_x})}}{\left(k_z-\sqrt{k_0^2-k_x^2-k_y^2}\right)\left(k_z+\sqrt{k_0^2-k_x^2-k_y^2}\right)}dk_z\\
&=-2\pi j\frac{e^{-j\sqrt{k_0^2-k_x^2-k_y^2}(z_{n_x}-z_{n'_x})}}{2\sqrt{k_0^2-k_x^2-k_y^2}}\\
&=-\pi j\frac{e^{-j\sqrt{k_0^2-k_x^2-k_y^2}(z_{n_x}-z_{n'_x})}}{2\sqrt{k_0^2-k_x^2-k_y^2}}
\end{aligned}
\tag{C.28}
$$

For $(z_{n_x} - z_{n'_x}) < 0$ the integration contour can be closed clockwise around the pole $k_z = -\sqrt{k_0^2 - k_x^2 - k_y^2}$ and the integral can be solved using the residue theorem:

$$\begin{aligned}
&\int_{-\infty}^{\infty} \frac{e^{-jk_z(z_{n_x}-z_{n'_x})}}{k_0^2 - k_x^2 - k_y^2 - k_z^2} dk_z \\
&= -\int_{-\infty}^{\infty} \frac{e^{-jk_z(z_{n_x}-z_{n'_x})}}{\left(k_z - \sqrt{k_0^2 - k_x^2 - k_y^2}\right)\left(k_z + \sqrt{k_0^2 - k_x^2 - k_y^2}\right)} dk_z \\
&= 2\pi j \frac{e^{j\sqrt{k_0^2-k_x^2-k_y^2}(z_{n_x}-z_{n'_x})}}{-2\sqrt{k_0^2 - k_x^2 - k_y^2}} \\
&= -\pi j \frac{e^{j\sqrt{k_0^2-k_x^2-k_y^2}(z_{n_x}-z_{n'_x})}}{2\sqrt{k_0^2 - k_x^2 - k_y^2}}
\end{aligned} \tag{C.29}$$

Combining equations (C.28) and (C.29) one finds that:

$$\int_{-\infty}^{\infty} \frac{e^{-jk_z(z_{n_x}-z_{n'_x})}}{k_0^2 - k_x^2 - k_y^2 - k_z^2} dk_z = -\pi j \frac{e^{-j\sqrt{k_0^2-k_x^2-k_y^2}|z_{n_x}-z_{n'_x}|}}{2\sqrt{k_0^2 - k_x^2 - k_y^2}} \tag{C.30}$$

Extracting the integral along x' from equation (C.27) gives:

$$\begin{aligned}
&\int_{x_{n'_x}-\frac{l_b}{2}}^{x_{n'_x}+\frac{l_b}{2}} b_{n'_x}(x' - x_{n'_x}) e^{jk_x x'} dx' \\
&= \int_{-\frac{l_b}{2}}^{\frac{l_b}{2}} b_{n'_x}(u) e^{jk_x u} du e^{jk_x x_{n'_x}} \\
&= B_{n'_x}(k_x) e^{jk_x x_{n'_x}}
\end{aligned} \tag{C.31}$$

where the change of variables $u = x' - x_{n'}$ is used to center the basis function around the origin. $B_{n'}(k_x)$ can be recognised to be the Fourier transform of the basis function. The exponential, $e^{jk_x x_{n'}}$, represents the phaseshift due to the displacement of the basis function from the origin. Similar steps can be performed for the integrals in y' and in x to obtain:

$$J_t(k_y) = \int_{-\frac{w}{2}}^{\frac{w}{2}} j_t(y') e^{jk_y y'} dy' = J_0\left(\frac{k_y w}{2}\right) \tag{C.32}$$

and

$$B^*_{n_x}(-k_x) e^{-jk_x x_{n_x}} = \int_{x_{n_x}-\frac{l_b}{2}}^{x_{n_x}+\frac{l_b}{2}} b^*_{n_x}(x - x_{n_x}) e^{-jk_x x} dx \tag{C.33}$$

where $J_t(k_y)$ and $B_{n_x}(k_x)$ are the Fourier transforms of $j_t(y')$ and b_{n_x} respectively. Substituting equations (C.30), (C.31), (C.32) and (C.33) into (C.27) gives:

$$Z_{x_{n'_x},x_{n_x}} = -\frac{1}{2\pi}\int_{-\infty}^{\infty} B_{n'_x}(k_x)B^*_{n_x}(-k_x)D_{n_x,n'_x}(k_x)e^{-jk_x(x_{n_x}-x_{n'_x})}dk_x \tag{C.34}$$

where

$$D_{n,n'}(k_x) = \frac{1}{2\pi}\int_{-\infty}^{\infty} J_t(k_y)G^{ej}_{xx}(k_x,k_y)e^{-j\sqrt{k_0^2-k_x^2-k_y^2}|z_{n_x}-z_{n'_x}|}dk_y \tag{C.35}$$

and

$$G^{ej}_{xx}(k_x,k_y) = -\frac{\zeta}{2k_0}\frac{\left(k_0^2-k_x^2\right)}{\sqrt{k_0^2-k_x^2-k_y^2}} \tag{C.36}$$

In the case when $|z_{n_x}-z_{n'_x}| = 0$ equation (C.35) reduces to:

$$\begin{aligned} D_{n,n'}(k_x) &= -\frac{1}{2\pi}\frac{\zeta}{2k_0}\left(k_0^2-k_x^2\right)\int_{-\infty}^{\infty}\frac{J_0\left(\frac{k_y w}{2}\right)}{\sqrt{k_0^2-k_x^2-k_y^2}}dk_y \\ &= -\frac{\zeta}{4k_0}\left(k_0^2-k_x^2\right)J_0\left(\sqrt{k_0^2-k_x^2}\frac{w}{4}\right)H_0^{(2)}\left(\sqrt{k_0^2-k_x^2}\frac{w}{4}\right) \end{aligned} \tag{C.37}$$

In the case when $|z_{n_x}-z_{n'_x}| \gg w$ equation (C.35) reduces to:

$$\begin{aligned} D_{n,n'}(k_x) &= -\frac{1}{2\pi}\frac{\zeta}{2k_0}\left(k_0^2-k_x^2\right)\int_{-\infty}^{\infty}\frac{J_0\left(\frac{k_y w}{2}\right)e^{-j\sqrt{k_0^2-k_x^2-k_y^2}|z_{n_x}-z_{n'_x}|}}{\sqrt{k_0^2-k_x^2-k_y^2}}dk_y \\ &\approx -\frac{\zeta}{4k_0}\left(k_0^2-k_x^2\right)H_0^{(2)}\left(\sqrt{k_0^2-k_x^2}|z_{n_x}-z_{n'_x}|\right) \end{aligned} \tag{C.38}$$

C.2.2 $Z_{z_{n'_z},x_{n_x}}$ in the spectral domain

Substituting the spectral expression for the xz-component of the Green's function in the expression for $Z_{z_{n'_z},x_{n_x}}$ found in equation (C.22) gives:

$$\begin{aligned} Z_{z_{n'_z},x_{n_x}} = &\int_{z_{n'_z}-\frac{l_b}{2}}^{z_{n'_z}+\frac{l_b}{2}}\int_{-\frac{w}{2}}^{\frac{w}{2}}\int_{x_{n_x}-\frac{l_b}{2}}^{x_{n_x}+\frac{l_b}{2}} b_{n'_z}(z'-z_{n'_z})j_t(y')b^*_{n_x}(x-x_{n_x}) \\ &\left(j\frac{\zeta}{k_0}\frac{1}{(2\pi)^3}\int_{-\infty}^{\infty}\int_{-\infty}^{\infty}\int_{-\infty}^{\infty}(-k_xk_z)\frac{e^{-jk_x(x-x_{n'_z})}e^{jk_yy'}e^{-jk_z(z_{n_x}-z')}}{k_0^2-k_x^2-k_y^2-k_z^2}dk_xdk_ydk_z\right)dxdy'dz' \end{aligned} \tag{C.39}$$

Extracting the integral along z' from equation (C.39) gives:

$$\begin{aligned}
&\int_{z_{n'_z}-\frac{l_b}{2}}^{z_{n'_z}+\frac{l_b}{2}} b_{n'_z}(z'-z_{n'_z})e^{jk_z z'}dz' \\
&= \int_{-\frac{l_b}{2}}^{\frac{l_b}{2}} b_{n'_z}(u)e^{jk_z u}due^{jk_z z_{n'_z}} \\
&= B_{n'_z}(k_z)e^{jk_z z_{n'_z}}
\end{aligned} \tag{C.40}$$

where the change of variables $u = z' - z_{n'}$ is used to center the basis function around the origin. $B_{n'_z}(k_z)$ can be recognised to be the Fourier transform of the basis function. The exponential, $e^{jk_z z_{n'_z}}$, represents the phaseshift due to the displacement of the basis function from the origin. Similar steps can be performed for the integrals in y' to obtain:

$$J_t(k_y) = \int_{-\frac{w}{2}}^{\frac{w}{2}} j_t(y')e^{jk_y y'}dy' = J_0\left(\frac{k_y w}{2}\right) \tag{C.41}$$

where $J_t(k_y)$ is the Fourier transform of $j_t(y')$. Subtituting equations (C.40) and (C.41) into equation (C.39) gives:

$$\begin{aligned}
Z_{z_{n'_z},x_{n_x}} = j\frac{\zeta}{k_0}\frac{1}{(2\pi)^3}\int_{x_{n_x}-\frac{l_b}{2}}^{x_{n_x}+\frac{l_b}{2}} b^*_{n_x}(x-x_{n_x})\int_{-\infty}^{\infty}\int_{-\infty}^{\infty}\int_{-\infty}^{\infty}(-k_x k_z) \\
B_{n'_z}(k_z)J_t(k_y)\frac{e^{-jk_x(x-x_{n'_z})}e^{-jk_z(z_{n_x}-z_{n'_z})}}{k_0^2-k_x^2-k_y^2-k_z^2}dk_x dk_y dk_z dx
\end{aligned} \tag{C.42}$$

Three cases must be considered, as is shown in figure C.3:

1. $x_{n'_z} < x_{n_x} - \frac{l_b}{2}$

2. $x_{n'_z} > x_{n_x} + \frac{l_b}{2}$

3. $x_{n_x} - \frac{l_b}{2} < x_{n'_z} < x_{n_x} + \frac{l_b}{2}$

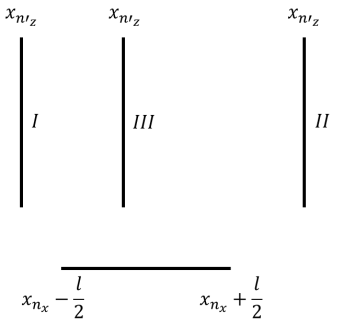

Figure C.3: Three cases of for $|x_{n_x} - x_{n'_z}|$.

Case I ($x_{n'_z} < x_{n_x} - \frac{l_b}{2}$)

Since $x - x_{n'_z} > 0 \forall x$ the integration contour for the integration along k_x can be closed counter clockwise around $k_x = \sqrt{k_0^2 - k_y^2 - k_z^2}$:

$$\begin{aligned}
&\int_{-\infty}^{\infty} k_x \frac{e^{-jk_x(x-x_{n'_z})}}{k_0^2 - k_x^2 - k_y^2 - k_z^2} dk_x \\
&= -\int_{-\infty}^{\infty} k_x \frac{e^{-jk_x(x-x_{n'_z})}}{\left(k_x - \sqrt{k_0^2 - k_y^2 - k_z^2}\right)\left(k_x + \sqrt{k_0^2 - k_y^2 - k_x^2}\right)} dk_x \\
&= -2\pi j \sqrt{k_0^2 - k_y^2 - k_z^2} \frac{e^{-j\sqrt{k_0^2 - k_y^2 - k_z^2}(x-x_{n'_z})}}{2\sqrt{k_0^2 - k_y^2 - k_z^2}} \\
&= -\pi j e^{-j\sqrt{k_0^2 - k_y^2 - k_z^2}|x-x_{n'_z}|}
\end{aligned} \tag{C.43}$$

The integral along x can now be solved to be:

$$B^*_{n_x}\left(-\sqrt{k_0^2 - k_y^2 - k_z^2}\right) e^{-j\sqrt{k_0^2 - k_y^2 - k_z^2}x_{n_x}} = \int_{x_{n_x}-\frac{l_b}{2}}^{x_{n_x}+\frac{l_b}{2}} b^*_{n_x}(x - x_{n_x}) e^{-j\sqrt{k_0^2 - k_y^2 - k_z^2}x} dx \tag{C.44}$$

Substituting equations (C.43) and (C.44) into (C.42):

$$\begin{aligned}
Z_{z_{n'_z}, x_{n_x}} = -\frac{\zeta}{k_0}\frac{1}{8\pi^2} \int_{-\infty}^{\infty}\int_{-\infty}^{\infty} k_z \\
B_{n'_z}(k_z) J_t(k_y) B^*_{n_x}\left(-\sqrt{k_0^2 - k_y^2 - k_z^2}\right) \frac{e^{-j\sqrt{k_0^2 - k_y^2 - k_z^2}|x_{n_x} - x_{n'_z}|} e^{-jk_z(z_{n_x} - z_{n'_z})}}{k_0^2 - k_y^2 - k_z^2} dk_y dk_z
\end{aligned} \tag{C.45}$$

Case II ($x_{n'_z} > x_{n_x} + \frac{l_b}{2}$)

Since $x - x_{n'_z} < 0 \forall x$ the integration contour for the integration along k_x can be closed clockwise around $k_x = -\sqrt{k_0^2 - k_y^2 - k_z^2}$:

$$\begin{aligned}
&\int_{-\infty}^{\infty} k_x \frac{e^{-jk_x(x-x_{n'_z})}}{k_0^2 - k_x^2 - k_y^2 - k_z^2} dk_x \\
&= -\int_{-\infty}^{\infty} k_x \frac{e^{-jk_x(x-x_{n'_z})}}{\left(k_x - \sqrt{k_0^2 - k_y^2 - k_z^2}\right)\left(k_x + \sqrt{k_0^2 - k_y^2 - k_x^2}\right)} dk_x \\
&= -2\pi j \sqrt{k_0^2 - k_y^2 - k_z^2} \frac{e^{j\sqrt{k_0^2-k_y^2-k_z^2}(x-x_{n'_z})}}{-2\sqrt{k_0^2 - k_y^2 - k_z^2}} \\
&= \pi j e^{-j\sqrt{k_0^2-k_y^2-k_z^2}|x-x_{n'_z}|}
\end{aligned} \tag{C.46}$$

The integral along x can now be solved to be:

$$B^*_{n_x}\left(-\sqrt{k_0^2 - k_y^2 - k_z^2}\right) e^{-j\sqrt{k_0^2-k_y^2-k_z^2}x_{n_x}} = \int_{x_{n_x}-\frac{l_b}{2}}^{x_{n_x}+\frac{l_b}{2}} b^*_{n_x}(x - x_{n_x}) e^{-j\sqrt{k_0^2-k_y^2-k_z^2}x} dx \tag{C.47}$$

Substituting equations (C.46) and (C.47) into (C.42):

$$\begin{aligned}
Z_{z_{n'_z}, x_{n_x}} = \frac{\zeta}{k_0} \frac{1}{8\pi^2} \int_{-\infty}^{\infty} \int_{-\infty}^{\infty} k_z \\
B_{n'_z}(k_z) J_t(k_y) B^*_{n_x}\left(-\sqrt{k_0^2 - k_y^2 - k_z^2}\right) \frac{e^{-j\sqrt{k_0^2-k_y^2-k_z^2}|x_{n_x}-x_{n'_z}|} e^{-jk_z(z_{n_x}-z_{n'_z})}}{k_0^2 - k_y^2 - k_z^2} dk_y dk_z
\end{aligned} \tag{C.48}$$

Case III ($x_{n_x} - \frac{l_b}{2} < x_{n'_z} < x_{n_x} + \frac{l_b}{2}$)

The integration domain along x is split in two: $x - x_{n'_z} > 0$ and $x - x_{n'_z} < 0$. The integral along k_x is closed counter clockwise for the values for x corresponding to $x - x_{n'_z} > 0$ and clockwise for the values of x corresponding to $x - x_{n'_z} < 0$ in the same way as shown for cases I and II. The integral along x is calculated in two parts:

$$\int_{x_{n_x}-\frac{l_b}{2}}^{x_{n_z}} b^*_{n_x}(x - x_{n_x}) e^{-j\sqrt{k_0^2-k_y^2-k_z^2}x} dx \tag{C.49}$$

and

$$\int_{x_{n_z}}^{x_{n_x}+\frac{l_b}{2}} b^*_{n_x}(x - x_{n_x}) e^{-j\sqrt{k_0^2-k_y^2-k_z^2}x} dx \tag{C.50}$$

The expression for the active impedance $Z_{z_{n'_z},x_{n_x}}$ can now be found to be:

$$Z_{z_{n'_z},x_{n_x}} = \frac{\zeta}{k_0}\frac{1}{8\pi^2}\int_{-\infty}^{\infty}\int_{-\infty}^{\infty} B_{n'_z}(k_z)J_t(k_y)\Bigg(- k_z \int_{x_{n_x}-\frac{l_b}{2}}^{x_{n_z}} b^*_{n_x}(x-x_{n_x})e^{-j\sqrt{k_0^2-k_y^2-k_z^2}x}dx$$
$$+ k_z \int_{x_{n_z}}^{x_{n_x}+\frac{l_b}{2}} b^*_{n_x}(x-x_{n_x})e^{-j\sqrt{k_0^2-k_y^2-k_z^2}x}dx\Bigg)\frac{e^{-j\sqrt{k_0^2-k_y^2-k_z^2}|x_{n_x}-x_{n'_z}|}e^{-jk_z(z_{n_x}-z_{n'_z})}}{k_0^2-k_y^2-k_z^2}dk_ydk_z \tag{C.51}$$

C.2.3 $Z_{x_{n'_x},z_{n_z}}$ in the spectral domain

Substituting the spectral expression for the zx-component of the Green's function in the expression for $Z_{x_{n'_x},z_{n_z}}$ found in equation (C.22) gives:

$$Z_{x_{n'_x},z_{n_z}} = \int_{x_{n'_x}-\frac{l_b}{2}}^{x_{n'_x}+\frac{l_b}{2}}\int_{-\frac{w}{2}}^{\frac{w}{2}}\int_{z_{n_z}-\frac{l_b}{2}}^{z_{n_z}+\frac{l_b}{2}} b_{n'_x}(x'-x_{n'_x})j_t(y')b^*_{n_z}(z-z_{n_z})$$
$$\left(j\frac{\zeta}{k_0}\frac{1}{(2\pi)^3}\int_{-\infty}^{\infty}\int_{-\infty}^{\infty}\int_{-\infty}^{\infty}(-k_xk_z)\frac{e^{-jk_x(x_{n_z}-x')}e^{jk_yy'}e^{-jk_z(z-z_{n'_x})}}{k_0^2-k_x^2-k_y^2-k_z^2}dk_xdk_ydk_z\right)dzdy'dx' \tag{C.52}$$

Extracting the integral along x' from equation (C.52) gives:

$$\begin{aligned}&\int_{x_{n'_x}-\frac{l_b}{2}}^{x_{n'_x}+\frac{l_b}{2}} b_{n'_x}(x'-x_{n'_x})e^{jk_xx'}dx' \\ &= \int_{-\frac{l_b}{2}}^{\frac{l_b}{2}} b_{n'_x}(u)e^{jk_xu}due^{jk_xx_{n'_x}} \\ &= B_{n'_x}(k_x)e^{jk_xx_{n'_x}}\end{aligned} \tag{C.53}$$

where the change of variables $u = x - x_{n'}$ is used to center the basis function around the origin. $B_{n'_x}(k_x)$ can be recognised to be the Fourier transform of the basis function. The exponential, $e^{jk_xx_{n'_x}}$, represents the phaseshift due to the displacement of the basis function from the origin. Similar steps can be performed for the integrals in y' to obtain:

$$J_t(k_y) = \int_{-\frac{w}{2}}^{\frac{w}{2}} j_t(y')e^{jk_yy'}dy' = J_0\left(\frac{k_yw}{2}\right) \tag{C.54}$$

where $J_t(k_y)$ is the Fourier transform of $j_t(y')$. Subtituting equations (C.40) and (C.41) into

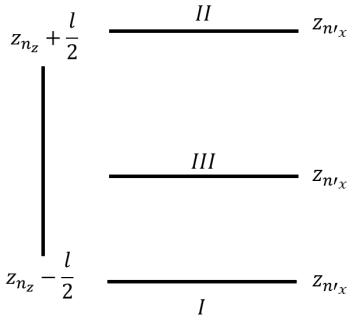

Figure C.4: Three cases of for $|z_{n_z} - z_{n'_x}|$.

equation (C.52) gives:

$$Z_{x_{n'_x},z_{n_z}} = j\frac{\zeta}{k_0}\frac{1}{(2\pi)^3}\int_{z_{n_z}-\frac{l_b}{2}}^{z_{n_z}+\frac{l_b}{2}} b^*_{n_z}(z-z_{n_z})\int_{-\infty}^{\infty}\int_{-\infty}^{\infty}\int_{-\infty}^{\infty}(-k_xk_z) \\ B_{n'_x}(k_x)J_t(k_y)\frac{e^{-jk_x(x_n-x_{n'_z})}e^{-jk_z(z-z_{n'_z})}}{k_0^2-k_x^2-k_y^2-k_z^2}dk_xdk_ydk_zdz \tag{C.55}$$

Three cases must be considered, as is shown in figure C.4:

1. $z_{n'_x} < z_{n_z} - \frac{l_b}{2}$
2. $z_{n'_x} > z_{n_z} + \frac{l_b}{2}$
3. $z_{n_z} - \frac{l_b}{2} < z_{n'_x} < z_{n_z} + \frac{l_b}{2}$

Case I ($z_{n'_x} < z_{n_z} - \frac{l_b}{2}$)

Since $z - z_{n'_x} > 0 \forall z$ the integration contour for the integration along k_z can be closed counter clockwise around $k_z = \sqrt{k_0^2 - k_x^2 - k_y^2}$:

$$\begin{aligned}
&\int_{-\infty}^{\infty} k_z\frac{e^{-jk_z(z-z_{n'_x})}}{k_0^2-k_x^2-k_y^2-k_z^2}dk_z \\
&= -\int_{-\infty}^{\infty} k_z\frac{e^{-jk_z(z-z_{n'_x})}}{\left(k_z-\sqrt{k_0^2-k_x^2-k_y^2}\right)\left(k_z+\sqrt{k_0^2-k_x^2-k_y^2}\right)}dk_z \\
&= -2\pi j\sqrt{k_0^2-k_x^2-k_y^2}\frac{e^{-j\sqrt{k_0^2-k_x^2-k_y^2}(z-z_{n'_x})}}{2\sqrt{k_0^2-k_x^2-k_y^2}} \\
&= -\pi j e^{-j\sqrt{k_0^2-k_x^2-k_y^2}|z-z_{n'_x}|}
\end{aligned} \tag{C.56}$$

The integral along z can now be solved to be:

$$B^*_{n_z}\left(-\sqrt{k_0^2-k_x^2-k_y^2}\right)e^{-j\sqrt{k_0^2-k_x^2-k_y^2}z_{n_z}} = \int_{z_{n_z}-\frac{l_b}{2}}^{z_{n_z}+\frac{l_b}{2}} b^*_{n_z}(z-z_{n_z})e^{-j\sqrt{k_0^2-k_x^2-k_y^2}z}dz \tag{C.57}$$

Substituting equations (C.56) and (C.57) into (C.55):

$$Z_{x_{n'_x},z_{n_z}} = -\frac{\zeta}{k_0}\frac{1}{8\pi^2}\int_{-\infty}^{\infty}\int_{-\infty}^{\infty} k_x \\ B_{n'_x}(k_x)J_t(k_y)B^*_{n_z}\left(-\sqrt{k_0^2-k_x^2-k_y^2}\right)\frac{e^{-j\sqrt{k_0^2-k_x^2-k_y^2}|z_{n_z}-z_{n'_x}|}e^{-jk_x(x_{n_z}-x_{n'_x})}}{k_0^2-k_x^2-k_y^2}dk_xdk_y \tag{C.58}$$

Case II ($z_{n'_x} > z_{n_z} + \frac{l_b}{2}$)

Since $z - z_{n'_x} < 0 \forall z$ the integration contour for the integration along k_z can be closed clockwise around $k_z = -\sqrt{k_0^2-k_x^2-k_y^2}$:

$$\begin{aligned}
&\int_{-\infty}^{\infty} k_z \frac{e^{-jk_z(z-z_{n'_x})}}{k_0^2-k_x^2-k_y^2-k_z^2}dk_z \\
&= -\int_{-\infty}^{\infty} k_z \frac{e^{-jk_z(z-z_{n'_x})}}{\left(k_z-\sqrt{k_0^2-k_x^2-k_y^2}\right)\left(k_z+\sqrt{k_0^2-k_x^2-k_y^2}\right)}dk_z \\
&= -2\pi j\sqrt{k_0^2-k_x^2-k_y^2}\frac{e^{j\sqrt{k_0^2-k_x^2-k_y^2}(z-z_{n'_x})}}{-2\sqrt{k_0^2-k_x^2-k_y^2}} \\
&= \pi j e^{-j\sqrt{k_0^2-k_x^2-k_y^2}|z-z_{n'_x}|}
\end{aligned} \tag{C.59}$$

The integral along z can now be solved to be:

$$B^*_{n_z}\left(-\sqrt{k_0^2-k_x^2-k_y^2}\right)e^{-j\sqrt{k_0^2-k_x^2-k_y^2}z_{n_z}} = \int_{z_{n_z}-\frac{l_b}{2}}^{z_{n_z}+\frac{l_b}{2}} b^*_{n_z}(z-z_{n_z})e^{-j\sqrt{k_0^2-k_x^2-k_y^2}z}dz \tag{C.60}$$

Substituting equations (C.59) and (C.60) into (C.55):

$$Z_{x_{n'_x},z_{n_z}} = \frac{\zeta}{k_0}\frac{1}{8\pi^2}\int_{-\infty}^{\infty}\int_{-\infty}^{\infty} k_x \\ B_{n'_x}(k_x)J_t(k_y)B^*_{n_z}\left(-\sqrt{k_0^2-k_x^2-k_y^2}\right)\frac{e^{-j\sqrt{k_0^2-k_x^2-k_y^2}|z_{n_z}-z_{n'_x}|}e^{-jk_x(x_{n_z}-x_{n'_x})}}{k_0^2-k_x^2-k_y^2}dk_xdk_y \tag{C.61}$$

Case III ($z_{n_z} - \frac{l_b}{2} < z_{n'_x} < z_{n_z} + \frac{l_b}{2}$)

The integration domain along z is split in two: $z - z_{n'_x} > 0$ and $z - z_{n'_x} < 0$. The integral along k_z is closed counter clockwise for the values for z corresponding to $z - z_{n'_x} > 0$ and clockwise for the values of z corresponding to $z - z_{n'_x} < 0$ in the same way as shown for cases I and II. The integral along z is calculated in two parts:

$$\int_{z_{n_z}-\frac{l_b}{2}}^{z_{n_x}} b^*_{n_z}(z-z_{n_z})e^{-j\sqrt{k_0^2-k_x^2-k_y^2}z}dz \tag{C.62}$$

and

$$\int_{z_{n_x}}^{z_{n_z}+\frac{l_b}{2}} b^*_{n_z}(z-z_{n_z})e^{-j\sqrt{k_0^2-k_x^2-k_y^2}z}dz \tag{C.63}$$

The expression for the active impedance $Z_{x_{n'_x},z_{n_z}}$ can now be found to be:

$$\begin{aligned} Z_{x_{n'_x},z_{n_z}} = \frac{\zeta}{k_0}\frac{1}{8\pi^2}\int_{-\infty}^{\infty}\int_{-\infty}^{\infty} B_{n'_x}(k_x)J_t(k_y)\Bigg(- k_x \int_{z_{n_z}-\frac{l_b}{2}}^{z_{n_x}} b^*_{n_z}(z-z_{n_z})e^{-j\sqrt{k_0^2-k_x^2-k_y^2}z}dz \\ + k_x \int_{z_{n_x}}^{z_{n_z}+\frac{l_b}{2}} b^*_{n_z}(z-z_{n_z})e^{-j\sqrt{k_0^2-k_x^2-k_y^2}z}dz\Bigg)\frac{e^{-j\sqrt{k_0^2-k_x^2-k_y^2}|z_{n_z}-z_{n'_x}|}e^{-jk_x(x_{n_z}-x_{n'_x})}}{k_0^2-k_x^2-k_y^2}dk_xdk_y \end{aligned} \tag{C.64}$$

C.2.4 $Z_{z_{n'_z},z_{n_z}}$ in the spectral domain

Substituting the spectral expression for the zz-component of the Green's function in the expression for $Z_{z_{n'_z},z_{n_z}}$ found in equation (C.22) gives:

$$\begin{aligned} Z_{z_{n'_z},z_{n_z}} = \int_{z_{n'_z}-\frac{l_b}{2}}^{z_{n'_z}+\frac{l_b}{2}}\int_{-\frac{w}{2}}^{\frac{w}{2}}\int_{z_{n_z}-\frac{l_b}{2}}^{z_{n_z}+\frac{l_b}{2}} b_{n'_z}(z'-z_{n'_z})j_t(y')b^*_{n_z}(z-z_{n_z}) \\ \left(j\frac{\zeta}{k_0}\frac{1}{(2\pi)^3}\int_{-\infty}^{\infty}\int_{-\infty}^{\infty}\int_{-\infty}^{\infty}(k_0^2-k_z^2)\frac{e^{-jk_x(x_{n_z}-x_{n'_z}}e^{jk_yy'}e^{-jk_z(z-z')}}{k_0^2-k_x^2-k_y^2-k_z^2}dk_xdk_ydk_z\right)dzdy'dz' \end{aligned} \tag{C.65}$$

Let us consider the integral in k_x first. For $(x_{n_z}-x_{n'_z})>0$ the integration contour can be closed counter clockwise around the pole $k_x=\sqrt{k_0^2-k_y^2-k_z^2}$ and the integral can be solved using the residue theorem:

$$\begin{aligned} &\int_{-\infty}^{\infty}\frac{e^{-jk_x(x_{n_z}-x_{n'_z})}}{k_0^2-k_x^2-k_y^2-k_z^2}dk_x \\ &= -\int_{-\infty}^{\infty}\frac{e^{-jk_x(x_{n_z}-x_{n'_z})}}{\left(k_x-\sqrt{k_0^2-k_y^2-k_z^2}\right)\left(k_x+\sqrt{k_0^2-k_y^2-k_z^2}\right)}dk_x \\ &= -2\pi j\frac{e^{-j\sqrt{k_0^2-k_y^2-k_z^2}(x_{n_z}-x_{n'_z})}}{2\sqrt{k_0^2-k_y^2-k_z^2}} \\ &= -\pi j\frac{e^{-j\sqrt{k_0^2-k_y^2-k_z^2}(x_{n_z}-x_{n'_z})}}{2\sqrt{k_0^2-k_y^2-k_z^2}} \end{aligned} \tag{C.66}$$

For $(x_{n_z} - x_{n'_z}) < 0$ the integration contour can be closed clockwise around the pole $k_x = -\sqrt{k_0^2 - k_z^2 - k_z^2}$ and the integral can be solved using the residue theorem:

$$\begin{aligned}
&\int_{-\infty}^{\infty} \frac{e^{-jk_x(x_{n_z} - x_{n'_z})}}{k_0^2 - k_x^2 - k_y^2 - k_z^2} dk_x \\
&= -\int_{-\infty}^{\infty} \frac{e^{-jk_x(x_{n_z} - x_{n'_z})}}{\left(k_x - \sqrt{k_0^2 - k_y^2 - k_z^2}\right)\left(k_x + \sqrt{k_0^2 - k_y^2 - k_z^2}\right)} dk_x \\
&= 2\pi j \frac{e^{j\sqrt{k_0^2 - k_y^2 - k_z^2}(x_{n_z} - x_{n'_z})}}{-2\sqrt{k_0^2 - k_y^2 - k_z^2}} \\
&= -\pi j \frac{e^{j\sqrt{k_0^2 - k_y^2 - k_z^2}(x_{n_z} - x_{n'_z})}}{2\sqrt{k_0^2 - k_y^2 - k_z^2}}
\end{aligned} \tag{C.67}$$

Combining equations (C.66) and (C.67) one finds that:

$$\int_{-\infty}^{\infty} \frac{e^{-jk_x(x_{n_z} - x_{n'_z})}}{k_0^2 - k_x^2 - k_y^2 - k_z^2} dk_x = -\pi j \frac{e^{-j\sqrt{k_0^2 - k_y^2 - k_z^2}|x_{n_z} - x_{n'_z}|}}{2\sqrt{k_0^2 - k_y^2 - k_z^2}} \tag{C.68}$$

Extracting the integral along z' from equation (C.65) gives:

$$\begin{aligned}
&\int_{z_{n'_z} - \frac{l_b}{2}}^{z_{n'_z} + \frac{l_b}{2}} b_{n'_z}(z' - z_{n'_z}) e^{jk_z z'} dz' \\
&= \int_{-\frac{l_b}{2}}^{\frac{l_b}{2}} b_{n'_z}(u) e^{jk_z u} du e^{jk_z z_{n'_z}} \\
&= B_{n'_z}(k_z) e^{jk_z z_{n'_z}}
\end{aligned} \tag{C.69}$$

where the change of variables $u = z' - z_{n'}$ is used to center the basis function around the origin. $B_{n'}(k_z)$ can be recognised to be the Fourier transform of the basis function. The exponential, $e^{jk_z z_{n'}}$, represents the phaseshift due to the displacement of the basis function from the origin. Similar steps can be performed for the integrals in y' and in z to obtain:

$$J_t(k_y) = \int_{-\frac{w}{2}}^{\frac{w}{2}} j_t(y') e^{jk_y y'} dy' = J_0\left(\frac{k_y w}{2}\right) \tag{C.70}$$

and

$$B^*_{n_z}(-k_z) e^{-jk_z z_{n_z}} = \int_{z_{n_z} - \frac{l_b}{2}}^{z_{n_z} + \frac{l_b}{2}} b^*_{n_z}(z - z_{n_z}) e^{-jk_z z} dz \tag{C.71}$$

where $J_t(k_y)$ and $B_{n_z}(k_z)$ are the Fourier transforms of $j_t(y')$ and b_{n_z} respectively. Substituting equations (C.68), (C.69), (C.70) and (C.71) into (C.65) gives:

$$Z_{z_{n'_z},z_{n_z}} = -\frac{1}{2\pi}\int_{-\infty}^{\infty} B_{n'_z}(k_z)B^*_{n_z}(-k_z)D_{n_z,n'_z}(k_z)e^{-jk_z(z_{n_z}-z_{n'_z})}dk_z \tag{C.72}$$

where

$$D_{n_z,n'_z}(k_z) = \frac{1}{2\pi}\int_{-\infty}^{\infty} J_t(k_y)G^{ej}_{zz}(k_y,k_z)e^{-j\sqrt{k_0^2-k_y^2-k_z^2}|x_{n_z}-x_{n'_z}|}dk_y \tag{C.73}$$

and

$$G^{ej}_{zz}(k_y,k_z) = -\frac{\zeta}{2k_0}\frac{\left(k_0^2-k_z^2\right)}{\sqrt{k_0^2-k_y^2-k_z^2}} \tag{C.74}$$

In the case when $|x_{n_z}-x_{n'_z}| = 0$ equation (C.73) reduces to:

$$\begin{aligned} D_{n,n'}(k_z) &= -\frac{1}{2\pi}\frac{\zeta}{2k_0}\left(k_0^2-k_z^2\right)\int_{-\infty}^{\infty}\frac{J_0\left(\frac{k_y w}{2}\right)}{\sqrt{k_0^2-k_y^2-k_z^2}}dk_y \\ &= -\frac{\zeta}{4k_0}\left(k_0^2-k_z^2\right)J_0\left(\sqrt{k_0^2-k_z^2}\frac{w}{4}\right)H_0^{(2)}\left(\sqrt{k_0^2-k_z^2}\frac{w}{4}\right) \end{aligned} \tag{C.75}$$

In the case when $|x_{n_z}-x_{n'_z}| \gg w$ equation (C.73) reduces to:

$$\begin{aligned} D_{n,n'}(k_z) &= -\frac{1}{2\pi}\frac{\zeta}{2k_0}\left(k_0^2-k_z^2\right)\int_{-\infty}^{\infty}\frac{J_0\left(\frac{k_y w}{2}\right)e^{-j\sqrt{k_0^2-k_y^2-k_z^2}|x_{n_z}-x_{n'_z}|}}{\sqrt{k_0^2-k_y^2-k_z^2}}dk_y \\ &\approx -\frac{\zeta}{4k_0}\left(k_0^2-k_z^2\right)H_0^{(2)}\left(\sqrt{k_0^2-k_z^2}|x_{n_z}-x_{n'_z}|\right) \end{aligned} \tag{C.76}$$

C.2.5 Voltages in spectral domain

Besides the active impedance also the voltages, as found in equation (C.23), can be expressed in the spectral domain:

$$
\begin{aligned}
v_{n_x} &= \frac{v_{m_x}}{\delta} \int_{x_{n_x}-\frac{l_b}{2}}^{x_{n_x}+\frac{l_b}{2}} \mathrm{rect}_\delta(x - x_{m_x}) b^*_{n_x}(x - x_{n_x}) dx \\
&= \frac{v_{m_x}}{\delta} \int_{x_{n_x}-\frac{l_b}{2}}^{x_{n_x}+\frac{l_b}{2}} \left(\frac{1}{2\pi} \int_{-\infty}^{\infty} \delta \,\mathrm{sinc}\left(\frac{k_x \delta}{2}\right) e^{-jk_x(x-x_{m_x})} dk_x \right) b^*_{n_x}(x - x_{n_x}) dx \\
&= \frac{v_{m_x}}{2\pi} \int_{-\infty}^{\infty} \mathrm{sinc}\left(\frac{k_x \delta}{2}\right) B^*_{n_x}(-k_x) e^{-jk_x(x_{n_x}-x_{m_x})} dk_x \\
v_{n_z} &= \frac{v_{m_z}}{\delta} \int_{z_{n_z}-\frac{l_b}{2}}^{z_{n_z}+\frac{l_b}{2}} \mathrm{rect}_\delta(z - z_{n_z}) b^*_{n_z}(z - z_{n_z}) dz \\
&= \frac{v_{m_z}}{\delta} \int_{z_{n_z}-\frac{l_b}{2}}^{z_{n_z}+\frac{l_b}{2}} \left(\frac{1}{2\pi} \int_{-\infty}^{\infty} \delta \,\mathrm{sinc}\left(\frac{k_z \delta}{2}\right) e^{-jk_z(z-z_{m_z})} dk_z \right) b^*_{n_z}(z - z_{n_z}) dz \\
&= \frac{v_{m_z}}{2\pi} \int_{-\infty}^{\infty} \mathrm{sinc}\left(\frac{k_z \delta}{2}\right) B^*_{n_z}(-k_z) e^{-jk_z(z_{n_z}-z_{m_z})} dk_z
\end{aligned}
\tag{C.77}
$$

C.3 Calculation of radiation pattern

This section will describe how the far field pattern can be found once the current vector $\boldsymbol{i}$ has been found. One can imagine a sphere with radius r centered in the origin. Every point on the surface of this sphere can be expressed in terms of two angles: the elevation angle θ and the azimuthal angle ϕ, where $\theta = 0$ is along the z-axis and $\phi = 0$ is along the x-axis. Every point on the surface of this sphere can be expressed in Cartesian coordinates as:

$$
\begin{aligned}
x_0 &= r \sin\theta \cos\phi \\
y_0 &= r \sin\theta \sin\phi \\
z_0 &= r \cos\theta
\end{aligned}
\tag{C.78}
$$

The electric field due to an electric current source can be found in any point $\boldsymbol{r}$ by calculating the convolution between the equivalent current, $\boldsymbol{j}_{eq}$, and the dyadic Green's function, $\boldsymbol{g}^{ej}$, evaluated in the point (x_0, y_0, z_0). Since convolution in the spatial domain is equivalent to multiplication in the spectral domain, the electric field can be found as:

$$
\boldsymbol{E}(x, y, z) = \frac{1}{(2\pi r)^2} \int_{-\infty}^{\infty} \int_{-\infty}^{\infty} \boldsymbol{J}_{eq}(k_x, k_y) \boldsymbol{G}^{ej}(k_x, k_y, z, z') e^{-jk_x x} e^{-jk_y y} dk_x dk_y \,. \tag{C.79}
$$

where $k_{x0} = k_0 \sin\theta\cos\phi$, $k_{y0} = k_0 \sin\theta \sin\phi$ and $k_{z0} = k_0 \cos\theta$. The equivalent current distributions of dipoles oriented along x and z, can be expressed as:

$$
\begin{aligned}
\boldsymbol{J}_{eq,x}(k_x, k_y) &= i_{n'_x} B_{n'_x}(k_x) J_t(k_y) \hat{\boldsymbol{x}} \\
\boldsymbol{J}_{eq,z}(k_y, k_z) &= i_{n'_z} B_{n'_z}(k_z) J_t(k_y) \hat{\boldsymbol{z}}
\end{aligned}
\tag{C.80}
$$

The total electric field due to all basis functions can be expressed as the sum of the individual contributions from every basis function. The total electric field in (x_0, y_0, z_0) can thus be found, by applying the stationary phase point approximation.

$$\boldsymbol{E}(x_0,y_0,z_0) = jk_{z0}\frac{1}{2\pi r}\left(\sum_{n'_x=1}^{N_x} i_{n'_x}B_{n'_x}(k_x)J_t(k_y)\hat{\boldsymbol{x}}\boldsymbol{G}^{ej}(k_{x0},k_{y0})e^{-jk_{x0}(x_0-x_{n'_x})}e^{-jk_{y0}(y_0-y_{n'_x})}\right.$$
$$\left.e^{-jk_{z0}(z_0-z_{n'_x})} + \sum_{n'_z=1}^{N_z} i_{n'_z}B_{n'_z}(k_z)J_t(k_y)\hat{\boldsymbol{z}}\boldsymbol{G}^{ej}(k_{y0},k_{z0})e^{-jk_{x0}(x_0-x_{n'_z})}e^{-jk_{y0}(y_0-y_{n'_z})}e^{-jk_{z0}(z_0-z_{n'_z})}\right) \tag{C.81}$$

From the electric field strength the radiation intensity can be found as:

$$U(\theta,\phi) = r^2\frac{1}{2\zeta}\left(|E_\theta|^2 + |E_\phi|^2\right) \tag{C.82}$$

where $E_\theta = E_x\cos\theta\cos\phi + E_y\cos\theta\sin\phi - E_z\sin\theta$ and $E_\phi = -E_x\sin\phi + E_y\cos\phi$ are the θ- and ϕ-components of the electric field, and ζ is the free-space impedance. The directivity is defined as the ratio of the radiation intensity in a direction (θ,ϕ) to the radiation intensity of an isotropic antenna radiating the same amount of power. The radiation intensity of an isotropic antenna is $U_0 = P_{rad}/4\pi$, where P_{rad} is the total radiated power and can be found by integrating the radiation intensity over the entire sphere:

$$P_{rad} = \int_0^{2\pi}\int_0^{\pi} U(\theta,\phi)\sin\theta d\theta d\phi \tag{C.83}$$

The directivity in every direction θ, ϕ is therefore:

$$D(\theta,\phi) = \frac{U(\theta,\phi)}{U_0} = 4\pi\frac{U(\theta,\phi)}{P_{rad}} \tag{C.84}$$

Appendix D

Convergence of a truncated sinusoidal basis function

It is stated in section 5.1 that the truncated sinusoidal basis function does not converge. The validity of the basis function is checked using a planar dipole with lenght $l = 0.5\lambda$. Let us consider such a planar dipole, as shown in figure D.1.

The basis functions in the spectral domain are:

$$\begin{aligned}
B_{up}(k_x) &= \frac{-e^{-jk_x\frac{b+a}{2}}}{2\sin\left(k_0\frac{l}{2}\right)}\left(e^{-jk_0\frac{l}{2}}\frac{e^{-jb(k_0-k_x)}-e^{-ja(k_0-k_x)}}{k_0-k_x}+e^{jk_0\frac{l}{2}}\frac{e^{jb(k_0+k_x)}-e^{ja(k_0+k_x)}}{k_0+k_x}\right)\forall(a<0,b<0)\\
B_{mid}(k_x) &= \frac{-e^{-jk_x\frac{b+a}{2}}}{2\sin\left(k_0\frac{l}{2}\right)}\left(\frac{2\cos\left(k_0\frac{l}{2}\right)}{k_0+k_x}+\frac{2\cos\left(k_0\frac{l}{2}\right)}{k_0-k_x}-e^{-jk_0\frac{l}{2}}\frac{e^{-ja(k_0-k_x)}}{k_0-k_x}\right.\\
&\quad\left.-e^{jk_0\frac{l}{2}}\frac{e^{-jb(k_0-k_x)}}{k_0-k_x}-e^{jk_0\frac{l}{2}}\frac{e^{ja(k_0+k_x)}}{k_0+k_x}-e^{-jk_0\frac{l}{2}}\frac{e^{jb(k_0+k_x)}}{k_0+k_x}\right)\forall(a<0,b>0)\\
B_{down}(k_x) &= \frac{e^{-jk_x\frac{b+a}{2}}}{2\sin\left(k_0\frac{l}{2}\right)}\left(e^{jk_0\frac{l}{2}}\frac{e^{-jb(k_0-k_x)}-e^{-ja(k_0-k_x)}}{k_0-k_x}+e^{-jk_0\frac{l}{2}}\frac{e^{jb(k_0+k_x)}-e^{ja(k_0+k_x)}}{k_0+k_x}\right)\forall(a>0,b>0)
\end{aligned} \tag{D.1}$$

where a is the x-coordinate of the left end point of the dipole part and b is the x-coordinate of the right end point with respect to the center of the dipole. The self impedance of a dipole part or the mutual impedance between two parts of the dipole is found to be:

$$Z_{xn'xn} = -\frac{1}{2\pi}\int_{-\infty}^{\infty} B_{n',x}(k_x)B^*_{n,x}(-k_x)D_{n,n'}(k_x)e^{-jk_x(x_n-x_{n'})}dk_x \tag{D.2}$$

where $D_{n,n'}(k_x) = \frac{1}{2\pi}\int_{-\infty}^{\infty} J_t(k_y)G^{ej}_{xx}(k_x,k_y)e^{-j\sqrt{k_0^2-k_x^2-k_y^2}|z_n-z_{n'}|}dk_y$ and $G^{ej}_{xx}(k_x,k_y) = -\frac{\zeta}{2k_0}\frac{(k_0^2-k_x^2)}{\sqrt{k_0^2-k_x^2-k_y^2}}$. Since for a planar dipole $|z_n - z_{n'}| = 0$:

$$D_{n,n'}(k_x) = -\frac{\zeta}{4k_0}\left(k_0^2-k_x^2\right)J_0\left(\sqrt{k_0^2-k_x^2}\frac{w}{4}\right)H_0^{(2)}\left(\sqrt{k_0^2-k_x^2}\frac{w}{4}\right) \tag{D.3}$$

As an example of the asymptotic expressions, and to show that the integrals do not converge, two of the individual components of the impedance matrix are considered: $Z_{up,up}$ and $Z_{up,mid}$. The remaining elements can be found in a similar way.

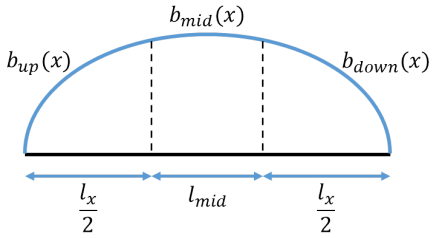

Figure D.1: Truncated sinusoidal basis function on a planar dipole. The sinusoidal basis function is cut in three parts: b_{up}, b_{mid} and b_{down}.

D.1 $Z_{up,up}$

Let us consider the basis function in the limit where $|k_x| \gg k_0$:

$$
\begin{aligned}
B(k_x) &= \frac{-e^{-jk_x\frac{b+a}{2}}}{2\sin\left(k_0\frac{l}{2}\right)}\left(e^{-jk_0\frac{l}{2}}\frac{e^{-jb(k_0-k_x)}-e^{-ja(k_0-k_x)}}{k_0-k_x}+e^{jk_0\frac{l}{2}}\frac{e^{jb(k_0+k_x)}-e^{ja(k_0+k_x)}}{k_0+k_x}\right)\\
&\approx \frac{-e^{-jk_x\left(\frac{b+a}{2}\right)}}{2\sin\left(k_0\frac{l}{2}\right)}\left(-e^{-jk_0\frac{l}{2}}\frac{e^{-jb(k_0-k_x)}-e^{-ja(k_0-k_x)}}{k_x}+e^{jk_0\frac{l}{2}}\frac{e^{jb(k_0+k_x)}-e^{ja(k_0+k_x)}}{k_x}\right)\\
&= \frac{-e^{-jk_x\left(\frac{b+a}{2}\right)}}{2\sin\left(k_0\frac{l}{2}\right)k_x}\left(-e^{-jk_0\frac{l}{2}}e^{-jb(k_0-k_x)}+e^{-jk_0\frac{l}{2}}e^{-ja(k_0-k_x)}+e^{jk_0\frac{l}{2}}e^{jb(k_0+k_x)}-e^{jk\frac{l}{2}}e^{ja(k_0+k_x)}\right)\\
&= \frac{-e^{-jk_x\left(\frac{b+a}{2}\right)}}{2\sin\left(k_0\frac{l}{2}\right)k_x}\left(-e^{-jk_0\frac{l}{2}}e^{-jbk_0}e^{jbk_x}+e^{-jk_0\frac{l}{2}}e^{-jak_0}e^{jak_x}+e^{jk_0\frac{l}{2}}e^{jbk_0}e^{jbk_x}-e^{jk_0\frac{l}{2}}e^{jak_0}e^{jak_x}\right)\\
&= \frac{-e^{-jk_x\left(\frac{b+a}{2}\right)}}{2\sin\left(k_0\frac{l}{2}\right)k_x}\left(-e^{-jk_0\left(\frac{l}{2}+b\right)}e^{jbk_x}+e^{-jk_0\left(\frac{l}{2}+a\right)}e^{jak_x}+e^{jk_0\left(\frac{l}{2}+b\right)}e^{jbk_x}-e^{jk_0\left(\frac{l}{2}+a\right)}e^{jak_x}\right)\\
&= \frac{-e^{-jk_x\left(\frac{b+a}{2}\right)}}{2\sin\left(k_0\frac{l}{2}\right)k_x}\left(e^{jbk_x}\left(e^{jk_0\left(\frac{l}{2}+b\right)}-e^{-jk_0\left(\frac{l}{2}+b\right)}\right)-e^{jak_x}\left(e^{jk_0\left(\frac{l}{2}+a\right)}-e^{-jk_0\left(\frac{l}{2}+a\right)}\right)\right)\\
&= \frac{-e^{-jk_x\left(\frac{b+a}{2}\right)}}{\sin\left(k_0\frac{l}{2}\right)k_x}\left(e^{jbk_x}j\sin\left(k_0\left(\frac{l}{2}+b\right)\right)-e^{jak_x}j\sin\left(k_0\left(\frac{l}{2}+a\right)\right)\right)\\
&= \left(\frac{j\sin\left(k_0\left(\frac{l}{2}+a\right)\right)}{\sin\left(k_0\frac{l}{2}\right)k_x}e^{jak_x}-\frac{j\sin\left(k_0\left(\frac{l}{2}+b\right)\right)}{\sin\left(k_0\frac{l}{2}\right)k_x}e^{jbk_x}\right)e^{-jk_x\left(\frac{b+a}{2}\right)}
\end{aligned}
\tag{D.4}
$$

Substituting $a=-l/2$ and $b=-l_{mid}/2$:

$$
\begin{aligned}
B(k_x) &= \left(\frac{j\sin\left(k_0\left(\frac{l}{2}-\frac{l}{2}\right)\right)}{\sin\left(k_0\frac{l}{2}\right)k_x}e^{-j\frac{l}{2}k_x}-\frac{j\sin\left(k_0\left(\frac{l}{2}-\frac{l_{mid}}{2}\right)\right)}{\sin\left(k_0\frac{l}{2}\right)k_x}e^{-j\frac{l_{mid}}{2}k_x}\right)e^{jk_x\left(\frac{\frac{l_{mid}}{2}+\frac{l}{2}}{2}\right)}\\
&= -\frac{j\sin\left(k_0\left(\frac{l}{2}-\frac{l_{mid}}{2}\right)\right)}{\sin\left(k_0\frac{l}{2}\right)k_x}e^{-j\frac{l_{mid}}{2}k_x}e^{jk_x\left(\frac{l_{mid}+l}{4}\right)}\\
&= -\frac{j\sin\left(k_0\left(\frac{l}{2}-\frac{l_{mid}}{2}\right)\right)}{\sin\left(k_0\frac{l}{2}\right)k_x}e^{-jk_x\left(\frac{l_{mid}-l}{4}\right)}
\end{aligned}
\tag{D.5}
$$

From equation (D.5) it is clear that:

$$B^*(-k_x)=B(k_x) \tag{D.6}$$

The function $D(k_x)$ for $|k_x| \gg k_0$ reduces to:

$$\begin{aligned}
D(k_x) &= -\frac{\zeta_0}{4k_0}(k_0^2 - k_x^2)J_0(\frac{w}{4}\sqrt{k_0^2 - k_x^2})H_0^{(2)}(\frac{w}{4}\sqrt{k_0^2 - k_x^2}) \\
&\approx \frac{\zeta_0}{4k_0}k_x^2 J_0(\frac{w}{4}(-j|k_x|))H_0^{(2)}(\frac{w}{4}(-j|k_x|)) \\
&= \frac{\zeta_0}{4k_0}k_x^2 J_0(-j\frac{w}{4}|k_x|)H_0^{(2)}(-j\frac{w}{4}|k_x|) \\
&= \frac{\zeta_0}{4k_0}k_x^2 I_0(|k_x|\frac{w}{4})\frac{2j}{\pi}K_0(|k_x|\frac{w}{4}) \\
&\approx \frac{\zeta_0}{4k_0}\frac{2j}{\pi}k_x^2\frac{e^{k_x\frac{w}{4}}}{\sqrt{2\pi|k_x|\frac{w}{4}}}\sqrt{\frac{\pi}{2|k_x|\frac{w}{4}}}e^{-k_x\frac{w}{4}} \\
&= \frac{\zeta_0}{4k_0}k_x^2\frac{j4}{\pi|k_x|w} \\
&= j\frac{\zeta_0}{\pi w k_0}|k_x|
\end{aligned} \tag{D.7}$$

The asymptotic expressions for the impedance $Z_{up,up}$ can now be found for $k_x \gg k_0$:

$$\begin{aligned}
Z_{up,up,pos} &= -\frac{1}{2\pi}\int_u^\infty B_{n'_x}(k_x)\,B^*_{n_x}(-k_x)\,D_{n,n'}(k_x)\,e^{-jk_x(x_n - x_{n'})}dk_x \\
&= -\frac{1}{2\pi}\int_u^\infty \left(-\frac{j\sin\left(k\left(\frac{l}{2} - \frac{l_{mid}}{2}\right)\right)}{\sin\left(k\frac{l}{2}\right)k_x}e^{-jk_x\left(\frac{l_{mid}-l}{4}\right)}\right)^2 j\frac{\zeta_0}{\pi w k_0}|k_x|dk_x \\
&= \frac{1}{2\pi}j\frac{\zeta_0}{\pi w k_0}\frac{\sin^2\left(k\left(\frac{l}{2} - \frac{l_{mid}}{2}\right)\right)}{\sin^2\left(k\frac{l}{2}\right)}\int_u^\infty \frac{e^{-jk_x\left(\frac{l_{mid}-l}{2}\right)}}{k_x}dk_x
\end{aligned} \tag{D.8}$$

and for $k_x \ll k_0$

$$\begin{aligned}
Z_{up,up,neg} &= -\frac{1}{2\pi}\int_{-\infty}^{-u} B_{n'_x}(k_x)\,B^*_{n_x}(-k_x)\,D_{n,n'}(k_x)\,e^{-jk_x(x_n - x_{n'})}dk_x \\
&= -\frac{1}{2\pi}\int_{-\infty}^{-u} \left(-\frac{j\sin\left(k\left(\frac{l}{2} - \frac{l_{mid}}{2}\right)\right)}{\sin\left(k\frac{l}{2}\right)k_x}e^{-jk_x\left(\frac{l_{mid}-l}{4}\right)}\right)^2 j\frac{\zeta_0}{\pi w k_0}|k_x|dk_x \\
&= \frac{1}{2\pi}j\frac{\zeta_0}{\pi w k_0}\frac{\sin^2\left(k\left(\frac{l}{2} - \frac{l_{mid}}{2}\right)\right)}{\sin^2\left(k\frac{l}{2}\right)}\int_{-\infty}^{-u} \frac{e^{-jk_x\left(\frac{l_{mid}-l}{2}\right)}}{-k_x}dk_x \\
&= \frac{1}{2\pi}j\frac{\zeta_0}{\pi w k_0}\frac{\sin^2\left(k\left(\frac{l}{2} - \frac{l_{mid}}{2}\right)\right)}{\sin^2\left(k\frac{l}{2}\right)}\int_{\infty}^{u} \frac{e^{jk'_x\left(\frac{l_{mid}-l}{2}\right)}}{k'_x}d(-k'_x) \\
&= \frac{1}{2\pi}j\frac{\zeta_0}{\pi w k_0}\frac{\sin^2\left(k\left(\frac{l}{2} - \frac{l_{mid}}{2}\right)\right)}{\sin^2\left(k\frac{l}{2}\right)}\int_{u}^{\infty} \frac{e^{jk'_x\left(\frac{l_{mid}-l}{2}\right)}}{k'_x}dk'_x
\end{aligned} \tag{D.9}$$

The integrals found in equations (D.8) and (D.9) do not converge.

D.2 $Z_{up,mid}$

It is shown in equation (D.4) that:

$$B(k_x) = \left(\frac{j\sin\left(k_0\left(\frac{l}{2} + a\right)\right)}{\sin\left(k_0\frac{l}{2}\right)k_x}e^{jak_x} - \frac{j\sin\left(k_0\left(\frac{l}{2} + b\right)\right)}{\sin\left(k_0\frac{l}{2}\right)k_x}e^{jbk_x}\right)e^{-jk_x\left(\frac{b+a}{2}\right)} \tag{D.10}$$

The asymptotic expression for middle basis function is:

$$\begin{aligned}
B(k_x) &= \frac{-e^{-jk_x\left(\frac{b+a}{2}\right)}}{2\sin\left(k_0\frac{l}{2}\right)}\left(\frac{2\cos\left(k_0\frac{l}{2}\right)}{k_0+k_x}+\frac{2\cos\left(k_0\frac{l}{2}\right)}{k_0-k_x}-e^{-jk_0\frac{l}{2}}\frac{e^{-ja(k_0-k_x)}}{k_0-k_x}\right.\\
&\qquad\left.-e^{jk_0\frac{l}{2}}\frac{e^{-jb(k_0-k_x)}}{k_0-k_x}-e^{jk_0\frac{l}{2}}\frac{e^{ja(k_0+k_x)}}{k_0+k_x}-e^{-jk_0\frac{l}{2}}\frac{e^{jb(k_0+k_x)}}{k_0+k_x}\right)\\
&\approx \frac{-e^{-jk_x\left(\frac{b+a}{2}\right)}}{2\sin\left(k_0\frac{l}{2}\right)}\left(\frac{2\cos\left(k_0\frac{l}{2}\right)}{k_x}-\frac{2\cos\left(k_0\frac{l}{2}\right)}{k_x}+e^{-jk_0\frac{l}{2}}\frac{e^{-ja(k_0-k_x)}}{k_x}\right.\\
&\qquad\left.+e^{jk_0\frac{l}{2}}\frac{e^{-jb(k_0-k_x)}}{k_x}-e^{jk_0\frac{l}{2}}\frac{e^{ja(k_0+k_x)}}{k_x}-e^{-jk_0\frac{l}{2}}\frac{e^{jb(k_0+k_x)}}{k_x}\right)\\
&= \frac{-e^{-jk_x\left(\frac{b+a}{2}\right)}}{2\sin\left(k_0\frac{l}{2}\right)k_x}\left(e^{-jk_0\frac{l}{2}}e^{-jak_0}e^{jak_x}+e^{jk_0\frac{l}{2}}e^{-jbk_0}e^{jbk_x}-e^{jk_0\frac{l}{2}}e^{jak_0}e^{jak_x}-e^{-jk_0\frac{l}{2}}e^{jbk_0}e^{jbk_x}\right)\\
&= \frac{-e^{-jk_x\left(\frac{b+a}{2}\right)}}{2\sin\left(k_0\frac{l}{2}\right)k_x}\left(e^{jak_x}\left(e^{-jk_0\left(\frac{l}{2}+a'\right)}-e^{jk_0\frac{l}{2}\left(\frac{l}{2}+a\right)}\right)+e^{jbk_x}\left(e^{jk_0\left(\frac{l}{2}-b\right)}-e^{-jk_0\left(\frac{l}{2}-b\right)}\right)\right)\\
&= \frac{e^{-jk_x\left(\frac{b+a}{2}\right)}}{\sin\left(k_0\frac{l}{2}\right)k_x}\left(e^{jak_x}j\sin\left(k_0\left(\frac{l}{2}+a\right)\right)-e^{jbk_x}j\sin\left(k_0\left(\frac{l}{2}-b\right)\right)\right)\\
&= \left(\frac{j\sin\left(k_0\left(\frac{l}{2}+a\right)\right)}{\sin\left(k_0\frac{l}{2}\right)k_x}e^{jak_x}-\frac{j\sin\left(k_0\left(\frac{l}{2}-b\right)\right)}{\sin\left(k_0\frac{l}{2}\right)k_x}e^{jbk_x}\right)e^{-jk_x\left(\frac{b+a}{2}\right)}\\
&= \left(\frac{j\sin\left(k_0\left(\frac{l}{2}-\frac{l_{mid}}{2}\right)\right)}{\sin\left(k_0\frac{l}{2}\right)k_x}e^{-j\frac{l_{mid}}{2}k_x}-\frac{j\sin\left(k_0\left(\frac{l}{2}-\frac{l_{mid}}{2}\right)\right)}{\sin\left(k_0\frac{l}{2}\right)k_x}e^{j\frac{l_{mid}}{2}k_x}\right)e^{-jk_x\left(\frac{\frac{l_{mid}}{2}-\frac{l_{mid}}{2}}{2}\right)}\\
&= \frac{j\sin\left(k_0\left(\frac{l}{2}-\frac{l_{mid}}{2}\right)\right)}{\sin\left(k_0\frac{l}{2}\right)k_x}\left(e^{-j\frac{l_{mid}}{2}k_x}-e^{j\frac{l_{mid}}{2}k_x}\right)
\end{aligned} \tag{D.11}$$

The asymptotic expressions for the impedance $Z_{up,mid}$ can now be found for $k_x \gg k_0$:

$$\begin{aligned}
Z_{up,mid,pos} &= -\frac{1}{2\pi}\int_u^\infty B_{n'_x}(k_x)\,B^*_{n_x}(-k_x)\,D_{n,n'}(k_x)\,e^{-jk_x(x_n-x_{n'})}dk_x\\
&= \frac{1}{2\pi}\int_u^\infty \frac{j\sin\left(k_0\left(\frac{l}{2}-\frac{l_{mid}}{2}\right)\right)}{\sin\left(k_0\frac{l}{2}\right)k_x}e^{-jk_x\left(\frac{l_{mid}-l}{4}\right)}\frac{j\sin\left(k_0\left(\frac{l}{2}-\frac{l_{mid}}{2}\right)\right)}{\sin\left(k_0\frac{l}{2}\right)k_x}\left(e^{-j\frac{l_{mid}}{2}k_x}-e^{j\frac{l_{mid}}{2}k_x}\right)\\
&\qquad j\frac{\zeta_0}{\pi w k_0}|k_x|e^{-jk_x\left(\frac{l_{mid}+l}{4}\right)}dk_x\\
&= -\frac{1}{2\pi}j\frac{\zeta_0}{\pi w k_0}\frac{\sin^2\left(k_0\left(\frac{l}{2}-\frac{l_{mid}}{2}\right)\right)}{\sin^2\left(k_0\frac{l}{2}\right)}\int_u^\infty e^{-jk_x\left(\frac{l_{mid}}{2}\right)}\left(e^{-j\frac{l_{mid}}{2}k_x}-e^{j\frac{l_{mid}}{2}k_x}\right)\frac{|k_x|}{k_x^2}dk_x\\
&= -\frac{1}{2\pi}j\frac{\zeta_0}{\pi w k_0}\frac{\sin^2\left(k_0\left(\frac{l}{2}-\frac{l_{mid}}{2}\right)\right)}{\sin^2\left(k_0\frac{l}{2}\right)}\int_u^\infty\left(e^{-jl_{mid}k_x}-1\right)\frac{1}{k_x}dk_x\\
&= -\frac{1}{2\pi}j\frac{\zeta_0}{\pi w k_0}\frac{\sin^2\left(k_0\left(\frac{l}{2}-\frac{l_{mid}}{2}\right)\right)}{\sin^2\left(k_0\frac{l}{2}\right)}\int_u^\infty\frac{e^{-jl_{mid}k_x}}{k_x}dk_x-\int_u^\infty\frac{1}{k_x}dk_x
\end{aligned} \tag{D.12}$$

and for $k_x \ll k_0$:

$$
\begin{aligned}
Z_{up,mid,neg} &= -\frac{1}{2\pi}\int_{-\infty}^{-u} B_{n'_x}(k_x)\, B^*_{n_x}(-k_x)\, D_{n,n'}(k_x)\, e^{-jk_x(x_n - x_{n'})} dk_x \\
&= \frac{1}{2\pi}\int_{-\infty}^{-u} \frac{j\sin\left(k_0\left(\frac{l}{2}-\frac{l_{mid}}{2}\right)\right)}{\sin\left(k_0\frac{l}{2}\right)k_x} e^{-jk_x\left(\frac{l_{mid}-l}{4}\right)} \frac{j\sin\left(k_0\left(\frac{l}{2}-\frac{l_{mid}}{2}\right)\right)}{\sin\left(k_0\frac{l}{2}\right)k_x} \left(e^{-j\frac{l_{mid}}{2}k_x} - e^{j\frac{l_{mid}}{2}k_x}\right) \\
&\qquad j\frac{\zeta_0}{\pi w k_0}|k_x| e^{-jk_x\left(\frac{l_{mid}+l}{4}\right)} dk_x \\
&= -\frac{1}{2\pi} j\frac{\zeta_0}{\pi w k_0} \frac{\sin^2\left(k_0\left(\frac{l}{2}-\frac{l_{mid}}{2}\right)\right)}{\sin^2\left(k_0\frac{l}{2}\right)} \int_{-\infty}^{-u} e^{-jk_x\left(\frac{l_{mid}}{2}\right)} \left(e^{-j\frac{l_{mid}}{2}k_x} - e^{j\frac{l_{mid}}{2}k_x}\right) \frac{|k_x|}{k_x^2} dk_x \\
&= -\frac{1}{2\pi} j\frac{\zeta_0}{\pi w k_0} \frac{\sin^2\left(k_0\left(\frac{l}{2}-\frac{l_{mid}}{2}\right)\right)}{\sin^2\left(k_0\frac{l}{2}\right)} \int_{-\infty}^{-u} \left(e^{-jl_{mid}k_x} - 1\right) \frac{-1}{k_x} dk_x \\
&= -\frac{1}{2\pi} j\frac{\zeta_0}{\pi w k_0} \frac{\sin^2\left(k_0\left(\frac{l}{2}-\frac{l_{mid}}{2}\right)\right)}{\sin^2\left(k_0\frac{l}{2}\right)} \int_{-\infty}^{-u} \frac{-e^{-jl_{mid}k_x}}{k_x} dk_x - \int_{-\infty}^{-u} \frac{-1}{k_x} dk_x \\
&= -\frac{1}{2\pi} j\frac{\zeta_0}{\pi w k_0} \frac{\sin^2\left(k_0\left(\frac{l}{2}-\frac{l_{mid}}{2}\right)\right)}{\sin^2\left(k_0\frac{l}{2}\right)} \int_{\infty}^{u} \frac{e^{jl_{mid}k'_x}}{k'_x} d\left(-k'_x\right) - \int_{\infty}^{u} \frac{1}{k'_x} d\left(-k'_x\right) \\
&= -\frac{1}{2\pi} j\frac{\zeta_0}{\pi w k_0} \frac{\sin^2\left(k_0\left(\frac{l}{2}-\frac{l_{mid}}{2}\right)\right)}{\sin^2\left(k_0\frac{l}{2}\right)} \int_{u}^{\infty} \frac{e^{jl_{mid}k'_x}}{k'_x} dk'_x - \int_{u}^{\infty} \frac{1}{k'_x} dk'_x
\end{aligned}
\tag{D.13}
$$

The integrals found in equations (D.12) and (D.13) do not converge.

Bibliography

[1] F. Tiezzi, D. Llorens, C. Dominguez and M. Fajardo, "A compact Ku-band transmit/receive low-profile antenna for broadband mobile satellite communications," *Proc. 4th European Conf. Antennas and Propag.*, Barcelona, Spain, 12-16 Apr. 2010, pp. 1-4.

[2] L. Baggen, S. Vaccaro. D.L. Del Rio, J. Padilla and R.T. Sánchez, "A compact phased array for satcom applications," *Int. Symp. Phased Array Systems & Technology.*, Waltham, MA, USA, 12-18 Oct. 2013, pp. 232-239

[3] S. Vaccaro, F. Tiezzi, M.F. Rúa and C.D.G. De Oro, "Ku-band low-profile Rx-only and Tx-Rx antennas for mobile satellite communications," *Int. Symp. Phased Array Systems and Technology.*, Boston, MA, USA, 12-15 Oct. 2010, pp. 536-542

[4] R. Bolt, D. Cavallo, G. Gerini, R. Grooters, D. Deurloo, R. Grooters, A. Neto, G. Toso, "Characterization of a Dual-Polarized Connected-Dipole Array for Ku-Band Mobile Terminals." *IEEE Trans. Antennas and propag.*, vol. 64, pp 591-598, Feb. 2016

[5] A. Catalani, F. Di Paolo, M. Migliorelli, L. Russo, G. Toso and P. Angeletti, "Ku band hemispherical fully electronic antenna for aircraft in flight entertainment." *Int. J. Antennas and Propag.*, vol. 2009, 7, Article ID 230650, doi:10.1155/2009/230650

[6] F. Tiezzi and S. Vaccaro,"Hybrid phased array antenna for mobile KU-band DVB-S services." *1st European Conf. Antennas and Propag.*, Nice, France, 6-10 Nov. 2006, pp. 1-4

[7] F. Tiezzi, S. Vaccaro, D. Llorens, C. Dominguez and M. Fajardo, "Ku-band hybrid phased array antennas for mobile satellite communication systems.", *7th European Conf. Antennas and Propag.*, Götenborg, Sweden, 8-12 Apr. 2013, pp. 1605-1608

[8] A.K. Bhattacharyya, "Active element pattern symmetry for asymmetrical element arrays.", *IEEE Antennas and Wireless Propag. Letters*, vol. 6, pp. 275-278, June 2007.

[9] S. Bruni, N. Llombart, A. Neto, G. Gerini and S. Maci, "Problem-Matched Basis Functions for Microstrip Coupled Slot Arrays Based on Transmission Line Green's Functions (TLGF)", *IEEE Trans. Antennas and Propag.*, vol. 53, pp. 3556-3567, Nov. 2005.

[10] C.A. Balanis, *Antenna theory: Analysis and design, 3rd ed.*, Hoboken: John Wiley & Sons, 2005.

[11] H. King, "Mutual impedance of unequal length antennas in echelon", *IRE Trans. Antennas and Propag.*, vol. 5, no. 3, pp. 306-313, 1957.

[12] J. Richmond and N. Geary, "Mutual impedance of nonplanar-skew sinusoidal dipoles"*IEEE Trans. Antennas and Propag.*, vol. 23, pp. 412-414, May 1975.